RHEOLOGY AND PROCESSING OF HIGH-DENSITY POLYETHYLENES (HDPEs): *EFFECTS OF MOLECULAR CHARACTERISTICS*

by

MAHMOUD ANSARI

B.A.Sc. Amirkabir University of Technology, Iran, 2003

M.A.Sc. Tarbiat Modares University, Iran, 2005

A THESIS SUBMITTED IN PARTIAL FULFILLMENT OF
THE REQUIREMENTS FOR THE DEGREE OF

DOCTOR OF PHILOSOPHY

in

THE FACULTY OF GRADUATE STUDIES

(Chemical and Biological Engineering)

THE UNIVERSITY OF BRITISH COLUMBIA

(Vancouver)

September 2012

ABSTRACT

In this study, the linear viscoelastic properties of two series of Ziegler-Natta and metallocene HDPEs (ZN-HDPEs and m-HDPEs respectively) of broad molecular weight distribution (MWD) have been studied. Relationships between the zero-shear viscosity and molecular weight (M_w) and molecular weight distribution show that the breadth of the molecular weight distribution (MWD) for m-HDPEs plays a significant role. Other interesting correlations between the crossover modulus and steady state compliance with MWD of both these classes of polymers have also been derived. Finally, the steady-shear viscosities from capillary rheometry are compared with LVE data to check the applicability of the empirical Cox-Merz rule. It is shown that the original Cox-Merz rule is approximately applicable for HDPEs for narrow to moderate MWD and fails for those HDPEs having a wide MWD due to the occurrence of wall slip.

The processing behavior of both series of HDPEs was investigated. Their melt fracture behaviour was studied primarily as a function of M_w and MWD, and operating conditions i.e. temperature and geometrical details and type of die (capillary, slit and annular). It is found that sharkskin and other melt fracture phenomena are very different for these two classes of polymers, although their rheological behaviors are nearly the same for many of these. It is also found that critical conditions for the onset of various melt fracture phenomena depend significantly on the type of die used for their study.

The slip behaviour of these resins was also studied as a function of M_w and MWD. It is found that the slip velocity increases with decrease of M_w, which expected to decay to zero as the M_w approaches a value with characteristic molecular dimension similar to surface asperities. For HDPEs that exhibit stick-slip transition (narrow to moderate MWD), the slip velocity has been found to increase with increase of polydispersity. The opposite dependence is shown for HDPEs of wider molecular weight distribution that do not exhibit stick-slip transition. A criterion is also developed as to the occurrence or not of the stick-slip transition which is found to depend strongly on M_w and its distribution.

PREFACE

The work of this thesis consists of *four* different manuscripts.

Chapter 5 is based on a manuscript that has been published.
Ansari, M., S.G. Hatzikiriakos, A.M. Sukhadia and D.C. Rohlfing (2011). "Rheology of Ziegler-Natta and metallocene high-density polyethylenes: broad molecular weight distribution effects." Rheologica Acta **50**(1): 17-27.

The materials covered in chapter 6 consist of two manuscripts, the first one is already published and the other one is accepted for publication.
Ansari, M., S.G. Hatzikiriakos, A.M. Sukhadia and D.C. Rohlfing (2012). "Melt Fracture of Two Broad Molecular Weight Distribution High-Density Polyethylenes." *Polymer Engineering and Science* **52**(4): 795-804.
Ansari, M., Y.W. Inn, A.M. Sukhadia, P.J. DesLauriers and S.G. Hatzikiriakos (2012). "Melt Fracture of HDPEs: Metallocene versus Ziegler-Natta and Broad MWD Effects." Accepted for publication in *Polymer*.

Chapter 7 has been prepared based on a submitted manuscript.
Ansari, M., Y.W. Inn, A.M. Sukhadia, P.J. DesLauriers and S.G. Hatzikiriakos (2012). "Wall slip of HDPEs: Molecular weight and molecular weight distribution effects."

All of the experiments and data analysis have been conducted by myself. The molecular weights and their distributions have been provided by Chevron-Phillips Chemical Company LP. The manuscripts were a collaborative effort between myself, my supervisor Prof. Savvas G. Hatzikiriakos and scientists of Chevron-Phillips Chemical Company LP who appear as co-authors in the manuscripts.

The initial and final drafts of this thesis were prepared by Mahmoud Ansari, with revisions edited and approved by Prof. Savvas G. Hatzikiriakos.

TABLE OF CONTENTS

LIST OF TABLES

LIST OF FIGURES

NOMENCLATURE

a_T	horizontal shift factor
b_T	vertical shift factor
G_c	crossover modulus, [Pa]
J_e^0	steady state creep compliance, [1/Pa]
ΔP_{end}	end pressure drop, [MPa]
a	Carreau-Yasuda model parameter
a	zero shear viscosity-M_w correlation: PI_w exponent
a	slip velocity-M_w pre-factor, [m/s/(g/mole)^3]
b	zero shear viscosity-M_w correlation: PI_z exponent
D_i	die inside diameter (Annulus), [mm]
D_o	die outside diameter (Annulus), [mm]
E_a	activation energy, [kcal/mole]
G^*	complex modulus, [Pa]
G'	elastic modulus (storage modulus), [Pa]
G''	viscous modulus (loss modulus), [Pa]
g_i	parsimonious relaxation modulus, [Pa]
H	die height (slit), [mm]
J	creep compliance, [1/Pa]
K	zero shear viscosity-M_w correlation pre-factor, [Pa.s/(g/mole)^a]
L	die length; length of material element, [mm]
L/D	die length to diameter ratio
L_0	initial length of material element, [mm]
M_0	monomer molecular weight, [g/mole]
M_c	critical molecular weight for the onset of entanglement, [gr/mole]
M_e	molecular weight between entanglements, [gr/mole]
M_i	mass of polymer chain with i monomer, [g/mole]
M_n	number average molecular weight, [g/mole]
M_w	weight average molecular weight, [g/mole]
M_z	z-moment of molecular weight, [g/mole]

M_{z+2}	(z+2)-moment of molecular weight, [g/mole]
n	shear thinning index
n_i	number of polymer chains with mass of M_i
PI_w	w-moment of polydispersity index
PI_z	z-moment of polydispersity index
Q	volumetric flow rate, [mm^3/s]
R	die radius, [mm]
r	r-direction distance in annulus, [mm]
R_g	radius of gyration, [μm]
t	time, [s]
T	temperature, [°C]
T_{ref}	reference temperature, [°C]
u_s	slip velocity, [mm/s]
W	die width (slit), [mm]
w_i	weight of all polymer chains with i monomer, [g/mole]
ΔP	pressure drop, [MPa]

Greek Letters

$\dot{\gamma}_{A,s}$	apparent shear rate corrected for slip, [1/s]
$\dot{\gamma}_A$	apparent shear rate, [1/s]
$\dot{\gamma}_c$	critical shear rate for the onset of sharkskin, [1/s]
$\alpha_{A,L}$	slip velocity-M_w pre-factor: lower branch, [$m.MPa^{-3}.s^{-1}$]
$\alpha_{A,U}$	slip velocity-M_w pre-factor: upper branch, [$m.MPa^{-3}.s^{-1}$]
α_B	slip velocity-M_w pre-factor: no stick-slip resins, [$m.MPa^{-4}.s^{-1}$]
$\dot{\gamma}$	shear rate, [1/s]
$\dot{\varepsilon}$	Hencky strain rate, [1/s]

η_E^+	uniaxial stress growth coefficient, [Pa.s]
η_R	reference viscosity, [Pa.s]
λ_i	i-th mode of parsimonious relaxation modulus, [s]
σ_{c1}	critical shear stress for the onset of sharkskin, [MPa]
σ_{c2}	upper critical shear stress for the onset of stick-slip, [MPa]
σ_{c3}	lower critical shear stress for the stick-slip effect, [MPa]
σ_{cr}	critical reference stress, [MPa]
$\sigma_{W,A}$	apparent wall shear stress, [MPa]
σ_W	wall shear stress, [MPa]
τ_{rz}	shear stress at location r, [MPa]
ω_c	crossover frequency, [rad/s]
2α	die entrance angle, [°]
α	zero shear viscosity-M_w correlation exponent
β	annulus geometrical parameter
ε	Hencky strain
γ_∞	ultimate recoil
η	shear viscosity, [Pa.s]
η^*	complex viscosity, [Pa.s]
η_0	zero shear viscosity, [Pa.s]
λ	Carreau-Yasuda model parameter: relaxation time, [s]
σ	shear stress, [MPa]
τ_0	elementary characteristic time [s]
ω	angular frequency, [rad/s]

Abbreviations

BN	Boron Nitride
EPDM	Ethylene propylene diene monomer
ESCR	Environmental Stress Crack Resistance
gmf	Gross Melt Fracture
HDPE	High-Density Polyethylene
LAOS	Large Angle Oscillatory Shear
LCB	Long Chain Branching
LDPE	Low-Density Polyethylene
LLDPE	Linear Low-Density Polyethylene
LVE	Linear Viscoelasticity Envelope
m-HDPE	Metallocene High-Density Polyethylene
MWD	Molecular Weight Distribution
PB	Polybutadiene
PCL	Polycaprolactone
PDI	Polydispersity Index
PDMS	Polydimethylsiloxane
PE	Polyethylene
PI	Polyisoprene
PLA	Polylactide
PP	Polypropylene
PPA	Polymer Processing Aid
PS	Polystyrene
SAOS	Small Angle Oscillatory Shear
SER	Sentmanat Extensional Rheometer
TTS	Time-Temperature Superposition
UHMWPE	Ultra-High Molecular Weight Polyethylene
ZN-HDPE	Ziegler-Natta High-Density Polyethylene

ACKNOWLEDGMENTS

First and foremost I would like to express my gratitude to my supervisor, Prof. Savvas G. Hatzikiriakos who I was honored to work with, for his constant support, skillful guidance, patience and great concern which made this work successful.

I would like to thank my committee members for their time, interest, insightful questions and helpful comments.

Sincere thanks to past and present group members from Rheology lab that I have had the pleasure to work with, for their inspirational discussions, constructive comments and also their effort to create an enjoyable environment to work.

My acknowledgment also goes to Chevron Phillips Chemical Company LP for their research grant that provided the necessary financial support and also the materials for this research.

Last but not least I wish to express my thanks to my parents, sisters, brothers, in-laws, friends and co-workers who encouraged, inspired and supported me spiritually. And most of all, I thank the only person who endured this long process with me, my wife for her endless love, great patience, support, encouragement and understanding especially during difficult times.

DEDICATION

To *Sareh*

1 INTRODUCTION

High-density Polythylene (HDPE) is the most applicable plastic in recent century [1] which can be synthesized by different type of processes and catalysts. Two major industrial catalysts to produce HDPEs are namely Zigler-Natta and metallocene catalysts. The advantage of using metallocene catalysts is to produce a product with controlled molecular weight (M_w) and molecular weight distribution (MWD) [2]. The HDPEs produced by these two methods are far different in mechanical and processing properties.

Extrusion is one of the most important routes of production plastic articles such as pipes, films and sheets. From the economical point of view, it is desirable to increase the rate of production without sacrificing product quality. However, this is limited by the occurrence of flow instabilities at flow rates greater than a critical value. These instabilities manifest themselves as surface defects on the surface of extrudates and are collectively known as melt fracture phenomena [3-6]. These include sharkskin (small amplitude periodic distortions) or surface melt fracture, slip-stick or oscillating melt fracture (alternating relatively smooth and distorted portion on the surface) and gross melt fracture (large amplitude periodic and/or non-periodic, chaotic distortions). Melt fracture has been observed in a number of polymers (mainly linear), more frequently on all types of linear polyethylenes including high-density polyethylenes which is the subject of the present work [7].

It has been reported that melt fracture phenomena depend strongly on the molecular characteristics of polyethylenes such as molecular weight and its distribution and levels of long chain branching [3-8]. To assess their processability and correlate it with their molecular structure, rheological methods are frequently employed [9]. In particular shear, extensional and capillary rheometry have been proven to be indispensable methods in assessing the processing behaviour of polyolefins and relate it to rheology [10].

The main objective of this work is to study the melt fracture behaviour of two series of HDPES, namely a series of Ziegler-Natta types (ZN-HDPE) and a second series of metallocene types (m-HDPE) all possessing a broad molecular weight distribution (MWD) not studied previously in

the literature. As these polymers possess excellent mechanical properties and poor processability it is desirable to understand the causes of this. In order to accomplish this, we first performed a thorough study of the rheology of these broad MWD resins particularly on the effects of molecular weight and molecular weight distribution. For example, relationships between rheological properties such as zero shear viscosity, steady state creep compliance, crossover frequency with molecular weight and its distributions are studied.

Consequently, their melt fracture performance in capillary, slit and annular rheometry was investigated. The effect of temperature on melt fracture is also examined which has been reported to be significant in some cases. Their processability is also studied as a function of molecular weight characteristics in capillary extrusion. Several interesting correlations between the critical conditions for the onset of instabilities (slip and melt fracture) and molecular characteristics are derived and discussed which points to the importance of molecular weight characteristics.

Polymer processing aids (PPA) are used in order to improve processability of polymer materials. These chemicals enhance the slippage of polymer melt on the die solid surface by forming a lubrication layer in between which results to higher production rates and better processability [11-13]. In this work, a fluoropolymer processing aid is used to examine its ability to eliminate or postpone melt fracture phenomena to higher shear rates.

The study of processability has led us to find that slippage plays a significant role in the surprisingly different processing behaviour of these polymers, and their slip behaviour is examined in detail. Slip is neither a recent discovery nor a phenomenon confined to the rheology of complex fluids such as molten polymers. Daniel Bernoulli, Coulomb, Poiseuille, Girard, Maxwell, Navier and Stokes are among those who considered the possible effects of slip in Newtonian fluid dynamics. Simply experimental observations were found consistent with the assumption of no-slip and therefore slip phenomena have received little attention in classical fluid mechanics (see Goldstein [14] for a summary).

The molecular dependence of slip velocity for all available HDPEs was studied. The slip velocity was determined by performing the Mooney analysis and deviation from their linear

viscoelastic behaviour [15]. A criterion for the occurrence of stick-slip transition proposed by Allal and Vergnes [16] is also examined and applied in our case. Based on the findings of this study, the flow curve of high-density polyethylenes (HDPEs) can be predicted solely from linear viscoelastic measurements.

2 LITERATURE REVIEW

This chapter presents the literature review on the subject of rheology and processing of polyethylenes. More specifically, the various types of polyethylene are presented; Rheological methods and pieces of equipment needed for this study are also discussed. Flow instabilities such as melt surface instabilities are described and the effects of different parameters such as processing conditions and material molecular characteristics are reviewed. Finally, the wall slip of polymer melts and more specifically that of polyethylenes and the effects of molecular characteristics are finally discussed.

2.1 Types of Polyethylenes

Plastic materials play a major role in our life through recent decades. One of the most important commodity plastic that is extensively used is polyethylene (PE). The chemical structure of this polymer has the repeating unit of ethylene group ($-CH_2-CH_2-$) and it was firstly synthesized by two British researchers, namely Reginald Gibson and Eric Fawcett in 1933 [17].

Thanks to different routes of production, it is rather of low cost to produce it compared to other plastics, and rather easy to process in several applications. Depending on the synthesis processing conditions and catalysts, different types of PEs namely high-density polyethylene (HDPE), low density polyethylene (LDPE), linear-low density polyethylene (LLDPE) and ultrahigh molecular weight polyethylene (UHMWPE) can be produced. These types of polyethylenes have different molecular structures, rheological properties, processing properties as well as mechanical properties [18-20]. Figure 2.1 is a schematic of the molecular structure of various types of polyethylene. It is noted that HDPE, the subject of the present work, has a linear structure.

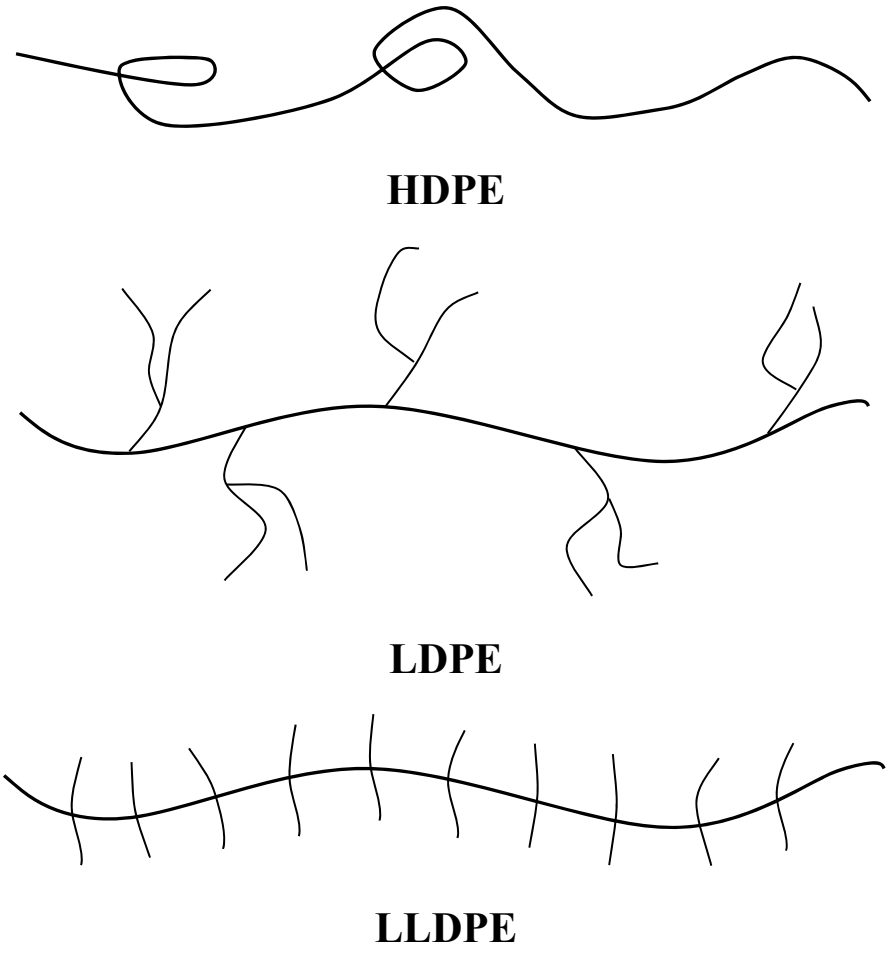

Figure 2.1. *Schematic representation of the microstructure of HDPE, LDPE and LLDPE.*

Among all types of PEs, HDPE has the longest history and areas of usage. There are two major processes of production: Ziegler-Natta and metallocene catalyst technologies. Use of metallocene catalysts can produce HDPEs with controlled molecular weight (M_w) and molecular weight distribution (MWD) [2]. This enhances its mechanical properties and as a result can be used in more demanding applications. For example HDPE is widely used in pipe industry, especially in water transportation and sewer applications, due to many advantages such as its chemical and corrosion resistance, ease of installation, and low cost of production and maintenance. This plastic passes the standard acceptable hoop stress (ring stiffness measure) by controlling the thickness; however it suffers from low environmental stress crack resistance (ESCR) [21, 22]. This defect could be solved to some extent by changing the molecular weight distribution from unimodal to bimodal [23]. Using metallocene catalysts it is possible to produce pipe grade HDPEs known as PE100 which exhibit bimodal MWD [24]. Although superior

mechanical properties are obtained for this class of polyethylenes, their processability becomes extremely difficult due to certain defects on products' surface that significantly limits the rate of production in extrusion applications.

2.2 Molecular Weight and Molecular Weight Distributions

Polymers are materials with large molecules consisted of many repetitive small simple molecules joint together by simple chemical bonds [25]. In most cases, because of their long length, these molecules are commonly known as polymer chains. In the case of synthesized polymers, because of random feature of the synthesizing process, it is impossible to assign a certain molar mass to the polymer [26]. In these systems, there are chains with different lengths, so there is a distribution of molar mass. To characterize these systems, statistical parameters such as the number average molecular weight, M_n are used:

$$M_n = \frac{\sum n_i.M_i}{\sum n_i} = \frac{\sum w_i}{\sum w_i/M_i} \tag{2.1.a}$$

where $w_i = n_i.M_i$ and n_i is the number of chains with molecular weight of M_i. This quantity, M_n, individually is not capable to describe a polymeric system. A number of other molecular averages are used, essentially higher moments of average molecular weights, which are defined by:

$$M_w = \frac{\sum w_i.M_i}{\sum w_i} = \frac{\sum n_i.M_i^2}{\sum n_i.M_i} \tag{2.1.b}$$

$$M_z = \frac{\sum w_i.M_i^2}{\sum w_i.M_i} = \frac{\sum n_i.M_i^3}{\sum n_i.M_i^2} \tag{2.1.c}$$

$$M_{z+j} = \frac{\sum w_i.M_i^{2+j}}{\sum w_i.M_i^{1+j}} = \frac{\sum n_i.M_i^{3+j}}{\sum n_i.M_i^{2+j}} \tag{2.1.d}$$

Where M_w is the weight average molecular weight and M_z and M_{z+1} are the z and z+1 average molecular weights. Even for cases where all these averages are known, it is impossible to have a complete picture of the distribution of molecular sizes of a particular polymeric system. Instead

the complete molecular weight distribution (MWD) is needed. Figure 2.2 shows a typical MWD of a unimodal HDPE.

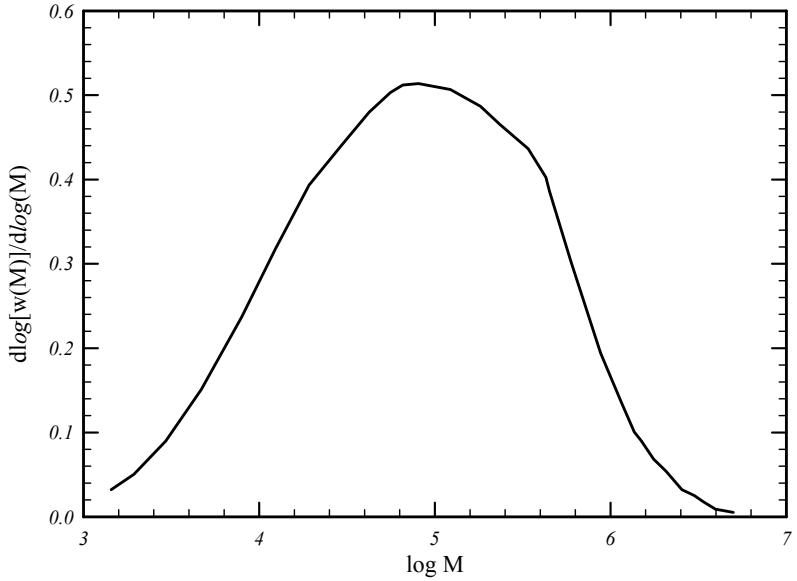

Figure 2.2. *A typical molecular weight distribution of a polymeric system.*

2.3 Rheology

Rheology is the science of flow and deformation of matter. Equations that relate deformation (strain) and rate of deformation (shear strain) to forces (stress) are known as *constitutive equations or rheological equations of state*. Such constitutive equations need to be compared in terms of their ability to model/predict the rheological response of real fluids/solids. From the scientific perspective, this goal can be attained by first setting up appropriate experiments in which simple flow histories are imposed to the material (such as simple shear or extension) and its response is recorded and compared with that of the model.

2.3.1 Rheological Experiments

Polymer melts and solutions are *viscoelastic* fluids which exhibit both viscous and elastic responses depending on the type of deformation. Due to this complex nature, more than one parameter is needed to describe their rheological properties. These parameters which are known

as material functions, including shear viscosity, first and second normal stress coefficients, steady state creep compliance, dynamic moduli and several others. In the following sections, some of the typical experiments in which these material functions are measured, are summarized.

2.3.1.1 Frequency Sweep

Frequency sweep is one of the most widely used experiment to characterize the rheological properties of polymers. According to this test the upper plate in parallel plate geometry is set into an oscillatory motion (sinusoidal rotational displacement or sinusoidal stress) and the stress or displacement is recorded [9].

In this type of experiment, the strain (stress) could be either within the linear or the nonlinear viscoelastic regime, which is called SAOS (small angle oscillatory shear) or LAOS (large angle oscillatory shear) respectively. SAOS is used in order to determine the dynamic moduli, G' (storage modulus), G'' (loss modulus) and the complex viscosity ($|\eta^*| \equiv \sqrt{G'^2+G''^2}/\omega$). Fig 2.3 shows typical data of G', G" and $|\eta^*|$ for a polyethylene.

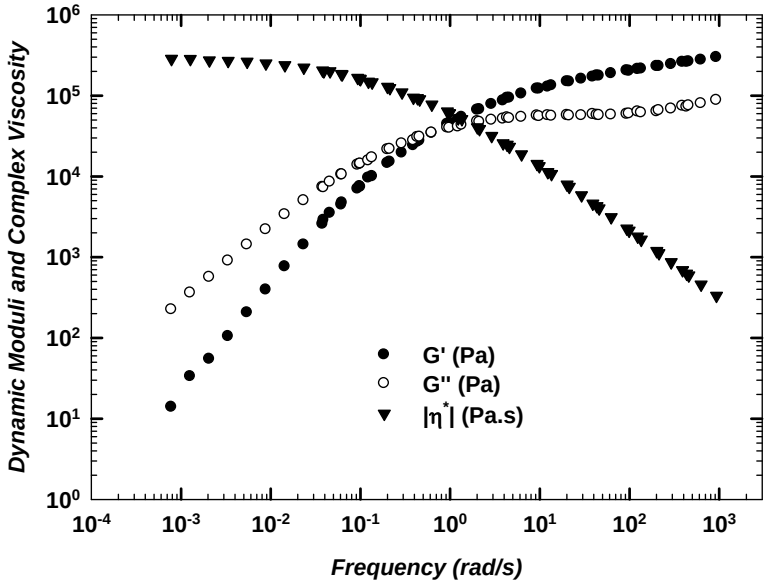

Figure 2.3. *Viscoelastic moduli and complex viscosity for a typical polyethylene obtained from frequency sweep experiments (SAOS).*

2.3.1.2 Creep and Creep Recovery

Creep is a transient test in which a constant stress is imposed to the sample and the strain is monitored with time [9]. Depending on the level of applied stress and type of material, a steady state response is reached. Figure 2.4 shows the typical response of a material and the material function of interest which is the steady state creep compliance (J_e^0). This can be measured based on the following equation or directly from the graph by extrapolation:

$$J(t) = J_e^0 + t/\eta_0 \tag{2.2.a}$$

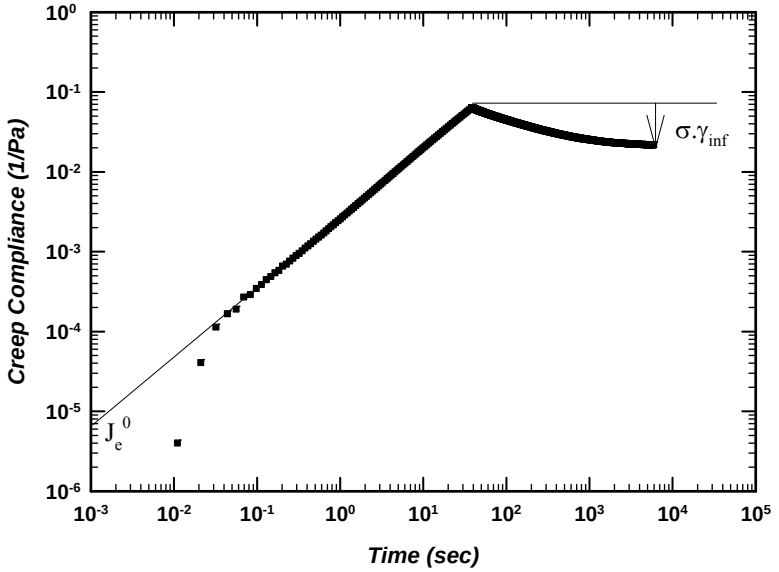

Figure 2.4. *A typical result of the creep and creep recovery experiment.*

If the stress is removed at a certain time (strain level), then due to the elastic nature of polymeric melts, it starts to recover the imposed strain (recoil); however due to its viscous character, this recoil would be completed after complete relaxation. The amount of strain recovered is called the ultimate recoil, γ_∞ (see Fig 2.4). Based on Boltzmann superposition (valid only in linear viscoelasticity) it can be shown that γ_∞ and J_e^0 follow the following equation [9]:

$$\gamma_\infty = \sigma J_e^0 = J_e^0 \eta_0 \dot{\gamma} \tag{2.2.b}$$

The steady state creep compliance is a weak function of M_w, however it has a strong dependency on the MWD [9]. There are some different measures of MWD to describe this correlation. Also many experiments have been performed to validate such relationships with different materials such as PS, branched PE & PDMS [27]. It is found based on available data so far that the following scaling is applicable:

$$J_e^0 \propto (M_{z+2} \times M_{z+1})/(M_z \times M_w) \tag{2.3}$$

which is mentioned by Kurata [28] and has been successfully used by Mills & Nevin [29] for a blend of two narrow molecular weight distributions PS.

2.3.1.3 Steady Shear

In this experiment, a constant shear rate is applied to the material and the steady state shear stress (response) is recorded. Repeating this experiment for several shear rates and plotting shear stress as a function of shear rate, defines the flow curve of the polymer. Viscosity is the main material function determined from this type of experiment (shear stress over shear rate). In some cases, the first and second normal stress difference coefficients are also measured. A typical graph for the flow curve for a molten polymer is shown in Fig 2.5.

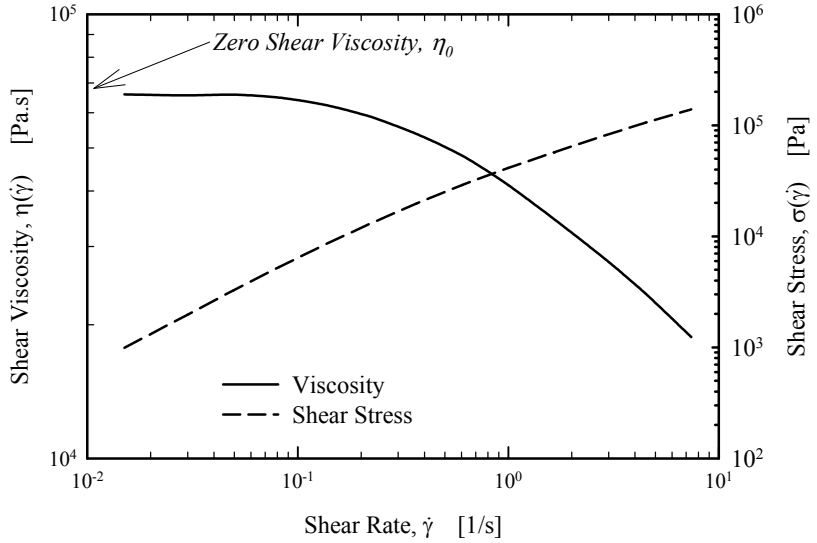

Figure 2.5. *A flow curve of a typical molten polymer obtained from a steady shear experiment.*

2.3.1.4 Uniaxial Extension

In an industrial polymer processing, the polymer melt or solution experiences a combination of different types of deformations i.e. shear and elongation (or extension). All of the above described experiments include only shear components and they are insufficient to completely characterize the rheological behaviour of a material. In fact elongational experiments have been shown to be more sensitive to subtle changes in the molecular structure and frequently are used to relate rheology and processability with molecular characteristics [9].

In a steady uniaxial elongation experiment, a sample of initial length L_o is stretched at a constant Hencky strain rare $\dot{\varepsilon} \equiv d\varepsilon / dt$ and its Hencky strain is related to L, the instantaneous sample length, according to:

$$\varepsilon(t) = ln\frac{L(t)}{L_0} \tag{2.4}$$

Moreover, taking into account the Boltzmann's superposition principle, it can be shown that in the case of transient elongation viscosity, at short time the following relationship is valid which is known as Trouton's rule (see Fig 2.6):

$$\eta_E^+(t) = 3\eta^+(t) \tag{2.5}$$

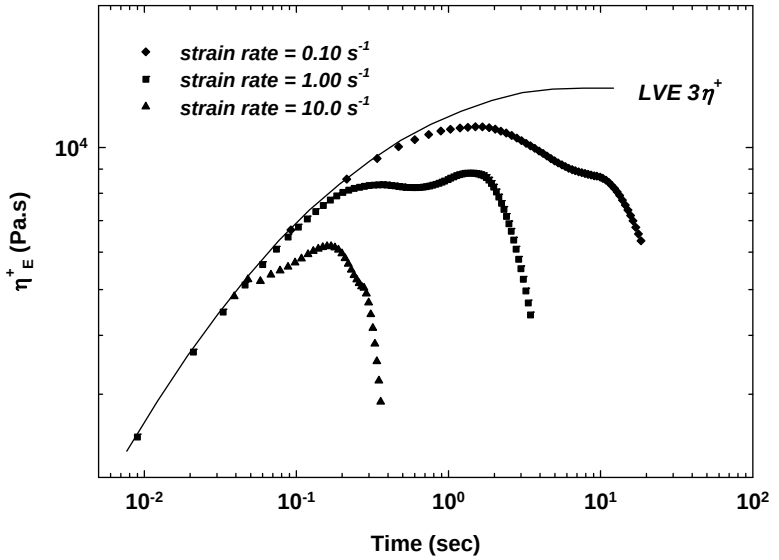

Figure 2.6. *A typical steady uniaxial shear experiment that shows the tensile stress growth coefficient as a function of time for several Hencky strain rates.*

2.3.2 Rheometers

Rheometer is the apparatus for measuring rheological properties. In the following sections the main rheometers and fixtures which have been used in this study are introduced.

2.3.2.1 Parallel Disks

Parallel disks are the most extensively used rheological fixture to produce simple shear (*Couette flo*w). It has two parallel concentric disks with specific diameter and distance (gap) between them. One disk can rotate with respect to the other (see Fig 2.7). In this fixture many types of experiments can be performed including the oscillation test (section 2.3.1.1) to generate the viscoelastic moduli of molten polymers plotted in Fig 2.3. Another advantage of this fixture is that only a small amount of material is needed. On the other hand it has some disadvantages such as the inability to reach high shear rates and strains (due to edge fracture of the sample and presence of secondary flows) and non-uniform strain (strain has a radial profile from zero at centre toward maximum at edges) [30]. In this fixture, the angular rotation is imposed and the torque is measured.

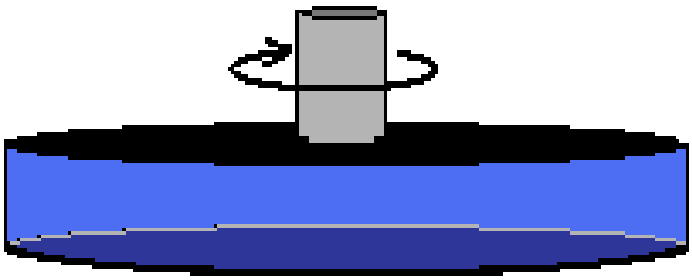

Figure 2.7. *Schematic illustration of parallel plates fixture.*

2.3.2.2 Extensional Rheometer (SER)

The Sentmanat Extensional Rheometer (SER) [10] is a suitable and easy-to-use fixture that can be used together with a rotational rheometer to generate uniaxial extensional data [31-33]. This rheometer consists of two drums (see Fig 2.8) where the main drum rotates by the host rheometer shaft and the slave drum counter-rotates due to the existence of intermeshing gears that connects the two drums. The sample could be either in a strip shape [34] or in a cylindrical shape [35]. The sample is held firmly in position by means of two clips. As a result the sample undergoes a uniform uniaxial stretching (extension). The possibility of using small amount of sample which results in better and faster controlling the temperature is one the most important advantages of this fixture. Moreover, contrary to other previous designed fixtures for uniaxial extension measurements, the imposed strain is not finite here. However, sagging is always a source of error which can be avoided by doing experiment as fast as possible. Another method is using an oil bath to immerse the sample in order to avoid sagging due to buoyancy forces.

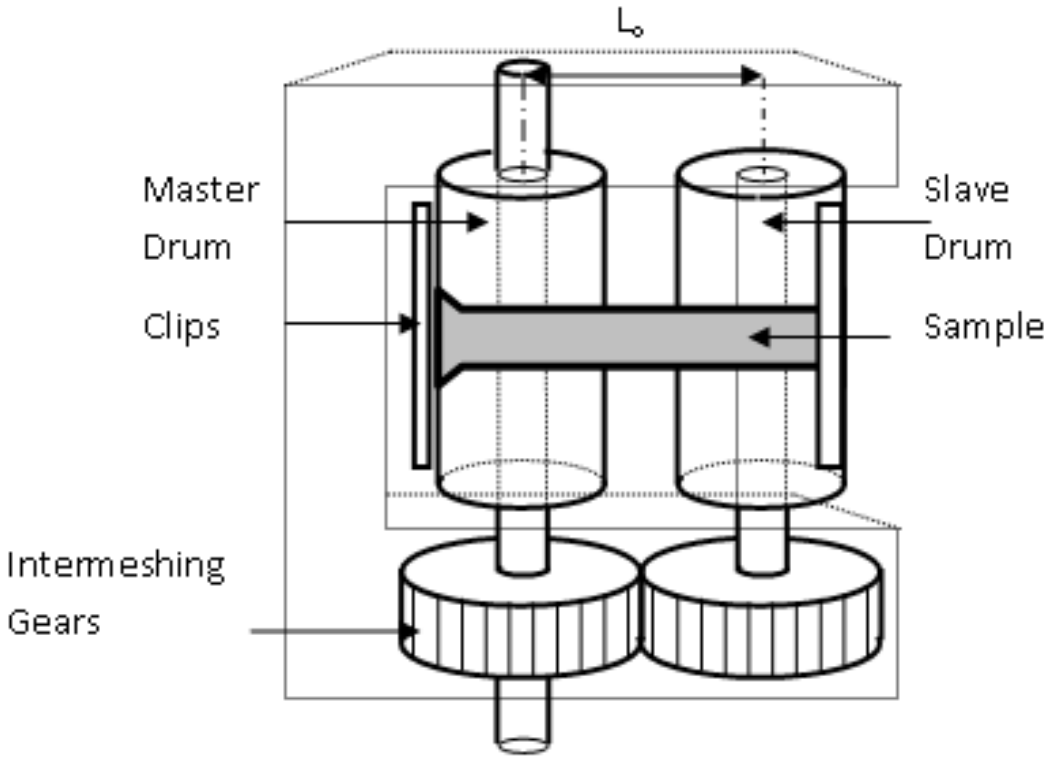

Figure 2.8. *Schematic of the Sentmanat Extensional Rheometer (SER).*

2.3.2.3 Capillary Rheometer

Capillary is one of the most industrially used instruments for measuring the *viscosity* of polymer melts. As shown in Fig 2.9, it consists of a reservoir (barrel) that contains initially the polymer melt and a piston which forces the material through the die which is located at the end of the barrel. The raw data from this device are the force needed to move the piston (pressure) and piston velocity (melt flow rate). Using the pressure and the velocity of the piston one may calculate the apparent shear stress and the apparent shear rate from the following equations:

$$\dot{\gamma}_A = 4Q/\pi R^3 \tag{2.6.a}$$

$$\sigma_A = R\Delta p/2L \tag{2.6.b}$$

Where Q, Δp, R and L are volumetric flow rate, applied pressure, die radius and die length respectively. These data are subject to two corrections.

One is the Rabinowitsch correction [9] that corrects the apparent shear rate to the true shear rate. The following equation is used for this purpose.

$$\dot{\gamma} = \frac{3n+1}{4n}\dot{\gamma}_A \tag{2.7}$$

Where "n" is viscosity shear thinning exponent defined as $n = d\log\tau_w / d\log\dot{\gamma}_A$.

The pressure should also be corrected for the extra pressure needed by the melt to flow from the reservoir into the capillary die (change of cross section). This is known as the Bagley correction. It can be calculated by plotting the pressure versus die length-to-diameter ratios (L/D) at fixed apparent shear rates. Then extrapolating the straight lines to zero L/D the excess pressure Δp_{end} can be calculated (see Fig 2.10). The true shear stress at the capillary wall can be calculated from (see Dealy and Wissbrun [9] for more details):

$$\sigma_w = \frac{\Delta p - \Delta p_{end}}{2(L/R)} \tag{2.8}$$

Finally slip at the wall can complicate the experimental data further and there are several studies and methods that can be used to analyze capillary data under slip [3, 8, 15, 36-38].

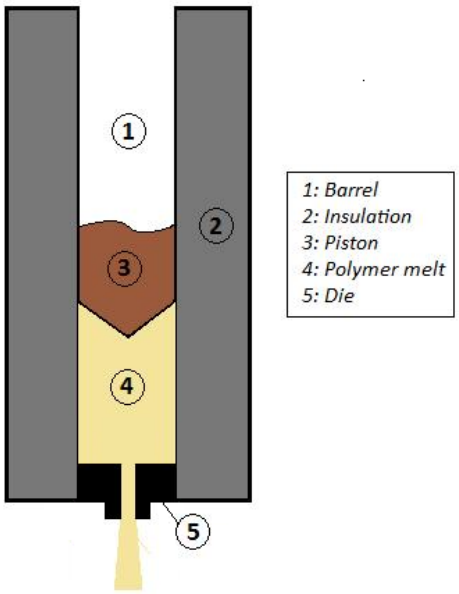

Figure 2.9. *Schematic diagram of a capillary viscometer.*

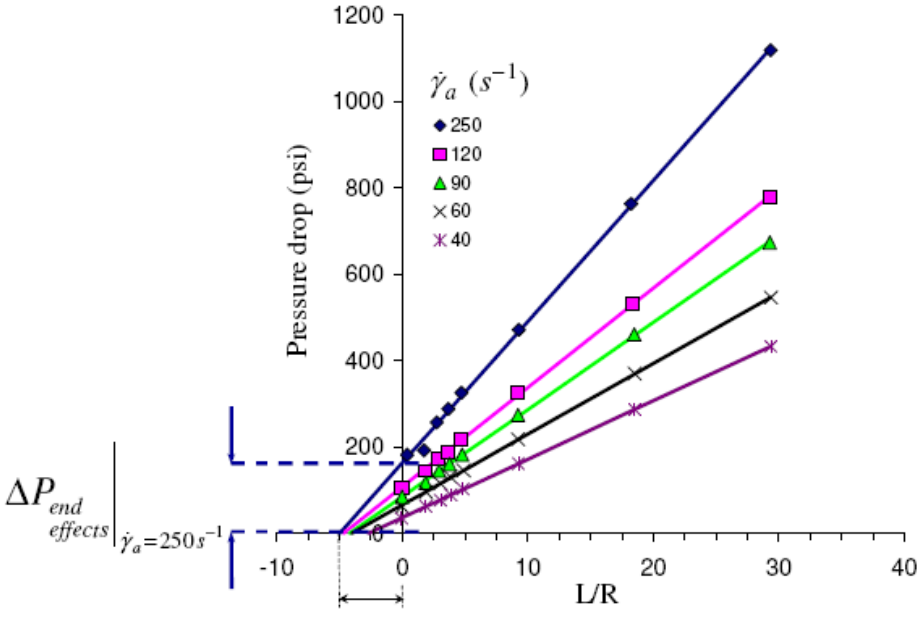

Figure 2.10. *Typical Bagley correction for capillary data. Each line corresponds to a shear rate.*

2.3.3 Zero Shear Viscosity and Molecular Characteristics

The melt rheology of entangled polymers is strongly influenced by M_w, its distribution and the level of long-chain branching [9, 39-42]. In particular, increase of polydispersity increases the level of shear thinning [42], while it has been reported that it has no influence on the zero shear viscosity, although some reports are contradictory. For example, Wasserman and Graessley [43], Garcia-Franco and Mead [44] and Kazatchkov et al [45] have reported that the zero shear viscosity of linear polymers does depend on the breadth of molecular weight for Ziegler-Natta HDPEs and LLDPEs with polydispersity index (*PDI*) in the range of 3-12. A weak dependence of the zero shear viscosity of linear polymers has also been predicted by the molecular theory of Pattamaprom and Larson [46].

It has also been reported that at a given molecular weight, the zero shear viscosity of m-HDPE are higher compared to that of ZN-HDPE and this is possibly due to the presence of a small undetectable level of long-chain branching [47-49]. The zero shear viscosity of m-HDPEs has been found to depend on M_w with an exponent of greater than 4, compared to the accepted value of 3.6 reported for ZN-HDPEs [50-52]. It is believe that for the case of broad molecular weight distribution HDPEs, the role on high M_w chains in the relaxation process is significant and therefore, the effect of z-moment of polydispersity should be considered [53].

2.4 Melt Fracture

Industrial polymer processing includes many different types of shaping processes including extrusion, injection molding, film blowing, fiber spinning and many others. From the economical point of view, it is desired to increase the rate of production without sacrificing product quality; however the rate of production is frequently limited by flow instabilities that lead to commercially unacceptable final products due to surface defects. These instabilities are collectively known as *melt fracture* [3, 54]. They are more specifically categorized into sharkskin or surface melt fracture, stick-slip or oscillating melt fracture and gross melt fracture. Typical images for each are presented in Fig 2.11.

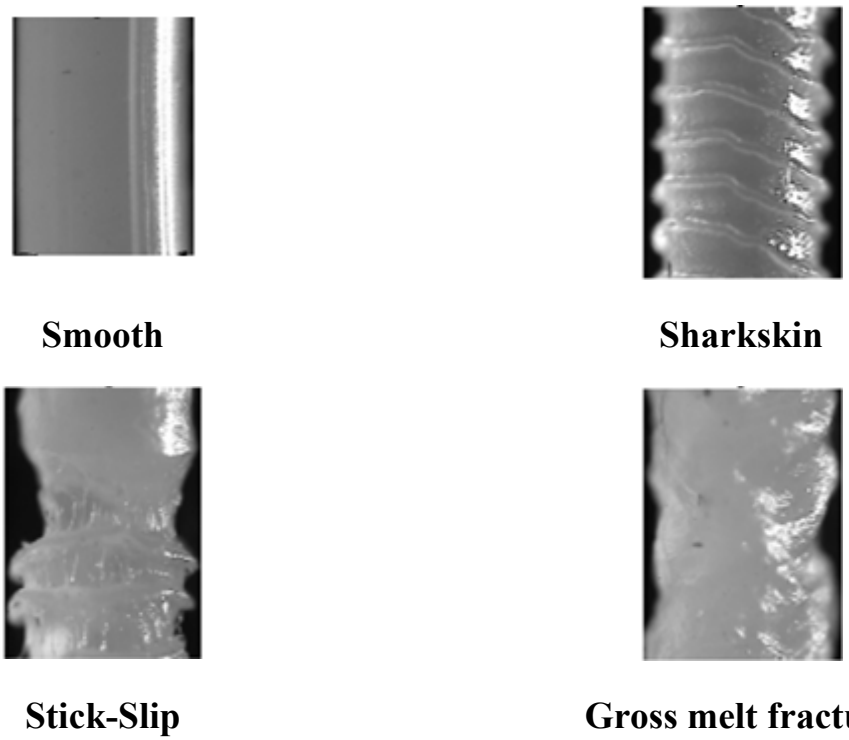

Figure 2.11. *Typical extrudate surface defects.*

2.4.1 Sharkskin Melt Fracture

2.4.1.1 Overview

Sharkskin is commonly the first observed instability that occurs during polymer processing (particularly linear polymers) at relatively low shear rates. This phenomenon manifests itself by small amplitude periodic irregularities on the surface of extrudates i.e. size are typically of about less than one-tenth of extrudate diameter [55].

It is believed that the first report on sharkskin observation is the experiments of Garvey and his co-workers in 1942 [56] on the extrusion of synthetic rubber compound. There are several thorough reviews available in the literature on the sharkskin phenomenon [57-59].

In the following section, a review of the sharkskin phenomenon is presented to outline the critical parameters that play a role on its origin and manifestations.

2.4.1.2 Mechanisms

Two different mechanisms have been proposed to explain the mechanism of occurrence of sharkskin.

The first mechanism which is known as exit stick-slip was firstly proposed by Vinogradov [60]. According to this, the stress at die exit (die lips) is greater compared to that of the die walls. Therefore, by increasing progressively the throughput, at a certain point the stress at the exit region reaches a critical value that promotes slip at the wall [3]. In this case, the melt starts to slip at the exit region of the die to relieve the extra stress. Taking into account that slip leads to less deformation and this decreases die swell [61], the die swell under slip is less than that under no-slip; thus the valleys in sharkskin defect are formed. Therefore according to this mechanism, sharkskin is due to a periodic slip boundary condition at the exit to the die. The experimental evidence that supports this mechanism is not convincing and the communication between Cogswell and Wang [62] discusses this.

The second mechanism for sharkskin which is the most accepted one has been proposed by Cogswell [63] and further explained by Migler et al [64]. This mechanism focuses on the fact that the velocity profile of polymer melt undergoes a sudden change from a parabolic shape inside the die region to an almost plug profile as it emerges from the die. This sudden change causes a stretching on extrudate that leads to surface rupture and thus surface melt fracture appears.

2.4.1.3 Effect of Die Geometry

Many groups have investigated the effects of capillary die dimensions on sharkskin [55, 65-68]. Experimental results show that at a fixed capillary length, the critical shear rate for the onset of sharkskin times the die diameter is a constant [69] while the severity of this instability (amplitude of distortions) increases linearly with the die diameter [65]. It has also been reported that at a fixed die diameter, the severity of sharkskin decreases with increase of the die length for sufficiently long dies (L/D>10 to achieve fully developed flow) [66]. The entrance angle has no significant effect on sharkskin [66].

The type of die (capillary versus slit versus annular) has been reported to have a significant effect for the onset of sharkskin. The results show that the critical stress for onset of sharkskin is higher in slit and annular dies compared to that for capillary dies [6, 70-72]. Such studies are extremely important from the industrial point of view as most of industrial processes such as pipe extrusion, blow molding and film blowing are performed with annular geometries rather than capillary ones. Therefore these studies can correlate results obtained in the laboratory with the industrial performance of the polymers.

2.4.1.4 Effect of Temperature

Considering the mechanism of sharkskin discussed above, it is clear that by increasing temperature, melt viscosity and other viscoelastic properties decrease and thus sharkskin would be postponed to higher shear rates. Therefore, one may expect that one way to eliminate sharkskin is to increase temperature. Although this is helpful to a certain extent, it has been shown that the critical stress is a weak function of temperature [60, 69, 73, 74]. Some studies also have shown that the die temperature (particularly at the exit) has a greater effect on sharkskin rather than the melt bulk temperature (barrel temperature) [75, 76]. Finally some experimental results have shown that there is a narrow window at the low temperature melt region in which smooth extrudate can be obtained [63, 77-80]. Crystallinity here is playing a significant role.

2.4.1.5 Effect of Molecular Structure

Regarding the molecular effects on sharkskin, it seems that by increasing the M_w, the critical stress for the onset of sharkskin decreases [74, 81-83]; while some other studies have shown a weak dependence on M_w [45, 84, 85]. Deeprasertkul et al [86] have reported that increase of M_w leads to more sever sharkskin; while it seems from their paper that there is no strong dependency on M_w. Moreover, it is clear that considering the power-law relation between zero shear viscosity and M_w (with a power index of 3.4), in all cases the critical shear rate for the onset of sharkskin is a decreasing function of the molecular weight.

The effect of MWD on critical shear stress for the onset of sharkskin is more complicated. It has been shown that with broadening the breadth of the MWD, the critical stress increases [87], or decreases [74] or is independent [69, 73, 88]. A possible reason for the existence of this complexity is that it becomes difficult to change the breadth of the MWD while keeping the M_w constant.

Kazatchkov et al [45] found that for a series of LLDPEs with constant M_w, the critical shear rate is an increasing function of molecular weight distribution. These authors have indicated that at a critical value of polydispersity index and above, sharkskin disappears completely. Fujiyama et al [84] found that the critical shear rate increases proportional to the square of M_z/M_w. Yamaguchi et al [89] have also shown that by increasing the molecular weight between entanglements (decreasing entanglement density), the critical stress decreases.

Allal et al [90] using an elastic theory provided a criterion for the onset of sharkskin based on a critical elongational stresses which depends on the plateau modulus, the M_w, the molecular weight between entanglements, M_e, and the polydispersity (will be discussed in chapter 6). Extending this study Allal and Vergnes [91] have proposed a molecular criterion for the occurrence and existence of sharkskin, including the parameters of the M_w and MWD and the entanglement characteristics. The theory was validated for data available for PS, PP and PE.

2.4.1.6 Effect of Processing Aid

In order to overcome sharkskin and to render the processes economically feasible, polymer processing aids (PPAs) are frequently used. PPAs can eliminate the flow instabilities known as sharkskin melt fracture and stick-slip or postpone them to higher flow rates. The end result is an increase of the productivity as well as an energy cost reduction, while high product quality is maintained. The additives mostly used for polyolefin extrusion processes are fluoropolymers [92-94]. Additional examples of other conventional processing aids such as stearates, silicon based polymers, hyperbranched polyethylenes and various polymer blend combinations have also been used. Finally Boron Nitride (BN) based PPAs have recently been proposed [95]. However, the most commercially relevant example is the use of fluoropolymer based PPAs to eliminate sharkskin melt fracture in linear polyethylenes.

Figure 2.12 shows the flow curve of a HDPE with and without fluoropolymer. It can be seen how typically a fluoropolymer acts in the extrusion of polyethylenes. As seen the addition of 1000ppm of fluoropolymers, significantly decreases the wall shear stress (due to significant slip) and postpones the onset of instabilities at significantly higher shear rates typically up to one order of magnitude (depending on the temperature and the type of polymer being extruded).

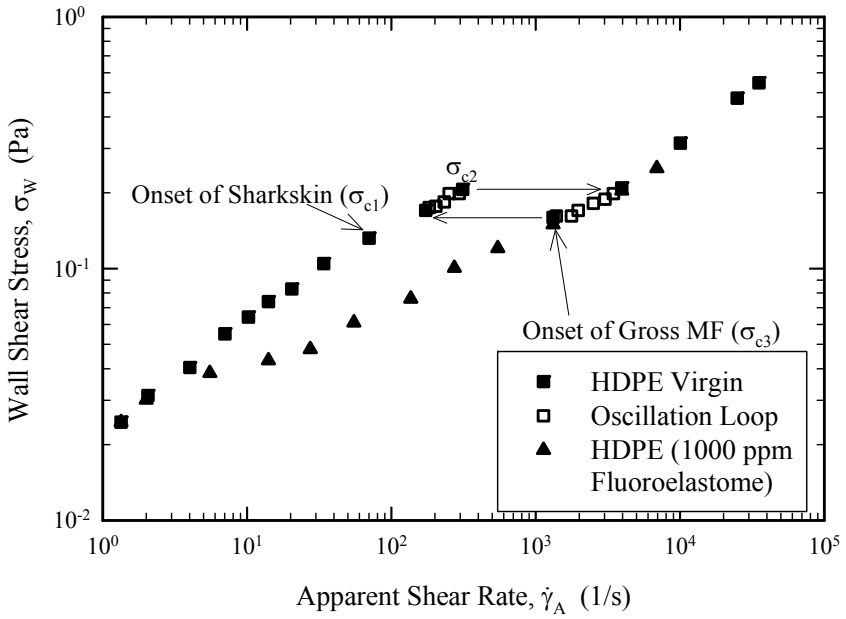

Figure 2.12. *The flow curve of a HDPE extruded in a pressure-driven capillary rheometer as virgin and in the presence of a fluoroelastomer (Adapted from reference [96]).*

2.4.2 Stick-Slip Melt Fracture

2.4.2.1 Overview

Extruding a polymer with linear molecular architecture such as LLDPE and HDPE, becomes unstable under certain flow conditions i.e. oscillations in pressure in spite of the face that the piston velocity is kept constant. This instability which is called stick-slip or oscillating melt fracture manifests itself by a discontinuity in the flow curve (Fig 2.12). The surface of the obtained extrudate exhibits a periodic appearance, namely alternating rough and smooth portions (Fig 2.11).

The works of Tordella [54] and Bagley et al [97] on the HDPEs are the first reports on this instability. However, more systematic studies on this subject have been done by Lupton and Regester [98] and Myerholtz [99]. Other terms rather than *stick-slip* and *oscillating melt fracture* have been used for this phenomenon such as *spurt flow* by Vinogradov et al [100, 101], *main flow instability* by Weill [102] and *cork flow* by El Kissi and Piau [103].

Stick-slip usually happens after sharkskin and before the gross melt fracture as flow rate increases. This discontinuity subdivides the flow curve into a low and a high flow rate branch. The important features of this instability are the critical shear stresses for these two branches (σ_{c2} and σ_{c3} in Fig. 2.12), the width of the discontinuity and the size and frequency of the pressure oscillations.

2.4.2.2 Mechanisms

The accepted mechanism for oscillating melt fracture consists of two major elements i.e. melt compressibility and melt slippage over the die solid wall. The melt compressibility compresses the material in the reservoir during the stick portion of the oscillation, which flows as extra when slip occurs. The main cause of slip is a sudden disentanglement of the bulk of the polymer from a monolayer of polymer molecules strongly adsorbed at the die wall. This leads to massive slip [62, 65, 104].

2.4.2.3 Effect of Die Geometry

Most of the previous studies have been done with capillary dies, although there are few works which reported that the critical shear stress for the onset of oscillation increases by switching from capillary to slit dies and the phenomenon totally vanishes in the case of annual dies [6, 70, 71].

The effect of L/D on the critical shear stress for the onset of stick-slip instability is not conclusive and depends on the experimental conditions and material under investigation. For the case of HDPE, it has been reported by different researchers [8, 99, 105, 106] that the upper critical stress, σ_{c2} (Fig 2.12) and also the discontinuity gap in the flow curve and the critical

stress difference (σ_{c2}- σ_{c3}) increases by increasing L/D, while the critical shear rate decreases. Vergnes et al [107] also reported a similar trend for EPDM. Wang and Drda [79, 108] for entangled linear polyethylenes and Ramamurthy [3] for LLDPE showed that σ_{c2} is almost independent of L/D. However, Kalika and Denn [109] observed that σ_{c2} reduces as L/D increased from 33.2 to 66.2 and 100.1. El Kissi and Piau [110] reported similar observation for PDMS.

For materials like HDPE [8, 15, 98] and LLDPE [3, 109] which exhibits stick-slip defect, the flow curve is subdivided into two branches as discussed above (Fig 2.12). In the low flow rate branch (before the discontinuity of stick-slip) the slip is weak due to adhesive failure of the interface. However at the high flow rate branch, it is massive and the velocity profile is almost plug flow. Lupton and Regester [98] reported that the slip velocities are 10 times higher in the high branch compared to that in the low flow rate branch. For data reported by Hatzikiriakos and Dealy [8] on HDPE, this ratio is even higher for some cases. The plug or nearly plug flow in the high flow rate branch have also been quantified for HDPEs [105, 111], LLDPEs [109] and EPDM [107].

2.4.2.4 Effect of Temperature

Previous studies with different polymers showed that temperature has a negligible effect on the critical stress for the onset of stick-slip, although the critical shear rate increases considerably [3, 63, 99, 100, 112]. For HDPE, it was observed that the high flow rate branch of the flow curve is almost insensitive to temperature, although the lower branch shifts to higher shear rates [8, 113].

Effect of temperature on the σ_{c2} is different for different polymers. For example it has been shown that for LLDPEs [3] and PDMS [110], that σ_{c2} is independent of temperature. Moreover, for the cases of PBs [100, 114], PIs [100] and fluoropolymer resins [12, 54] it is a weak increasing function, while for the HDPEs [8, 79] and ethylene–propylene copolymer [101] the dependency can be much stronger.

2.4.2.5 Effect of Molecular Structure

Reducing the M_w and broadening MWD leads to suppression of the stick-slip instability and the flow curve becomes a continuous one (with no discontinuity) for polymers with sufficiently low M_w and broad MWD. This has been verified for different polymers such as HDPEs [8, 99, 115, 116], LLDPEs [3], PBs [100, 112, 114, 117], PIs [100, 112, 118, 119], PDMS [110] and PSs [118, 119]. For the case of LLDPE different effects have also been reported i.e. σ_{c2} decreases with increasing M_w [120].

Broadening the MWD has the same effect as lowering the M_w [3, 99, 112, 114]. Experiments by Myerholtz [99] on HDPEs with different MWD showed that by broadening the MWD, the hysteresis loop in the flow curve becomes smaller until completely vanishes for very broad MWD, producing a continuous flow curve. Similar observations has been reported by Vinogradov et al [112] for PBs. Wang et al [108, 114] reported that for monodisperse PB melts the σ_{c2} is independent of M_w, while for HDPE they found the following scaling $\sigma_{c2} \propto M_w^{-0.5}$. This scaling is also valid for the data of Hatzikiriakos and Dealy [8] on HDPEs.

2.4.3 Gross Melt Fracture

2.4.3.1 Overview

Gross melt fracture (gmf) occurs at sufficiently high shear rates regardless of the type of polymer. In this phenomenon, the extrudate exits the die in an irregular manner and exhibits severe distortions. These instabilities happen in the order of extrudate volume, and therefore sometimes gmf is referred to as *volume melt fracture* in order to be distinguished from sharkskin or *surface melt fracture* [3, 69, 121]. The cross section of extrudate is also not constant within its length. As it is mentioned before, the main difference between the previous discussed melt fracture instabilities (sharkskin and stick-slip) and gmf is that it can happen for all types of polymers. A thorough review in this subject has been done by Kim and Dealy [122].

2.4.3.2 Mechanisms

While the origin of sharkskin is located at the die exit, the gross melt fracture initiates at the die entry region [54, 59, 123-127]. In the entry area into the die, the polymer melt experiences a considerable amount of elongational stress in the direction of flow, near the flow centerline [128]. At sufficiently high flow rates, melt strands can no longer bear the elongational stress and break. At this point the streamlines become irregular and flow breaks into several layers where each layer moves with its own velocity causing the chaotic extrudate appearance of the melt as it exits the die.

2.4.3.3 Effect of Die Geometry

Since the origin of gmf is at the die entrance, the die diameter does not affect the phenomenon. However, capillary die can alter gmf in two ways. Firstly, the severity of extrudate distortion decreases with increasing of the die length. Due to larger length of the die the melt partially relaxes and perhaps partially restores its continuity inside the die. Secondly, by increasing the die length, the pressure in the die entrance region increases and therefore, at a given shear rate, flow is shifted toward the stick-slip flow region [129].

The die entrance angle has a more accountable effect on gmf. It has been shown [130] that reducing the entrance angle, causes gmf to be postponed to higher flow rates and it also reduces the severity of the extrusion distortion. This is due to lower tensile stress experienced by the melt when the entry angle decreases. Kim and Dealy [122] reported that this effect is only observable when the entrance angle is less than 90°.

2.4.3.4 Effect of Molecular Structure

Piau et al [131] found that the gmf is almost independent of die material. This supports the idea that gmf is mainly a function of polymer nature and therefore, the molecular structure of the polymer plays a significant role.

Available data on the effect of M_w on the critical shear stress for the onset of gmf showed that it has a decreasing effect, although the effect of MWD is confusing. Vlachopoulos et al [73, 82] for HDPE, PP and PS reported that σ_{c3} scales inversely with M_w, while MWD had practically no effect. Baik and Tzoganakis [74] reported the same trend for M_w on polypropylenes, although they also found that MWD cause a decrease on σ_{c3}. Data for HDPEs reported by Kim and Dealy [132] showed a completely different trend, i.e. σ_{c3} was independent of M_w, and varied linearly with MWD.

2.4.4 Wall Slip of Polymers

2.4.4.1 Overview

Unlike Newtonian fluids, polymer melts slip over solid surfaces violating the classical no-slip boundary condition of fluid mechanics [3, 15, 133-136]. According to the slip theory developed by Brochard-Wyart and de Gennes [137], polymer melts slip no matter how small are the applied forces (shear stresses). This has been verified by direct slip measurements using optical techniques [138, 139]. From macroscopic slip measurements i.e. capillary extrusion, a critical shear stress for the onset of slip, σ_{c1} is frequently defined for practical reasons depending on the work of adhesion of the interfaces involved [4, 136, 140-143].

2.4.4.2 Mechanisms

Two are the main mechanisms of slip, namely direct desorption of molecules from the interface and disentanglement of molecules from a monolayer adsorbed on the interface. The first slip mechanism accounts for relatively small deviations from the no-slip boundary condition, and it has been observed at relatively small values of the wall shear stress. In this region, the mechanism of slip is direct detachment/desorption of a few chains from the wall that leads to measurable slip velocities even from macroscopic rheological measurements [140, 141, 144].

At a second critical wall shear stress value, σ_{c2} a transition from weak to strong slip has been observed and this causes the discontinuity in the flow curve discussed above in Fig 2.12 [3, 8, 79, 108, 145, 146]. The velocity profile in this slip regime approaches that of plug flow. The

mechanism of slip in this regime is sudden disentanglement of the polymer chains in the bulk from those in a monolayer of polymer chains adsorbed at the wall [91, 124, 147].

The transition from weak to strong slip has been observed in the capillary flow of linear molten polyethylenes [3, 109]. This transition is mainly a characteristic of linear polymers typically with relatively narrow molecular weight distribution, including linear polyethylenes such as high density (HDPEs) and linear low density polyethylenes (LLDPEs) [3, 147], polyisoprenes (PIs) [112, 148], polybutadienes (PBs) [149], fluoropolymers [12], polydimethylsiloxanes (PDMSs) [110, 150] and lately polycaprolactones (PCLs) [151]. As a result, the flow curve of such polymers is a discontinuous one, consisted of two branches, namely a low flow-rate branch (weak slip) and a high flow-rate branch (strong slip) as discussed above in the context of Fig 2.12. On the other hand, linear polymers (high-density polyethylenes) of significantly wide molecular weight distribution do not exhibit this transition [99].

2.4.4.3 Effect of Molecular Characteristics

Several studies have attempted to quantify the slip velocity as a function of wall shear stress, wall normal stress, and temperature [3, 15, 98, 133, 135, 152]. However, very few studies have attempted to address the dependence of slip velocity on molecular weight characteristics, such as molecular weight (M_w) and polydispersity index ($PI \equiv M_w/M_n$). Mhetar and Archer [153, 154] and Park et al [149], for the case of nearly monodisperse polybutadiens, Awati et al [155] and Mackay and Henson [156] for nearly monodisperse polystyrenes and Othman et al [157] for narrow molecular weight distribution polylactides (PLAs) (polydispersity less than 2) have shown that the slip velocity increases with decrease of molecular weight. Considering the convective constraint release mechanism for bulk and tethered chains, Joshi et al [158] proposed some scaling relationships which are in agreement with these experimental observations. Hatzikiriakos and Dealy [15] studied the slip velocity of a series of polydisperse HDPEs (polydispersity index in the range from 3.2 to 9.4) and scaled their slip velocity data with a critical shear stress for the onset of slip, σ_{c1} (determined from the macroscopic dependence of the flow curve on capillary diameter) and polydispersity to produce a master slip curve which was a decreasing function of polydispersity.

As stressed by Brochard-Wyart and de Gennes [137] polymers slip no matter how small are the applied forces and therefore the critical shear stress, σ_{c1}, cannot be easily defined. However, σ_{c1} is simply a convenient parameter which can be defined from macroscopic rheological experiments, where the flow curves start exhibiting a diameter dependency. Alternative interpretation of the data reported by Hatzikiriakos and Dealy [15] is discussed below and it shown that the slip velocity of the HDPEs studied by Hatzikiriakos and Dealy [15] increases with decrease of molecular weight and with increase of polydispersity.

3 THESIS OBJECTIVES AND ORGANIZATION

3.1 Thesis Objectives

The main of objective of this study is to understand the rheology and processing (melt fracture phenomena) of two series of broad molecular weight distribution Ziegler-Natta (ZN) and metallocene HDPEs as functions of molecular parameters such as MW and MWD. In other words to understand the critical parameters that play a role in the melt fracture phenomena of wide molecular weight distribution HDPEs and correlate them with molecular parameters and rheological properties.

The particular and detailed objectives of this project are listed below:

1- Study the shear and extensional rheology of two series of metallocene and ZN HDPEs with a relatively broad molecular weight distribution over a wide range of temperatures using a parallel plate and an extensional rheometer. This includes the effects of molecular weight and molecular weight distribution on the rheological properties such as zero shear viscosity, steady-state compliance and crossover frequency.

2- Study the processing behaviour of the HDPE resins over a wide range of temperatures by using a capillary rheometer and a variety of capillary, slit and annular dies. In other words the objective is to assess the effects of die geometry (including die diameter, length-to-diameter ration and entrance angle) on the critical parameters for the onset of sharkskin melt fracture.

3- Identify theoretical and phenomenological relationships which relate the rheological parameters such as zero shear viscosity and steady-state creep compliance to M_w and MWD. These relationships can be extended to relate critical conditions for the onset of the flow instabilities (mainly surface melt fracture or sharkskin) with measures of M_w and its distribution.

4- Identify the critical parameters (essentially rheological) that play a role in the processing of these polymers as this can be assessed by their melt fracture performance. The question here is how to explain the large differences in the processability of the ZN-HDPEs and m-HDPEs, although their rheological properties are not much different.

5- Study the effect of molecular weight and its distribution on the slip of the available resins in order to shed light on the role of slip on the melt fracture behaviour. Moreover, it is an objective to develop a criterion based on molecular characteristics for the occurrence of stick-slip melt fracture.

3.2 Thesis Organization

The organization of this dissertation is as follows. A brief introduction to the problem of interest is presented in chapter 1. This is followed by introducing the different types of polyethylenes and their molecular characterization in chapter 2. This chapter also presents a literature review on the subject including different rheological experiments and rheological instruments used to carry out the experimental work. Moreover, previous reports on the rheology of HDPEs their slip and melt fracture behavior are also reviewed chapter 3 presents the objectives and the organization of the thesis. In chapter 4, the materials and methods used in this research are discussed. In chapter 5, the linear viscoelastic properties as well as extensional rheology of all the resins are presented. The effects of molecular characteristics on the rheological parameters are discussed (Objective 1). Chapter 6 provides all the results on the melt fracture properties of these resins considering the effect of molecular characteristics and processing conditions (Objective 2). The effects of M_w and MWD on the critical conditions for the onset of melt fracture (Objective 3) along with their proposed correlations with rheological parameters (Objective 4) are discussed. Chapter 7 reports the slip velocities and its dependency on M_w and MWD (Objective 5). This chapter also includes a discussion on the slip mechanisms in order to develop a molecular based criterion for the onset of stick-slip melt fracture. Finally, chapter 8 summarizes the important conclusions from the results of this research and provides recommendations for future work.

4 MATERIALS AND METHODOLOGY

4.1 Materials

Two groups of high density polyethylenes (HDPEs) are studied, namely a group of Ziegler-Natta referred to as ZN-HDPEs and a second group of metallocene referred to as m-HDPEs, all provided by Chevron Phillips Chemical Company LP. A characteristic difference of these polymers with those used in other studies [47, 48] is that they all possess a much wider molecular weight distribution. Table 4.1 lists all resins used in the present study along with various measures of their molecular weights. These values are carefully measured using high temperature GPC by Chevron Phillips Chemical Company LP. As can be seen, the polydispersity index, *PDI*, varies from 11 to 17 and 12-42 for the ZN-HDPEs and m-HDPEs, respectively. Among the m-HDPEs, the last two ones (m-HDPE-13 and m-HDPE-19) have PDI values in the range of the ZN-HDPEs (10-15), while the polydispersity of the rest of m-HDPEs are well above these, typically greater than 19. In addition, for many m-HDPEs the number average molecular weight (M_n) changes while weight average molecular weight (M_w) is approximately the same. This enables us to study the effects of molecular characteristics of these samples in a more systematic way.

4.2 Methodology

4.2.1 Linear Viscoelasticity

The linear viscoelastic properties of all resins have been studied using the Anton Paar MCR501, a stress/strain-controlled rheometer. Two types of tests have been performed; small amplitude oscillatory shear (SAOS) and creep tests. Both types of experiments have been performed with the 25mm parallel disk geometry and a gap of about 1 mm. For this type of experiment, the reproducibility is within ±3%. To avoid degradation particularly for the case of creep tests, all experiments have been run under nitrogen environment. The frequency sweep tests were carried out at temperatures ranging from 150°C to 230°C, over 20^{o}C increments. The various curves were shifted by means of applying the time-temperature superposition (TTS) in order to generate the master curves at the reference temperature of T_{ref}=190°C. All samples were found to be

thermorheologically simple as they obeyed the time-temperature superposition (TTS) principle. The resulted master curves did not contain the terminal zone at low frequencies for many polymers and thus the zero shear viscosity could not be inferred with certainty solely from these data. One way to extend the data to even lower frequencies is using a stress relaxation (step strain) experiment run for long time. Then the stress relaxation data were used to calculate the relaxation moduli using the Boltzmann superposition principle [9]. This procedure has been applied for all polymers and found that the generated data agreed well with G', G" from SAOS, while resulted the zero shear viscosities in many cases. Furthermore, creep experiments have been performed with stress level of 10 Pa as another means of determining the zero-shear viscosities. The zero-shear viscosity values were found to be in agreement with those generated by stress relaxation.

Table 4.1. *List of HDPEs used in this study and their different moments of molecular weights.*

Resin	M_n (Kg/mole)	M_w (Kg/mole)	PDI=M_w/M_n	M_z (Kg/mole)	M_z/M_w
ZN-HDPE-0	23.0	328.4	14.3	1541.0	4.7
ZN-HDPE-5	18.7	328.7	17.6	1500.7	4.6
ZN-HDPE-6	26.8	296.2	11.1	1244.3	4.2
ZN-HDPE-10	29.6	320.3	10.8	1443.4	4.5
ZN-HDPE-11	26.6	290.4	10.9	1372.3	4.7
ZN-HDPE-12	22.8	291.0	12.8	1588.8	5.5
ZN-HDPE-13	21.8	270.4	12.4	1449.9	5.4
ZN-HDPE-14	21.7	259.6	12.0	1477.2	5.7
ZN-HDPE-15	18.0	228.3	12.7	1319.8	5.8
ZN-HDPE-16	16.0	193.3	12.1	1277.5	6.6
m-HDPE-1	5.3	222.5	42.0	876.7	3.9
m-HDPE-8	10.8	272.4	25.2	972.5	3.6
m-HDPE-9	12.8	269.9	21.1	1081.0	4.0
m-HDPE-10	12.5	266.2	21.3	1049.0	3.9
m-HDPE-11	13.0	248.5	19.1	1041.0	4.3
m-HDPE-12	11.6	229.8	19.8	1048.0	4.6
m-HDPE-13	14.5	210.5	14.5	678.9	3.2
m-HDPE-19	18.1	212.7	11.8	579.9	2.7

4.2.2 Extensional Rheology

Their extensional behaviour in simple uniaxial extension has been studied using the second generation Sentmanat Extensional Rheometer (SER2) housed in the Anton Paar MCR501 rotational rheometer. More information regarding this fixture can be found elsewhere [10, 31, 32]. The tests were conducted at T=150°C, over a wide range of Hencky strain rates, namely 0.01, 0.1, 1.0, 10.0 and 20.0 s^{-1}. Rectangular samples with 6-8 mm width and thickness of 0.5–0.7 mm were used. It should be noted that due to their high viscosities, the samples have shown no sign of sagging. The reproducibility of this experiment is within ±10%.

4.2.3 Processing Study

The processing behaviour was characterized by using an Instron constant speed capillary rheometer fitted with several capillary dies of various lengths, diameters and entrance angles. For example, to determine the slip behaviour of the polymers, capillary experiments were performed using dies having the same length-to-diameter (L/D) ratio and different diameters [8]. Furthermore, determination of Bagley correction required the use of capillary dies having the same diameter and different length-to-diameter (L/D) ratios [9]. Slit and annular dies were also used in this study in order to examine the effects of die geometry type on the processability of polymers. Table 4.2 summarizes the dies used in this study along with their characteristic dimensions. It is worthwhile to mention that the barrel of the capillary rheometer used has four individual heating zones from barrel to the die land in order to keep temperature uniform along the barrel. The reproducibility of this experiment is within ±10%.

Table 4.2. *Characteristic dimensions of capillary, slit and annular dies used in this study.*

Capillary die	**D (mm)**		**L/D**	**2α**
	0.51		20	15^o, 30^o, 45^o, 60^o & 90^o
	0.79		5, 16, 32	180^o
	0.79, 1.22, 2.11		16	180^o
Slit die	**H (mm)**	**L (mm)**	**W (mm)**	**L/H**
	0.47	20.68	2.54	44
Annular die	**D_o (mm)**	**D_i (mm)**	**D_i/D_o**	**$L/(D_o-D_i)$**
	2.54	1.54	0.61	10

5 RHEOLOGY OF HDPEs

In this chapter, the rheological properties of ZN-HDPEs and m-HDPEs are presented. As all these resins have relatively large molecular weights and broad molecular weight distributions, it is interesting to study the effects of molecular characteristics on their rheological parameters such as zero shear viscosity and steady state compliance.

5.1 Linear Viscoelasticity

Fig. 5.1 depicts the master curves of the dynamic moduli G' and G" and the complex viscosity for two representative samples of m-HDPE-8 and ZN-HDPE-6 at the reference temperature of 190°C (the viscoelastic moduli and complex viscosity of all the HDPEs studied in this work are plotted in Appendix A.1, Figs. A.1-A.16). As discussed in section 4.2.1, to reach the Newtonian regime in order to infer the zero shear viscosity, stress relaxation results were used along with creep tests. As seen the experimental data obtained from these three independent tests agree well.

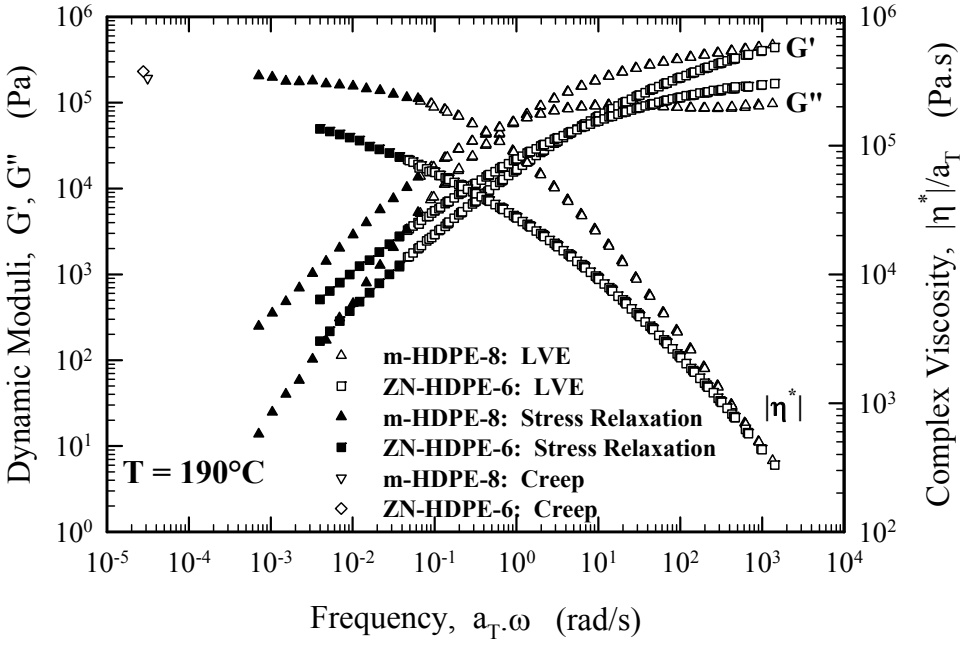

Figure 5.1. *Master curves of storage and loss moduli for a metallocene (m-HDPE-8) and Ziegler-Natta (ZN-HDPE-6) polyethylene resins at T_{ref} = 190°C. Data were obtained from frequency sweep linear viscoelastic measurements (LVE), stress relaxation and creep tests.*

From the linear viscoelastic moduli curves the crossover frequency, ω_c, can be defined as the frequency at which $G'(\omega_c) = G''(\omega_c) = G_c(\omega_c)$, where G_c is referred to as the crossover modulus. This parameter is important because it separates the viscous and elastic behaviour and it has been used in the past to relate it with various measures of the molecular weight distribution [48, 159]. It has been shown that this parameter is a decreasing function of polydispersity index [48]. This is due to increase of elastic modulus with polydispersity. Utracki and Schlund [159] found that the following equation holds for G_c and the polydispersity index $PDI \equiv M_w/M_n$ for a series of linear low-density polyethylenes (LLDPEs):

$$G_c(Pa) = 8.4 \times 10^5 (M_w/M_n)^{-1.385} \tag{5.1}$$

Vega et al [48] have compared this equation to their data for ZN and m-HDPEs. Fig. 5.2 depicts the experimental results obtained in the present work along with those of Vega et al [48] and Raju et al [50]. Eq. 5.1 proposed by Utracki and Schlund [159] is also plotted on Fig. 5.2 as a straight solid line. It is interesting to note that the data obtained in the present work for both m-HDPEs and ZN-HDPEs are in general agreement with those of Vega et al [48], pointing to the correct trend that G_c is a decreasing function of the polydispersity index, as Eq. 5.1 implies.

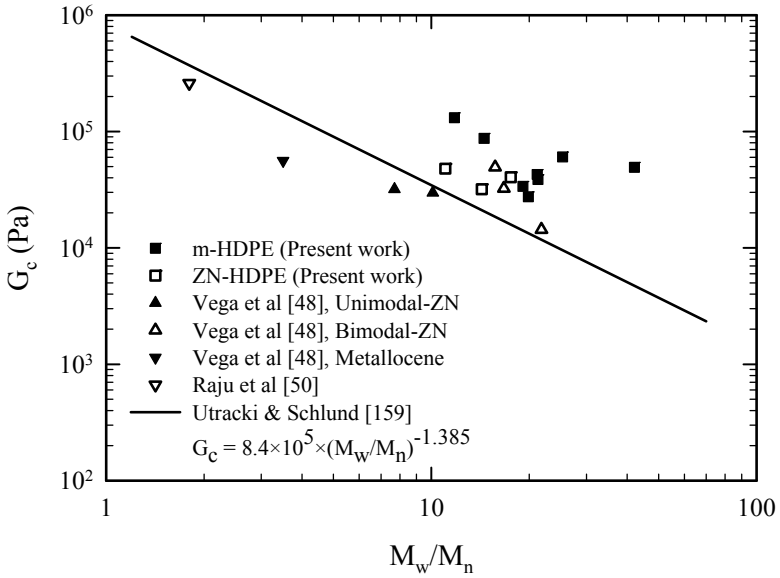

Figure 5.2. *The crossover modulus as a function of polydispersity index, M_w/M_n, at T=190°C for several sets of data for ZN and m-HDPEs. The solid line is Eq. 5.1 proposed by Utracki and Schlund [159].*

For broad molecular weight distribution resins, higher moments of the molecular weight distributions can correlate better with G_c. Fig. 5.3 plots the crossover modulus, G_c, as a function of M_z/M_w, where it is shown that a power law relationship (Eq. 5.2) fits well the data for the HDPEs studied in this work.

$$G_c(Pa) = 3.1 \times 10^6 (M_z/M_w)^{-3.1} \tag{5.2}$$

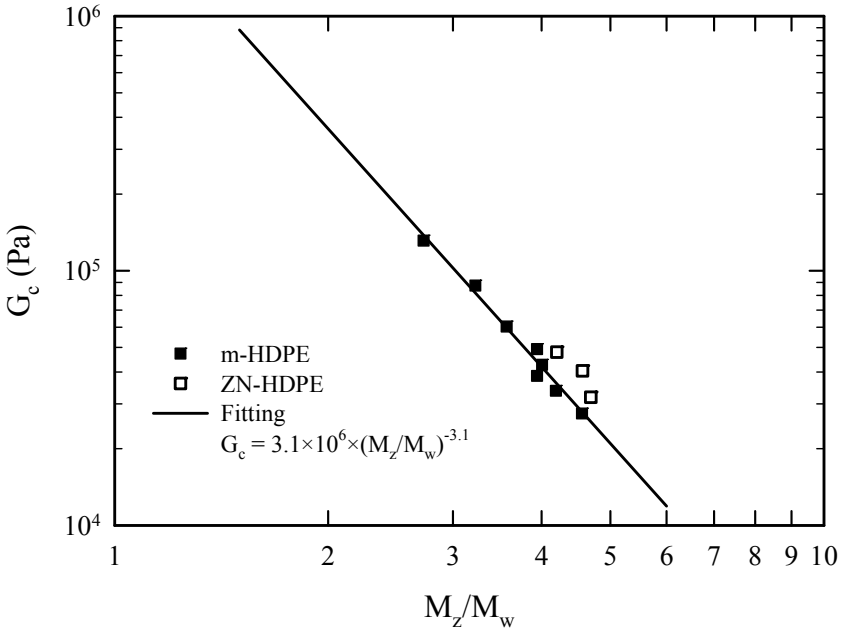

Figure 5.3. *The crossover modulus as a function of M_z/M_w for the HDPEs studied in the present work at T=190°C, showing the existence of a correlation represented by Eq. 5.2.*

5.2 Zero Shear Viscosity

Fig. 5.4 shows the complex viscosity of all resins at 190°C obtained from frequency sweep (LVE), stress relaxation and creep experiments as described above. For the sake of clarity each curve has been multiplied by a factor listed in Fig. 5.4. The Newtonian flow regime has been reached in most cases with a few exceptions particularly for the high M_w resins. For these cases creep tests were run to determine these values which are also plotted in Fig. 5.4. In addition, the data were fitted with the Carreau-Yasuda model Eq. 5.3 to obtain the zero-shear viscosity as a model parameter.

$$\eta(\dot{\gamma}) = \eta_0[1 + (\lambda\dot{\gamma})^a]^{(n-1)/a} \tag{5.3}$$

The values obtained by this method were in agreement with those obtained independently from the combined frequency sweep, stress relaxation and creep data. The determined parameters of the Carreau-Yasuda model for best fit to the experimental data are listed in Table 5.1 and model fits are plotted in Fig. 5.4 as continuous lines. As confirmed by Stadler et al [160], the Carreau-Yasuda model works well for representing the viscosity curve of linear polydisperse HDPEs (similar to our materials). Table 5.1 lists the values of zero-shear viscosity at 150°C and 190°C, the steady state creep compliance, J_e^0 and the energy of activation for all samples obtained from applying the TTS principle (see Appendix A.2 for the list of shift factors).

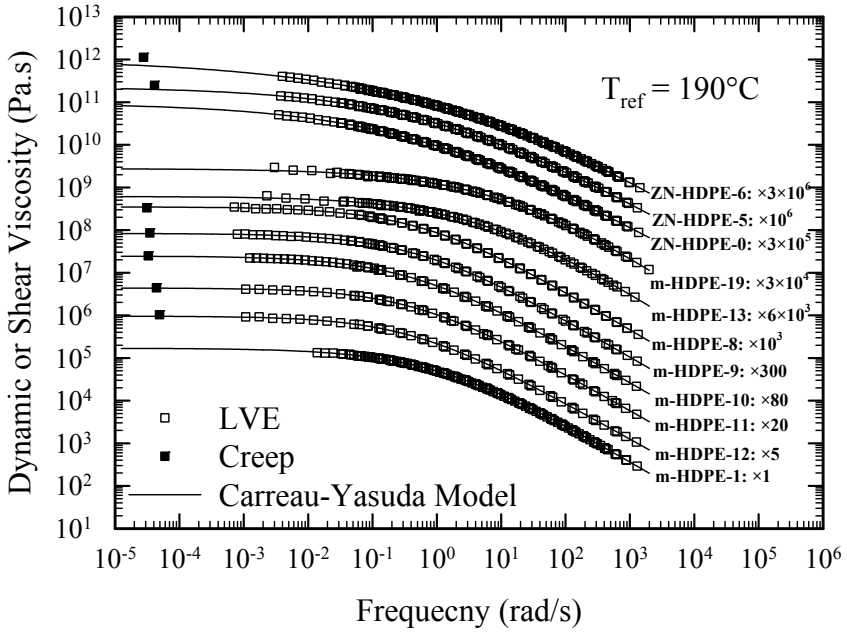

Figure 5.4. *The complex viscosity material function of all resins obtained from frequency sweep (LVE), stress relaxation and creep tests at the reference temperature of T_{ref}=190°C.*

The dependence of the zero shear viscosity, η_0, on M_w has gained a great interest in literature, because it could be used as an evidence of LCB and broadness of the MWD [42, 160, 161]. It is generally accepted that η_0 depends on the M_w according to Eq. 5.4, with an exponent α equal to 1 for M_w below the critical molecular weight for entanglements, M_c, and with an exponent of α equal to about 3.4 for M_w above M_c.

$$\eta_0 = KM_w^{\alpha} \tag{5.4}$$

Wood-Adams et al [52] reported a value of $K = 6.8 \times 10^{-15}$ and an exponent $\alpha = 3.6$ at 150°C for a series of linear polyethylenes (LLDPs). Stadler et al [161] found a higher coefficient for *K* for linear HDPEs, that is $K = 9 \times 10^{-15}$ with an exponent $\alpha = 3.6$ at 150°C. The same exponent of 3.6 has also been reported by Wasserman and Graessley [43] and Raju et al [50] and therefore it is the accepted universal exponent in the literature for linear polyethylenes.

Fig. 5.5 summarizes these findings in the literature along with the data of the present work. It can be seen that the zero shear viscosities, η_0, of m-HDPEs in the present work are higher than those reported by Wood-Adams et al [52] and Stadler et al [161], which is typically found for metallocene HDPEs [48, 49]. The power exponent of our correlated data shows an exponent of 4.5 as in Fig. 5.5. This is an indication of either of the presence of a small amount of Long Chain Branching (LCB) or an effect of the high polydispersity or a combination of both. To investigate this further, the energy of activation E_a determined from the application of the TTS principle is a useful quantity (all listed in Table 5.1).

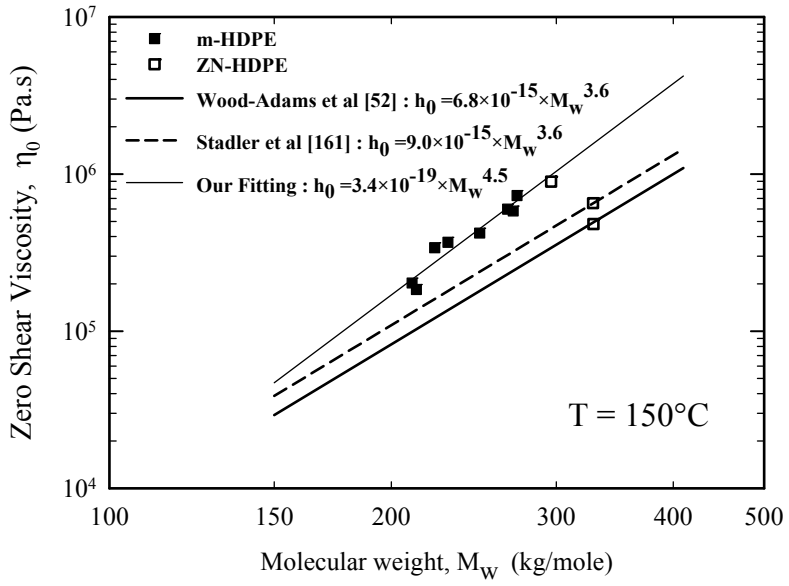

Figure 5.5. *The zero shear viscosity dependency to molecular weight at T=150°C.*

First, the application of (TTS) to obtain the master curves did not require the application of vertical shift, which is frequently required for highly branched polymers [41, 162]. High values of the activation energy E_a imply the presence of LCB or polydispersity [41]. The values determined in the presence work were higher than 7 kcal/mol for ZN-HDPEs, and in the range of 5.5-7 kcal/mol for the m-HDPEs. Values for E_a for narrow molecular weight HDPEs in the absence of LCB are expected to be in the range of 5-5.5 kcal/mol [51, 125, 163]. Vega et al [48] reported values between 5-5.5 kcal/mol for conventional bimodal PEs, which were explained to be due to low molecular weight tails and not to LCB. Furthermore, their reported values of E_a for m-HDPEs were in the range of 7-9 kcal/mol which were possibly attributed to the presence of low levels of LCB [49]. In our case the E_a values for the m-HDPEs are lower and possibly not due to LCB. Hatzikiriakos [41] found a correlation of polydispersity with E_a for a series of LLDPEs and reported values between 6-8.5 Kcal/mol. Therefore, in the present case the relatively high values of E_a seem to be due more to the broadness of the MWD and less to the presence of LCB. A similar comparison and discussion for the zero shear viscosity of various sets of data reported in the literature at 190°C follows.

The presence of long chain branching can be also verified by comparing the radius of gyration (R_g) of m-HDPEs detected by light scattering with a reference for linear polymers. Fig. 5.6 shows such a comparison and gives a good agreement with the linear reference. It can be concluded that the m-HDPEs studied in this work do not possess any LCB.

Raju et al [50] studied a series of fractionated polydisperse linear HDPEs and reported an exponent of 3.6 and a proportionality constant of $K = 3.4 \times 10^{-15}$ for Eq. 5.4. However, Vega et al [48] reported a power exponent of 4.2 with $K = 2.3 \times 10^{-17}$ for nearly monodisperse metallocene HDPE of low levels of LCB. Fig. 5.7 depicts our data at T=190°C (Table 5.1) and the equations of Raju et al [50] for linear monodisperse HDPEs and that of Vega et al [48] for nearly monodisperse branched m-HDPEs. Our data lie between these two sets indicating that levels of LCB (if present) are much less than those in the m-HDPEs studied by Vega et al [48] who reported that they were undetectable with analytical methods.

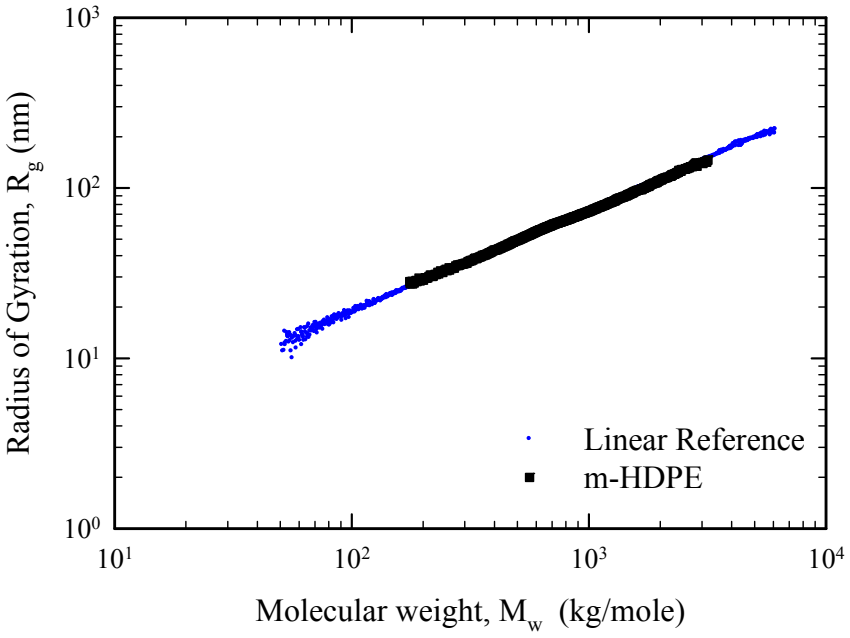

Figure 5.6. *The radius of gyration of metallocene HDPEs (filled squares) as a function of molecular weight together with a linear reference, verifying the absence of long chain branching in their structure.*

Table 5.1. *Rheological parameters of the materials.*

Resin	E_a	J_e^0 (T=170°C)	η_0 (T=150°C)	*Carreau-Yasuda Model Parameters* (T=190°C)			
	(kcal/mol)	*(1/Pa)*	*(Pa.s)*	η_0 *(Pa.s)*	λ (s)	*n*	*a*
ZN-HDPE-0	7.6		653639	314290	1.60	0.14	0.29
ZN-HDPE-5	7.5		480690	226620	0.82	0.11	0.30
ZN-HDPE-6	7.3		894972	348190	0.07	-0.12	0.20
m-HDPE-1	6.9		339908	168990	0.91	0.11	0.49
m-HDPE-8	6.9	1.11×10^{-5}	729620	350700	1.51	0.10	0.52
m-HDPE-9	7.0	1.62×10^{-5}	582082	278270	1.90	0.12	0.53
m-HDPE-10	5.5	1.90×10^{-5}	598497	307760	2.37	0.12	0.51
m-HDPE-11	6.0	2.33×10^{-5}	421544	218770	2.14	0.14	0.55
m-HDPE-12	5.7	2.67×10^{-5}	368463	191660	2.40	0.15	0.55
m-HDPE-13	6.3		202839	102760	0.18	0.02	0.42
m-HDPE-19	6.8		184135	91364	0.06	-0.05	0.39

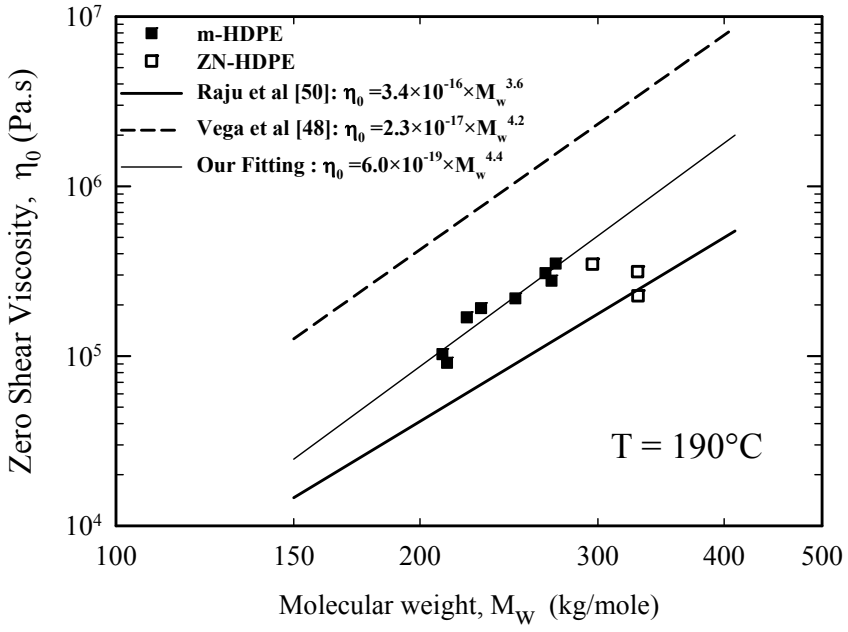

Figure 5.7. *The zero shear viscosity dependency on molecular weight at T=190°C.*

Wasserman and Graessley [43] have presented a more general correlation for the zero shear viscosity of linear polymers that allows the zero shear viscosity to be not only a function of M_w, but also a function of different measures of polydispersity. Their proposed correlation is:

$$\eta_0 = KM_w^{\alpha}(M_w/M_n)^a(M_z/M_w)^b \tag{5.5}$$

Previous studies on polyethylenes have revealed that for polyethylenes the coefficients "*a*" and "*b*" are 0 and 1 respectively [43, 44, 161]. Stadler et al [161] has shown that at T=150°C, Eq. 5.5 is valid with $K = 4.1 \times 10^{-15}$, $\alpha = 3.6$, a=0 and b=1. den Doelder [164] also has proposed exponent b as 0.9 using the double reptation single exponential model for the case of polydisperse polymers. These results are also consistent with modelling efforts by Nobile and Cocchini [165, 166] and Cocchini and Nobile [167]. Fig. 5.8 shows that by considering this modification (effect of polydispersity), our data fall on a straight line with a slope of 3.6 at both temperatures of 150°C and 190°C (accepted universal exponent for linear polymers) and agrees remarkably well with the correlation derived by Stadler et al [161] using their own experimental data. The fact that the new slope of the corrected data for polydispersity effects is 3.6, is perhaps an indirect indication of the absence of LCB from our m-HDPEs. It is noted that the range of

M_z/M_w covered by Stadler et al [161] was from 1.5 to 3.8, whereas in this case this is extended from 2.7 to 4.7 indicating that our resins have a much broader MWD and thus the effect of polydispersity might be more significant.

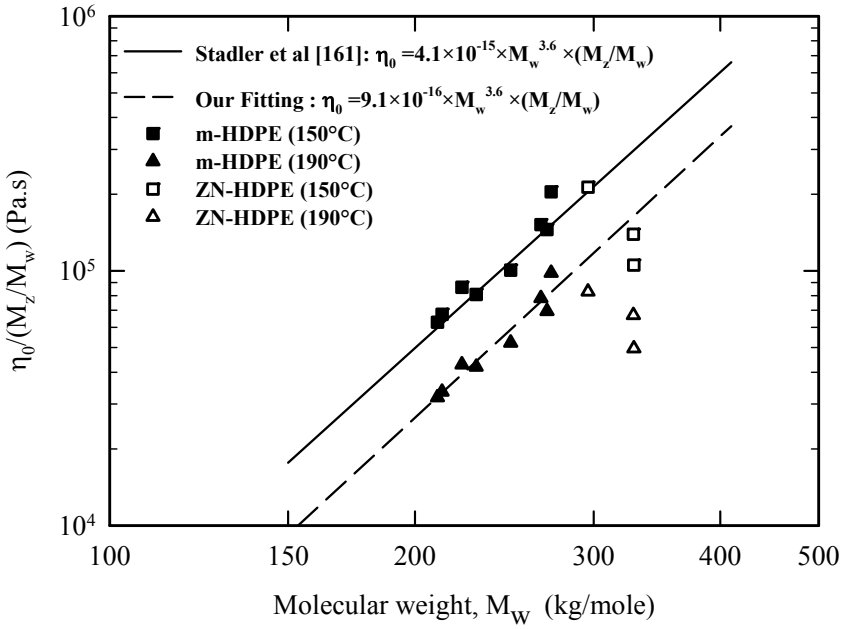

Figure 5.8. *Correlation of zero shear viscosity with M_w taking MWD into account at T=150°C & T=190°C.*

5.3 Steady State Creep Compliance

Fig. 5.9 shows typical creep test results for two samples (m-HDPE 9 and 11) using a 10 Pa shear stress value. From creep tests, the steady state creep compliance (J_e^0) can be determined by extrapolating the steady state linear portion of the compliance curve to time zero, according to the following equation [9]:

$$\lim_{t\to\infty} J_e = J_e^0 + t/\eta_0 \tag{5.6}$$

To verify that steady state conditions have been reached, Eq. 5.6 has been used to check the linearity of the final portion of the curves.

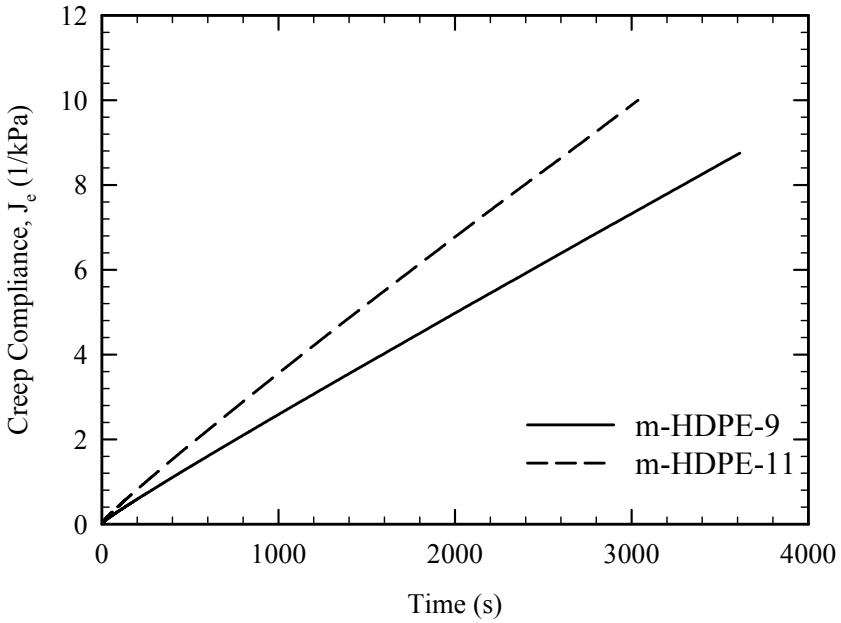

Figure 5.9. *Creep test results for two samples m-HDPE-9 and m-HDPE-11 using a constant shear stress of 10 Pa at T=170°C .*

Rather than viscosity which is a function of molecular weight, it is widely accepted that the steady state creep compliance does not relate to M_w, but it is very sensitive to measures of the molecular weight distribution for molecular weights greater than the critical molecular weight for entanglements, M_c [42]. There are many relations (empirical and theoretical) proposed to relate J_e^0 with molecular weight distribution. Two of them are the most accepted in the literature since they have been verified experimentally. The first one was proposed by Mieras and Rijn [168] (Eq. 5.7a) and has been tested successfully for polystyrene (PS), HDPEs and polydimethylosiloxanes (PDMSs) by Mills [12, 169]. The second relation is that proposed by Agarwal [27] (Eq. 5.7b) and explained theoretically by Kurata [28]. This was found to work well for PSs [29, 170-173].

$$J_e^0 \propto (M_z/M_w)^{3.7} \tag{5.7a}$$

$$J_e^0 \propto (M_z \times M_{z+1})/(M_n \times M_w) \tag{5.7b}$$

Fig. 5.10a depicts the experimental values for m-HDPEs of the present work together with Eqs. 5.7a and 5.7b and the experimental data reported by Mills [174]. As shown in the figure, our data

follow Eq. 5.7a well. However, it should be noted that our data are lower than reported by Mills [174] by about 1 order of magnitude at the same molecular weight distribution. Gabriel and Münstedt [175] and Resch et al [176] have shown that molecular structure such as LCB plays a significant role in melt elasticity i.e. steady state creep compliance. However detailed information on the molecular structure of HDPEs used by Mills [174] is lacking and the origin of this difference cannot be concluded.

Another correlation has been also proposed by den Doelder [164] based on the double reptation single exponential model (Eq. 5.7c):

$$J_e^0 \propto (M_{z+1}/M_w)^{2.2} \times (M_{z+1}/M_z)^{2.2} \tag{5.7c}$$

As it is clear from Fig. 5.10b, this correlation also describes well the experimental data of the present work.

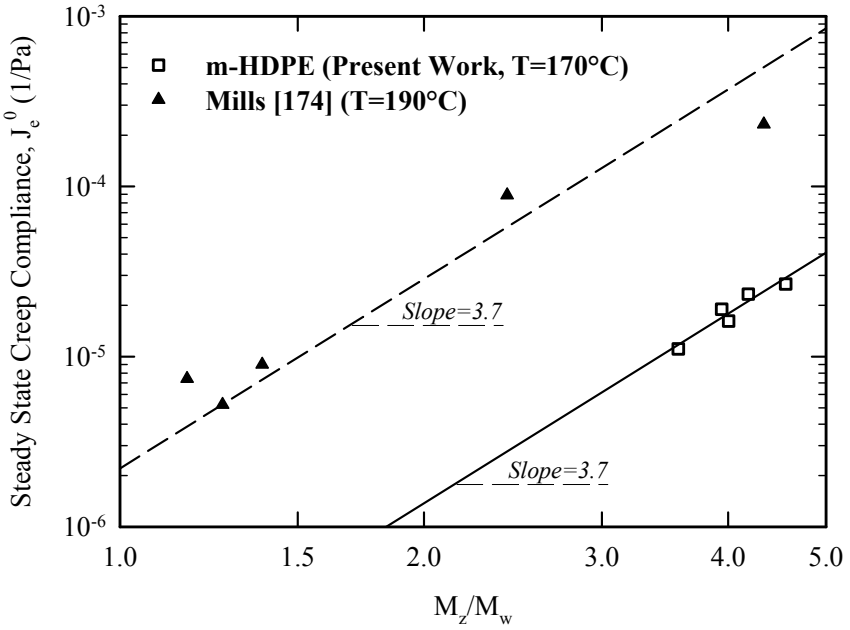

Figure 5.10a. *Correlation between steady state creep compliance and the measure of MWD, M_z/M_w for several HDPE resins.*

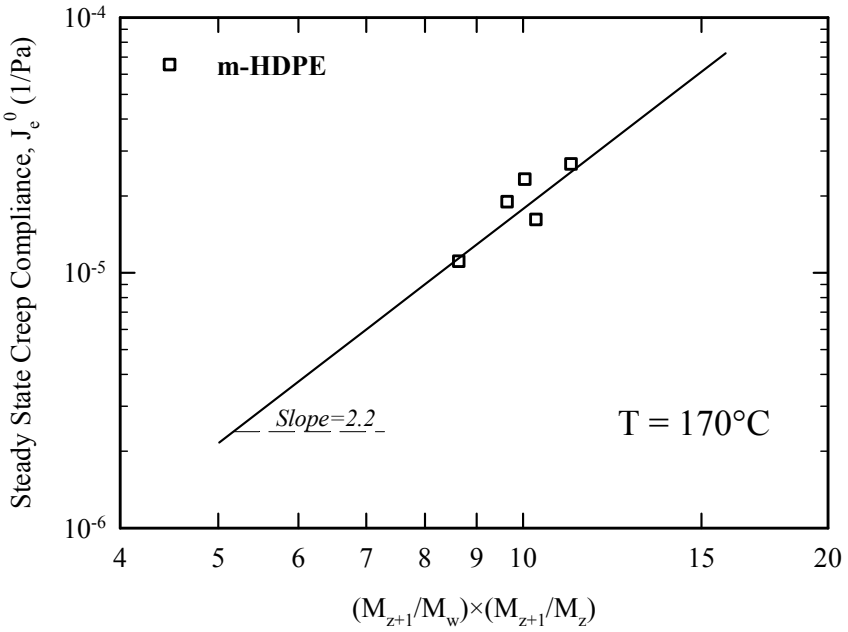

Figure 5.10b. *Correlation between steady state creep compliance and a measure of MWD, $M_{z+1}^2/M_w\,M_z$ for m-HDPE resins. The slope is 2.2 as it is expected according to Eq. 5.7c proposed by den Doelder [164].*

5.4 Summary

In this chapter, the rheological properties of broad molecular weight distribution ZN and m-HDPEs have been examined. The zero shear viscosity showed a power-law correlation with molecular weight, but the exponent was greater than the universal exponent of 3.6. As it was shown that there is no branching for m-HDPEs resins, it was assumed that for these high molecular weight polymers, the effect of very long molecules needs to be considered. This was done by introducing the z-moment of molecular weight into the correlation. Once the effect of molecular weight distribution has been taken into account, the exponent of 3.6 was recovered. It should be noted that the effect of polydispersity was in accordance with previous studies. The crossover modulus also shows a power-law dependence on the z-moment polydispersity, M_z/M_w.

Finally, the correlation of steady state compliance with different measures of polydispersity was checked. Our experimental results for m-HDPE resins were in good agreement with different proposed correlations in the literature.

6 MELT FRACTURE OF HDPEs

In this chapter, the melt fracture instabilities of ZN-HDPEs and m-HDPEs are studied. The effects of temperature, addition of a processing aid, type of die (cylindrical, slit and annular) and geometrical details, as well as molecular characteristics such as molecular weight and its distribution on the different modes of melt fracture are investigated. Some interesting correlations for the onset of instabilities and molecular and rheological parameters are also derived.

6.1 Uniaxial Extensional Rheology

According to the accepted mechanisms for the different types of melt fractures [31, 63, 64], the elongational part of the flow in the die inlet (gross melt fracture) and outlet (sharkskin) plays a key role in the phenomena. Therefore, studying the uniaxial extensional properties would be a matter of interest in order to have a better understanding of the processing properties of polymer melts [32].

Fig. 6.1 depicts the uniaxial extensional results of resins m-HDPE-1 and ZN-HDPE-0 at T=150°C and different Hencky strain rates. Similar graphs for several other ZN and m-HDPEs can be found in Appendix B. The continuous lines represent $3\eta^+$ determined from linear viscoelastic measurements by calculating the parsimonious relaxation spectrum $\{G_i, \lambda_i\}$ of both resins [177, 178] from the following expression (Parsimonious relaxation spectra for all the resins are listed in Appendix A.3):

$$\eta_E^+ = 3\sum_i \frac{G_i}{\lambda_i}[1 - exp(-t/\lambda_i)] \tag{6.1}$$

It is noted that both resins follow Trouton's rule at short times.

As it is shown in Fig. 6.1, the LVE $3\eta^+$ for the metallocene resin is higher than ZN-HDPE-0 in the shown time span. The resin m-HDPE-1 ruptures at relatively longer times, which shows its higher extensibility and capability to store energy. Another interesting feature of this figure is

that the m-HDPE-1 shows a necking behaviour at Hencky strains higher than 1.0 s^{-1}. This necking is accompanied by a two steps rupture. The first rupture is incomplete and happens at the edges of the sample (necking), although the sample still withstands the tensile stress. The necked sample is further extended, becomes opaque, which is sign of crystallinity until it eventually breaks up. Based on these results, the ZN-HDPE is expected to exhibit better processability.

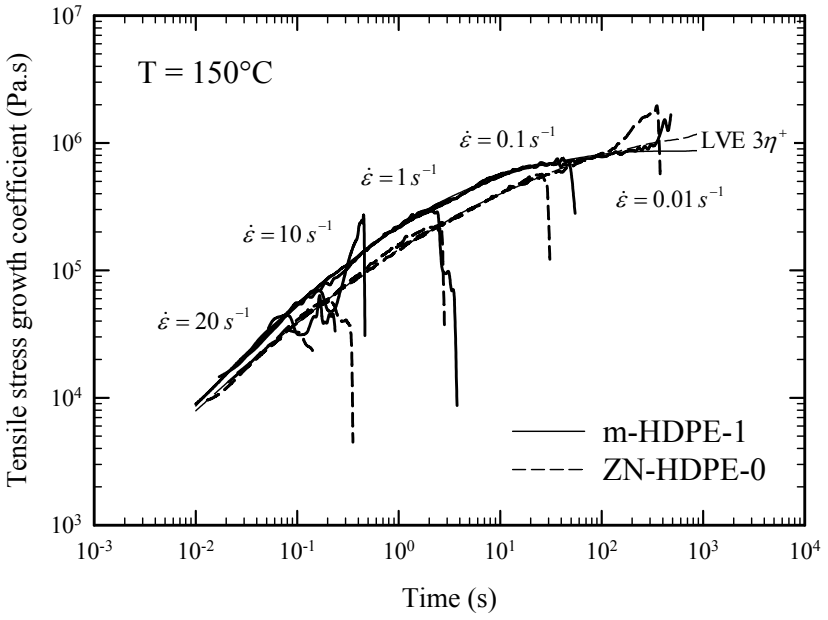

Figure 6.1. *The tensile stress growth coefficient of resins m-HDPE-1 and ZN-HDPE-0 at several Hencky strain rates, at T=150°C. The line labeled as LVE* $3\eta^+$ *line has been calculated from fitting linear viscoelastic measurements with a parsimonious relaxation spectrum and use of Eq. 6.1.*

6.2 Capillary Rheometry

Figs. 6.2a and 6.2b depict the capillary flow curves for the resins m-HDPE-1 and ZN-HDPE-0, respectively at different temperatures, namely from 140 to 230°C. Similar graphs that depict the flow curves of several other ZN and m-HDPEs can be found in Appendix C.1. The temperature dependency of metallocene resin is slightly milder than its ZN counterpart. This can be deduced by the activation energy values obtained by the application of TTS principle to obtain the LVE master curves presented in chapter 5 (Table 5.1). These are 6.90 kcal/mole for m-HDPE-1 and 7.29 kcal/mole for ZN-HDPE-0, typical values for linear polymers with a very broad MWD [41].

The same shift factors were used to superpose the capillary data plotted in Figs 6.2a and 6.2b. The results are shown in Figs 6.3a and 6.3b. The superposition is excellent, except for the flow curves obtained at low temperatures and high apparent shear rates. This is clearly due to the effect of flow induced crystallization (FIC) which seems to be more dominant for m-HDPE-1 compared to ZN-HDPE-0. For example Fig 6.3a shows that the flow curves for m-HDPE-1 even at the temperature as high as T=160°C shows lack of superposition due to FIC. It is noted that the melting points for the two resins are T=126.7°C and T=127.5°C for the m-HDPE-1 and ZN-HDPE-0 respectively. As it was discussed in the previous section, FIC crystallization was found to be more dominant for m-HDPE-1 from the uniaxial experiments that leads to necking. The higher heat of fusion for the metallocene resin which is 174.5 J/gr compared to the one of ZN-HDPE-0 which is 143.6 J/gr would be another sign of its higher tendency to crystallize.

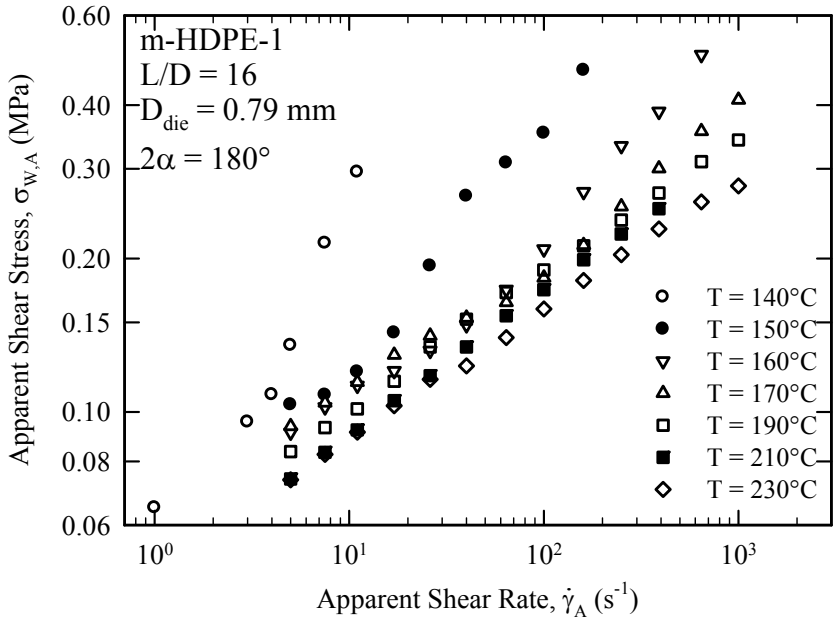

Figure 6.2a. *The flow curves of resin m-HDPE-1 in capillary extrusion at different temperatures.*

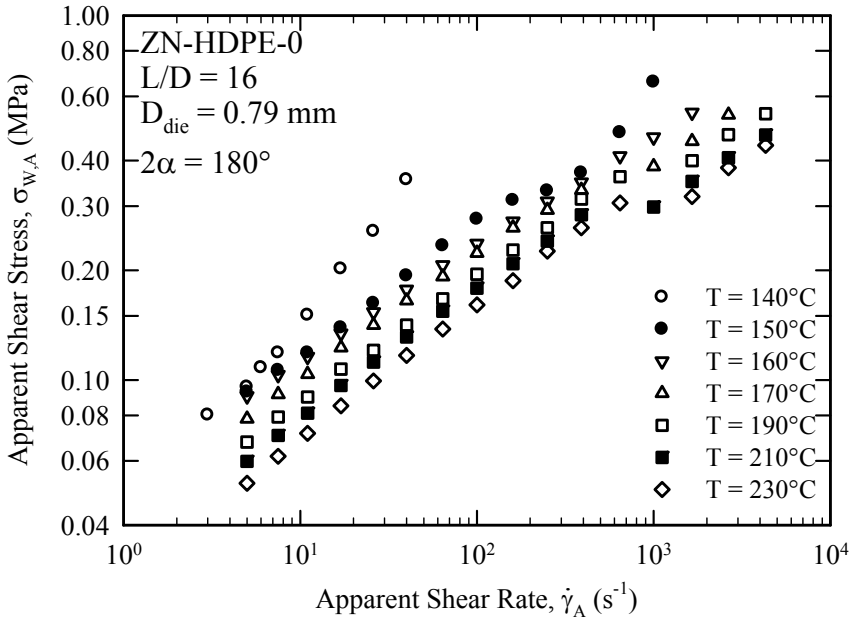

Figure 6.2b. *The flow curves of resin ZN-HDPE-0 in capillary extrusion at different temperatures.*

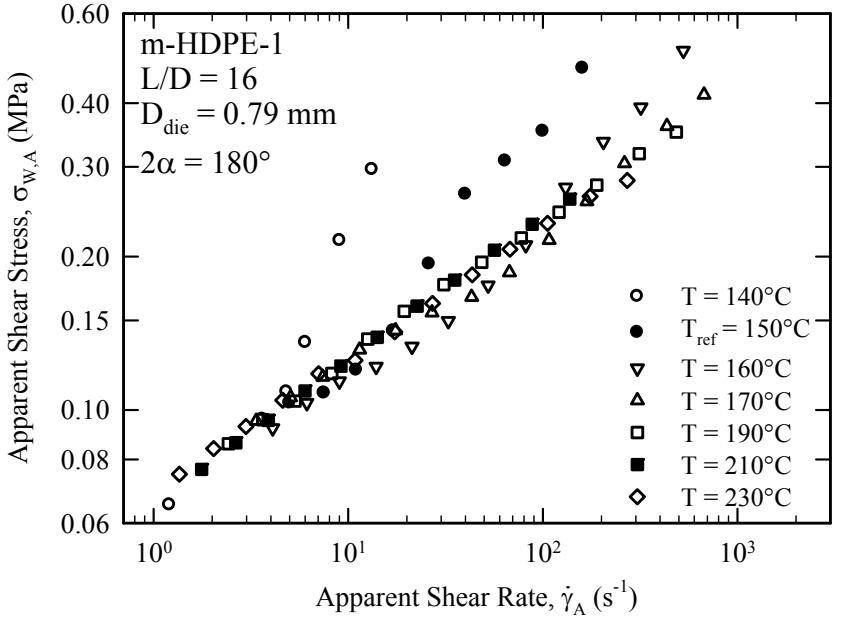

Figure 6.3a. *The master flow curve of resin m-HDPE-1 at T_{ref} = 150°C, obtained by superposing the data plotted in Fig. 6.2a by using shift factors determined from LVE.*

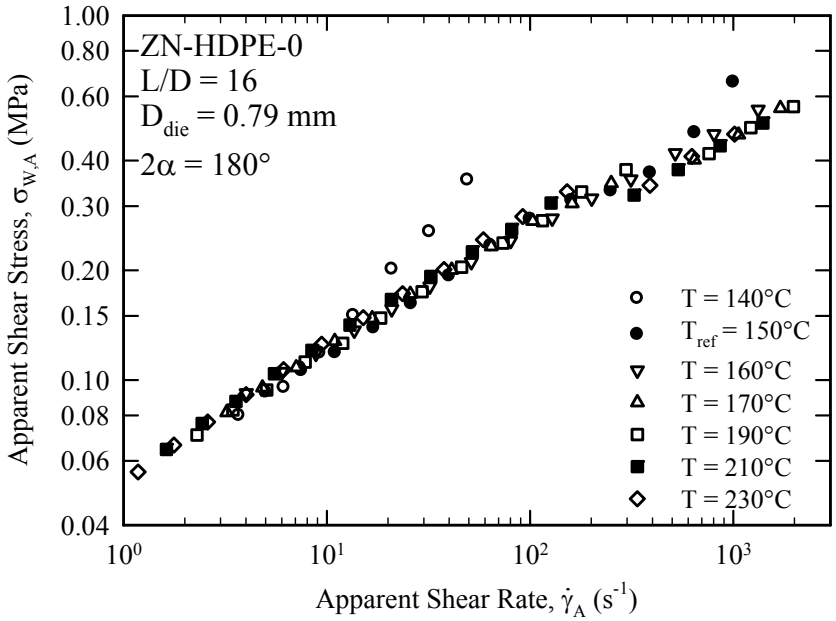

Figure 6.3b. *The master flow curve of resin ZN-HDPE-0 at T_{ref} = 150°C, obtained by superposing the data plotted in Fig. 6.2b by using shift factors determined from LVE.*

6.2.1 Melt Fracture and Typical Flow Curves for HDPEs

Linear polymers like HDPE and LLDPE of narrow molecular weight distribution generally show a discontinuity in their flow curve that separates their flow curve into two distinct parts. The flow in this regime is unstable, in other words the flow rate and pressure drop oscillate between two extreme values, a phenomenon known as stick-slip or oscillating melt fracture. Fig. 6.4a shows such a behavior for resin ZN-HDPE-10 at T=190°C. As seen the flow curve is divided into two branches, namely a low and a high flow-rate branches [34, 179]. In the low flow-rate branch, the velocity profile of the melt in the die region is almost parabolic and the magnitude of slippage is typically low. On the other hand, in the high flow-rate branch the velocity profile is almost plug like. The two branches are connected to each other through a hysteresis loop as shown in Fig 6.4a.

Three are three relevant critical shear stresses that are of importance in the melt fracture phenomena under discussion, namely the critical shear stress for the onset of sharkskin (σ_{c1}), the

critical shear stress for the onset of stick-slip (σ_{c2}) and the critical shear stress for the onset of gross melt fracture (σ_{c3}). The first two critical shear stresses, σ_{c1} and σ_{c2}, refer to the low flow-rate branch, while σ_{c3} to the high flow-rate branch. During the pressure oscillations the shear stress in the wall of the capillary oscillates between σ_{c2} and σ_{c3}. The difference $\sigma_{c2} - \sigma_{c3}$ defines the magnitude of the oscillations.

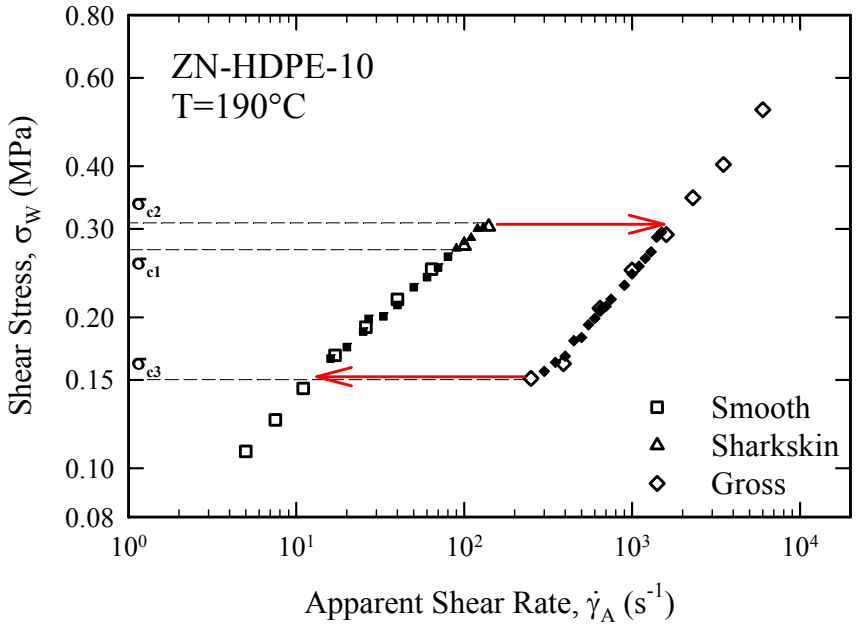

Figure 6.4a. *The flow curve of ZN-HDPE-10 at T=190°C which shows the stick-slip transition as a hysteresis loop that connects two distinct branches. Several experiments were performed to completely define the hysteresis loop. The relevant critical stresses are those for the onset of sharkskin, σ_{c1}, for the onset of stick-slip, σ_{c2} and for the onset of gross melt fracture, σ_{c3}.*

Contrary to the ZN resins, most of the metallocene resins, particularly those with PDI>19, do not exhibit any stick-slip instability and their flow curve is rather a continuous one. Fig. 6.4b shows such a typical flow curve for resin m-HDPE-8 at 190°C. In this case, there are two relevant critical shear stress values, namely the critical shear stress for the onset of sharkskin (σ_{c1}), and the critical shear stress for the onset of gross melt fracture (σ_{c3}). It is worthwhile to mention that in this case σ_{c1} is always less than σ_{c3}. However, this is not true for the case of HDPEs that exhibit stick-slip transition (see Fig. 6.4a).

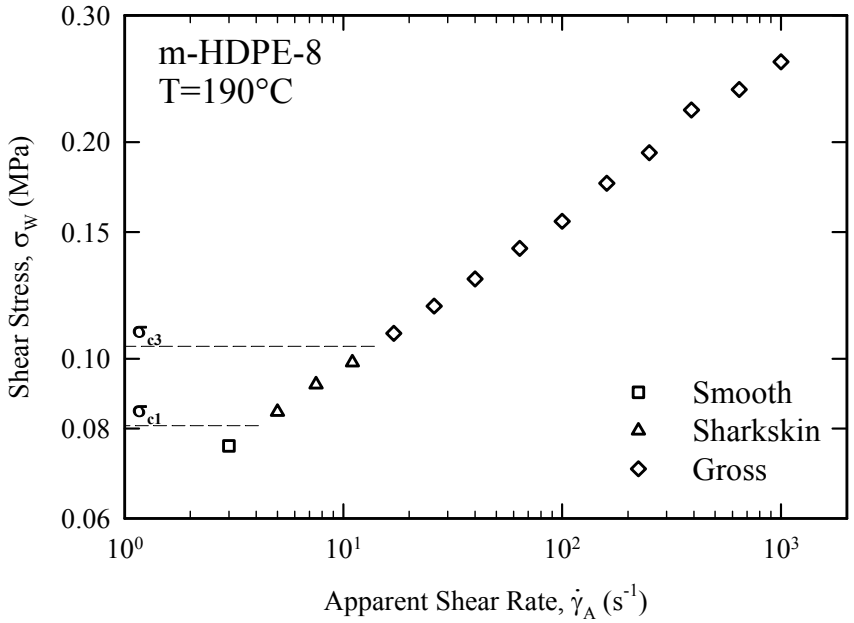

Figure 6.4b. *The flow curve of m-HDPE-8 at T=190°C appears to be a continuous one. The critical stresses for the onset of sharkskin and gross melt fracture are also shown as σ_{c1} and σ_{c3} respectively.*

6.2.2 Effect of Molecular Weight

Fig. 6.5 shows the effect of molecular weight on the shape of flow curve for resins ZN-HDPE-10 to ZN-HDPE-16. These resins have almost the same polydispersity and different molecular weight, M_w. It is clear that the size of the discontinuity (size of the hysteresis loop) decreases by decreasing the molecular weight. In other words, as the molecular weight decreases, the difference $\sigma_{c2} - \sigma_{c3}$ (magnitude of the oscillations) decreases and the two branches come closer. Essentially, the hysteresis loop shrinks in both the horizontal and vertical directions. Also the critical shear stress for the onset of stick-slip transition appears to slightly decrease with increase of molecular weight as will be discussed later. Below a certain molecular weight, M_w, the flow curve becomes continuous (no stick-slip transition) as was also reported by Myerholtz [99] and Blyler and Hart [115]. Another interesting feature of this figure is that the high flow rate branch of the flow curve is independent of M_w.

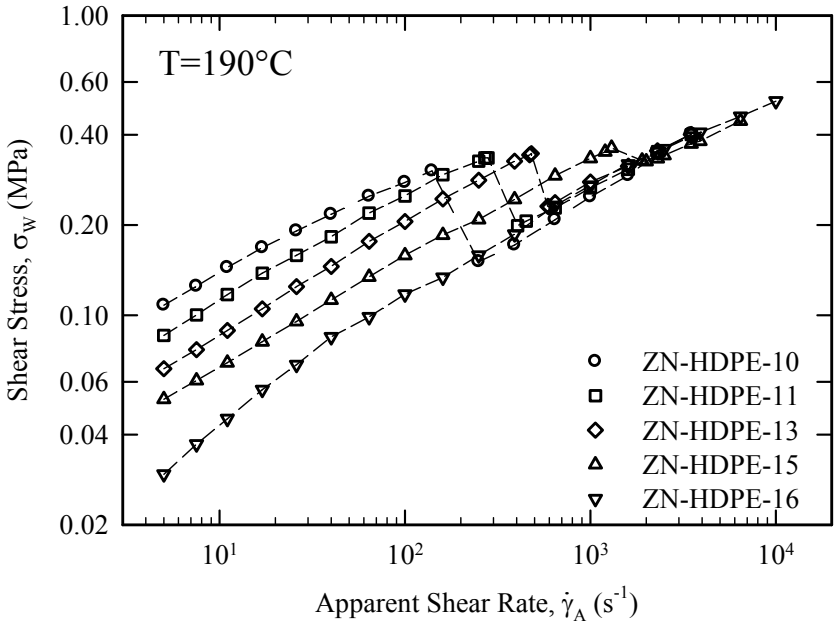

Figure 6.5. *The flow curves of some of the ZN-HDPE resins with similar PDI, and different molecular weight at T=190°C. The size of stick-slip discontinuity in the flow curve decreases with decrease of the molecular weight.*

6.2.3 Effect of Molecular Weight Distribution

Fig. 6.6 depicts the flow curves of three different HDPEs having almost the same M_w and different polydispersities, namely 11, 18 and 25. As it is clear, the effect of increasing the polydispersity is similar to the effect of decreasing the molecular weight. In other words as PDI increases, the size of the hysteresis loop decreases in both horizontal (the two distinct branches come closer) and vertical directions and the magnitude of the oscillations $\sigma_{c2} - \sigma_{c3}$ also decrease. For polymers with PDI>19 the stick-slip transition disappears. Note the flow curve of HDPE-8 in Fig. 6.6 and several other flow curves for HDPEs with PDI>19 in Fig. 6.7. Finally, the high flow rate branch of the flow curve appears to be independent of polydispersity as well. For example see how they all come together at high shear stress values in Fig. 6.7. In this flow regime, the HDPEs slip is considerably high (nearly plug flow) and the friction of monomer with the wall becomes the relevant parameter that controls the level of stress developed [8].

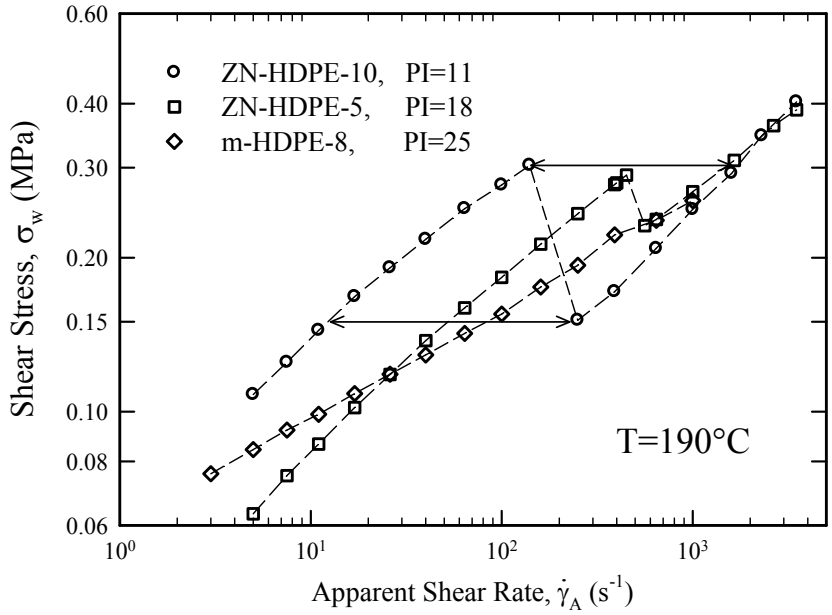

Figure 6.6. *The flow curves of ZN-HDPE-10, ZN-HDPE-5 and m-HDPE-8 at T=190°C that show the effect of polydispersity. The size of the stick-slip discontinuity (size of the hysteresis loop) in the flow curve decreases with increase of polydispersity.*

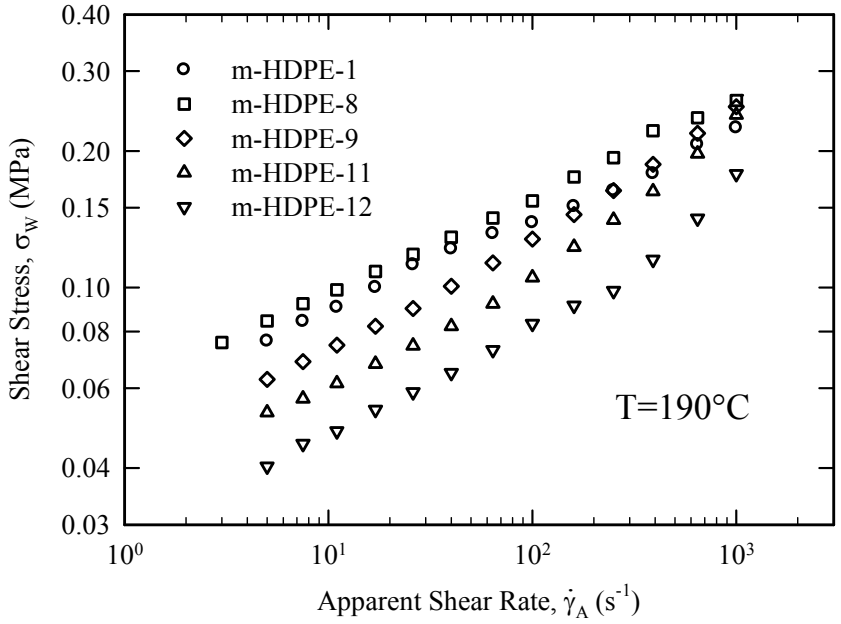

Figure 6.7. *The flow curves of the m-HDPEs with PDI>19 at T=190°C. All flow curves are continuous because of the wide molecular weight distribution.*

6.2.4 Stick-Slip: Molecular Criterion for the Onset

As discussed in previous sections, the magnitude of the oscillations in the stick-slip transition is a function of M_w and its distribution. The most acceptable mechanistic molecular explanation for this phenomenon is the entanglement-disentanglement transition between the tethered molecules attached to the solid wall and the molecules in the bulk [137]. According to these authors, the tethered chains can be stretched in the direction of flow since they are entangled to the bulk molecules. After a critical shear stress, these entanglements could not sustain the load, since the tethered chains cannot be stretched further due to their contour length limitation. As a result of the sudden disentanglement, a transition from weak to strong slip is obtained at σ_{c2} (see Fig. 6.6). In this state the tethered chains slowly recover their random coil shape until they re-entangled with surrounding chains at σ_{c3} (see Fig. 6.6) and be stretched again. The disentangled bulk chains also can slip over them during this period. This cyclic process leads to an oscillation in shear stress exerting by molecules, essentially a hysteresis loop defined by the two arrows in Fig. 6.6 for ZN-HDPE-10. Based on this analogy, it is expected to suppress stick-slip effect by introducing short chains (e.g. increasing the molecular weight distribution), as they prefer to migrate to the wall and act as tethered chains [153, 180]. These short tethered chains do not have the ability to be oriented much by flow and therefore the bulk chains can slip over them gradually (instead of catastrophic disentanglement and abrupt slippage in the case of long tethered chains) by increasing the shear stress [158]. This has been also verified experimentally by Myerholtz [99] and Blyler and Hart [115].

As it is depicted in Fig. 6.7, it appears that once PDI increases above 19 and closer to 20, the stick slip flow regime disappears and the flow curves are monotonically increasing functions of the shear rate. However, PDI is not the only criterion for the occurrence of stick-slip. Allal and Vergnes [16] have argued that in order to eliminate this defect, the entanglement at the solid-polymer interface should be removed. These authors argued that the size of these interfacial molecules must be lower than a few times of the molecular weight between entanglements, M_e, with the exact number depending on the chemical structure of the polymer and nature of the solid material. They have developed the following criteria for the absence of stick-slip flow from a class of linear polymers:

$$M_w/M_e < \lambda \times PDI \quad \text{(no stick-slip)} \tag{6.2}$$

where *PDI* is the polydispersity index and λ is a constant depending on the polymer chemical structure and the solid wall material. Assuming a value for M_e=1.2 kg/mole for polyethylenes and $M_c=2M_e$, a value of 12 is obtained for λ, where M_c is the critical molecular weight for the onset of entanglements [16]. Fig. 6.8 demonstrates that the criterion of Eq. 6.2 based on the weight average molecular weight and polydispersity index for stick-slip existence can describe the flow behaviour of HDPEs examined in this work as well as those studied by Hatzikiriakos and Dealy [8]. Eq. 6.2 as an equality is represented by the continuous straight line in Fig. 6.8 and separates the domain (*PDI, M_w*) in two areas, namely the stick-slip and the no stick-slip domains.

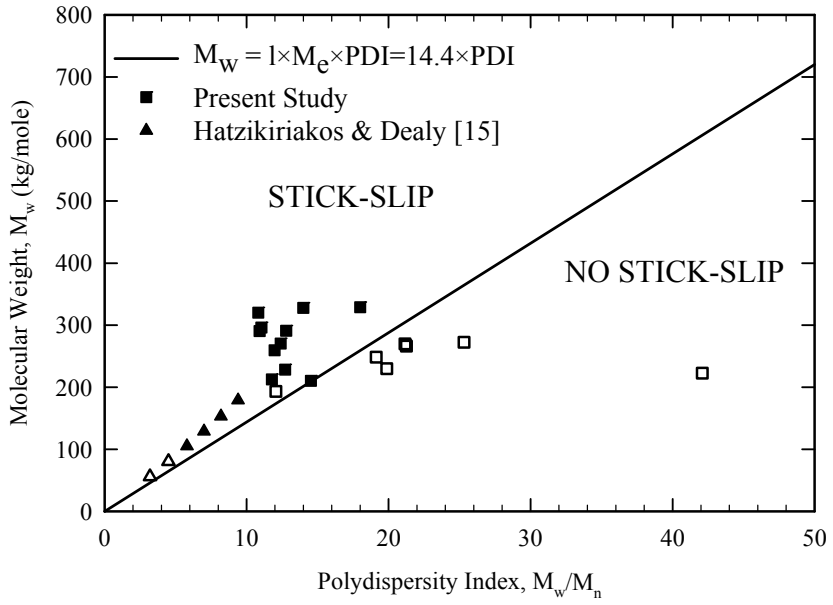

Figure 6.8. *Criterion for the occurrence of stick-slip transition for HDPE resins. Open symbols represent resins with no stick-slip transition while filled symbols those that exhibit this transition. The continuous line is $M_w=12\times PDI\times M_e$. In general Eq. 6.2 represents the data adequately well.*

6.3 Effects of Processing Conditions on Melt Fracture

6.3.1 Effect of Temperature

Fig. 6.9a and 6.9b illustrate the processability maps of resins m-HDPE-1 and ZN-HDPE-0 in capillary extrusion experiments as a function of apparent shear rate and temperature. Similar processability maps for several other ZN and m-HDPEs can be found in Appendix D. The various symbols on the map indicate smooth, sharkskin and gross melt fracture appearance of samples extruded at a given temperature and apparent shear rate. It is clear that the processability of ZN-HDPE-0 is superior compared to that of m-HDPE-1. This can be also seen from the critical shear rates and stresses for the onset of melt fracture at various temperatures listed in Table 6.1 for both polymers (The critical apparent shear rates and apparent shear stresses for most of the resins are listed in Appendix D). Therefore, the processability of the two resins with similar rheology is distinctly different mainly due to the broadness of their molecular weight distribution.

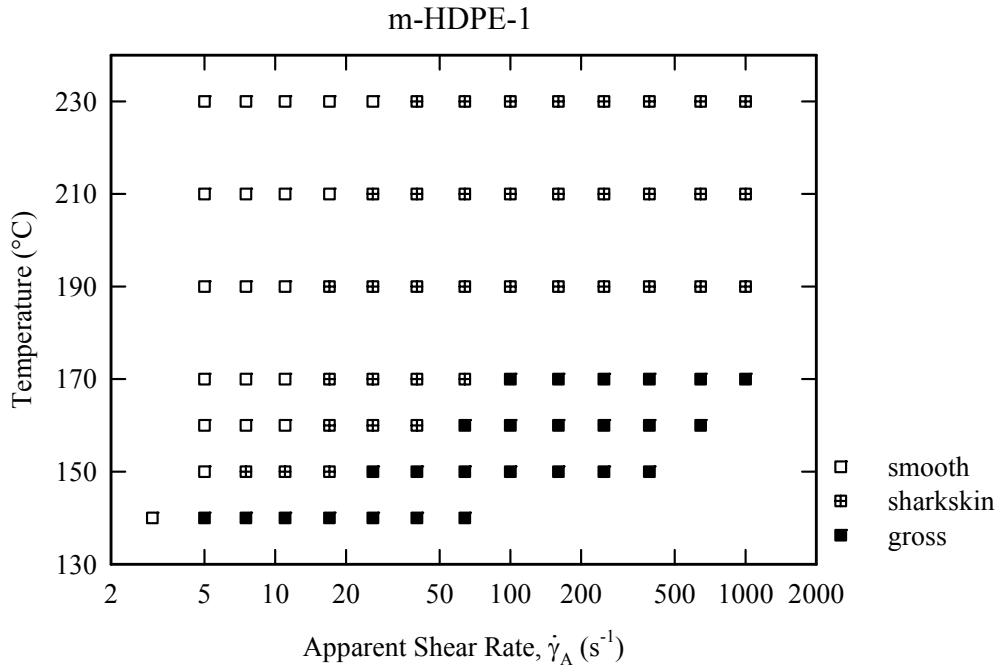

Figure 6.9a. *Processability map of resin m-HDPE-1 in capillary extrusion as a function of apparent shear rate and temperature. Various symbols indicate smooth, sharkskin or gross melt fracture appearance of samples extruded at given temperature and apparent shear rate.*

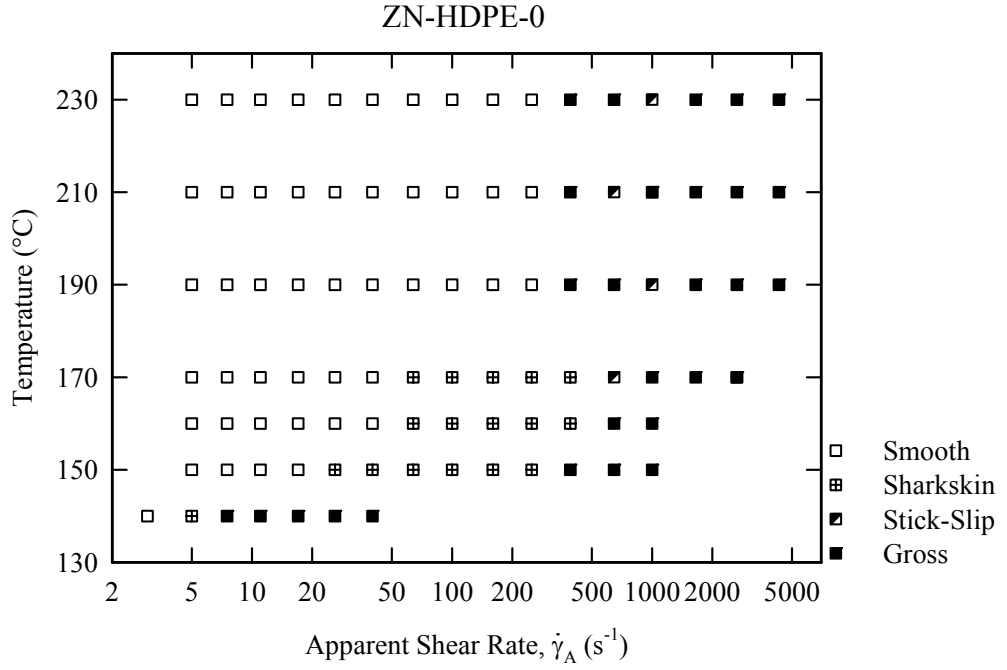

Figure 6.9b. *Processability map of resin ZN-HDPE-0 in capillary extrusion as a function of apparent shear rate and temperature. Various symbols indicate smooth, sharkskin or gross melt fracture appearance of samples extruded at given temperature and apparent shear rate.*

Table 6.1. *Critical apparent shear rates and shear stresses for the onset of sharkskin melt fracture in capillary die for both resins at different temperatures. Note that only gross melt fracture is obtained for ZN-HDPE-0 at high temperatures.*

Temperature (°C)	*m-HDPE-1*		*ZN-HDPE-0*	
	$\dot{\gamma}_{A,cr}$ (s^{-1})	$\sigma_{A,cr}$(MPa)	$\dot{\gamma}_{A,cr}$ (s^{-1})	$\sigma_{A,cr}$(MPa)
140	3.9	0.11	3.8	0.09
150	6.1	0.11	21	0.15
160	13.7	0.12	50	0.19
170	13.7	0.12	50	0.18
190	13.7	0.11	312	0.29*
210	21.0	0.11	312	0.26*
230	32.2	0.12	312	0.24*

* *Gross melt fracture*

At low temperatures, the first extrudate defect that is observed is sharkskin; while by increasing the temperature, sharkskin is obtained at higher and higher apparent shear rates, it eventually disappears at temperatures greater than about 190^{o}C. At these high temperatures gross melt fracture occurs. Moreover, inspecting the critical shear rates and stresses listed in Table 6.1, it can be concluded that the critical shear stress for the onset of sharkskin is a weak function of temperature, also in agreement with other reports in the literature [15, 181].

Although the critical stress for the onset of sharkskin is a weak function of temperature, it is sensitive to molecular weight distribution [3, 45, 69]. Kazatchkov et al [45] showed that for linear low-density polyethylenes having PDI>9, sharkskin instability was not a serious problem. While this is the case in the present study for 9<PDI<19, for resins with PDI>19, sharkskin becomes a serious problem as it occurs at critical shear stress values of significantly less than 0.1 MPa [3, 4, 45, 64].

Finally, the critical shear stress values of 0.24-0.30 MPa for the onset of gross melt fracture also agree well with previous reports [3, 58, 63, 100, 112]. For example Hatzikiriakos and Dealy [8] have reported critical shear stress in the range of 0.22-0.50 MPa for various HDPEs.

While the results for ZN-HDPE-0 overall agree with those reported in the literature, the results for the m-HDPE-1, are quite surprising. Given its high PDI of about 40, the critical shear stresses for the onset of sharkskin at around 0.1 MPa is typical for very narrow molecular weight distribution HDPEs [3, 7, 45, 134]. It is also noted that no stick-slip instability was obtained which is mainly due to the high PDI. Moreover, as it will be shown in the next chapter, the m-HDPE-1 resin exhibits significant slippage on the die wall surface and this has also an impact on its processability in the presence of processing aids.

Table 6.2 summarizes the critical shear stresses for the onset of various instabilities for all HDPEs at various temperatures. Once again these values are independent of temperature. One striking difference between the HDPEs with PDI>19 (first group) and the second group is the distinctly different critical values. The first group exhibits sharkskin at relatively low critical shear stress values, typically less than about 0.1 MPa. They exhibit no stick-slip and their flow curve is monotonically increasing, exhibiting significant slip and failure of the Cox-Merz rule as

reported by Ansari et al [182]. The second group exhibits critical shear stress values above 0.15 MPa and in most cases above 0.20 MPa. They all exhibit stick-slip transition with low slip at the low flow curve branch.

Table 6.2. *Critical shear stresses for the onset of different types of melt fractures.*

Material	*T (°C)*	*Critical shear stress (MPa)*		
		Sharkskin, σ_{c1}	*Stick-slip,* σ_{c2}	*Gross*
ZN-HDPE-0	150-230	0.15-0.18 (150-170°C)	0.29	0.29-0.34
ZN-HDPE-5	170-230	N/A	0.30	0.28-0.31
ZN-HDPE-6	170-230	0.16-0.20 (150-170°C)	0.33	0.29-0.32
ZN-HDPE-10	190	0.27	0.30	0.15
ZN-HDPE-11	190	0.28	0.33	0.20
ZN-HDPE-12	190	0.27	0.34	0.21
ZN-HDPE-13	190	0.27	0.35	0.22
ZN-HDPE-14	190	0.26	0.36	0.25
ZN-HDPE-15	190	0.24	0.36	0.33
ZN-HDPE-16	190	0.26	N/A	0.42
m-HDPE-1	150-230	0.10	N/A	0.16 (150-170°C)
m-HDPE-8	150-210	0.08	N/A	0.10
m-HDPE-9	150-210	0.07	N/A	0.09
m-HDPE-10	150-210	0.07 (150-190°C)	N/A	0.09 (150-190°C)
m-HDPE-11	150-210	0.06 (150-190°C)	N/A	0.09 (150-190°C)
m-HDPE-12	150-210	0.05 (150-190°C)	N/A	0.1 (150-190°C)
m-HDPE-13	170-210	0.10	0.36	0.20
m-HDPE-19	170-210	0.14-0.15	0.37	0.25

6.3.2 Effect of Die Type

The type of die (capillary versus slit versus annular) has been reported to have a significant effect on the critical conditions for the onset of sharkskin. The results show that the critical stress for onset of sharkskin is higher in slit and significantly higher in annular dies compared to that in capillary dies [6, 70-72, 183]. For example Delgadillo et al [6] have performed extrusion experiments for a linear low-density polyethylene with capillary, slit and annular dies. They have reported that the critical stresses for the onset of sharkskin, oscillating and gross melt fracture differ significantly depending on the die geometry used. Oscillating melt fracture was obtained with capillary and slit dies but it was absent in annular die extrusion. Such studies are extremely important from the industrial point of view as most of industrial processes such as pipe extrusion,

blow molding and film blowing include annular flow geometries rather than capillary/slit ones. Therefore, such studies can correlate results obtained in the laboratory with the industrial (production scale) performance of the polymers.

Three types of die have been used to check the effect, i.e. capillary, slit and annular. The die dimensions are listed in Table 4.2. Figs. 6.10a and 6.10b depict the flow curves of m-HDPE-1 and ZN-HDPE-0 respectively, through these dies. The apparent shear rates are defined as

$$\begin{aligned} \dot{\gamma}_A &= 8Q/\pi D^3 \qquad (capillary) \\ \dot{\gamma}_A &= 6Q/WH^2 \qquad (slit) \\ \dot{\gamma}_A &= 48Q/\pi(D_o - D_i)^2\,(D_o + D_i) \qquad (annular) \end{aligned} \tag{6.3}$$

where Q is the volumetric flow rate. The wall shear stress for the annular die is not uniform across the thickness and therefore we have calculated two flow curves for this case, which correspond to the shear stress values at inner and outer surfaces. The stresses have been calculated using the following formula, which is based on the assumption of a power-law fluid [184]:

$$\tau_{rz} = \frac{\Delta p D}{4L}\left(\frac{2r}{D} - \beta^2 \frac{D}{2r}\right) \tag{6.4}$$

where τ_{rz} is the shear stress at radius r, Δp is the pressure drop, L is the length of the die land, and β is the parameter depending on the geometry and the power law index [184].

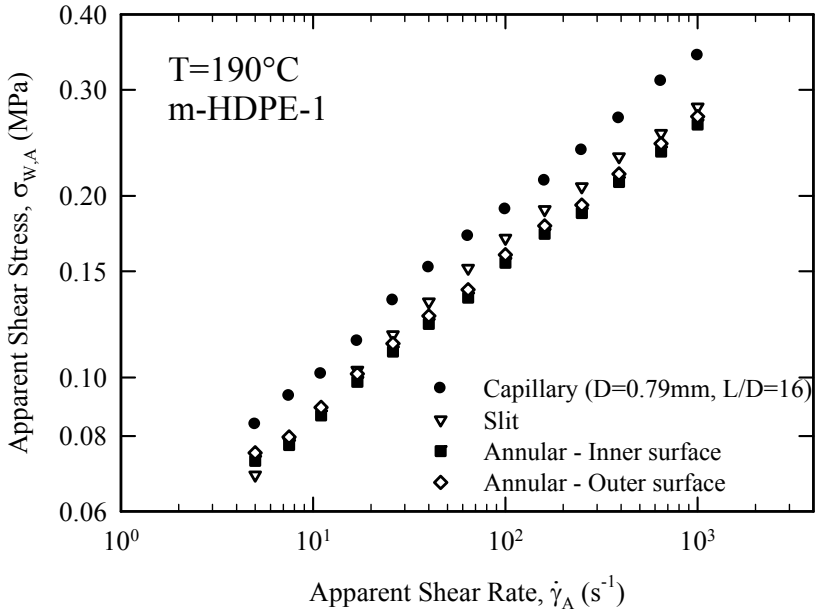

Figure 6.10a. *Flow curves of the resin m-HDPE-1 for different die types at T=190°C*

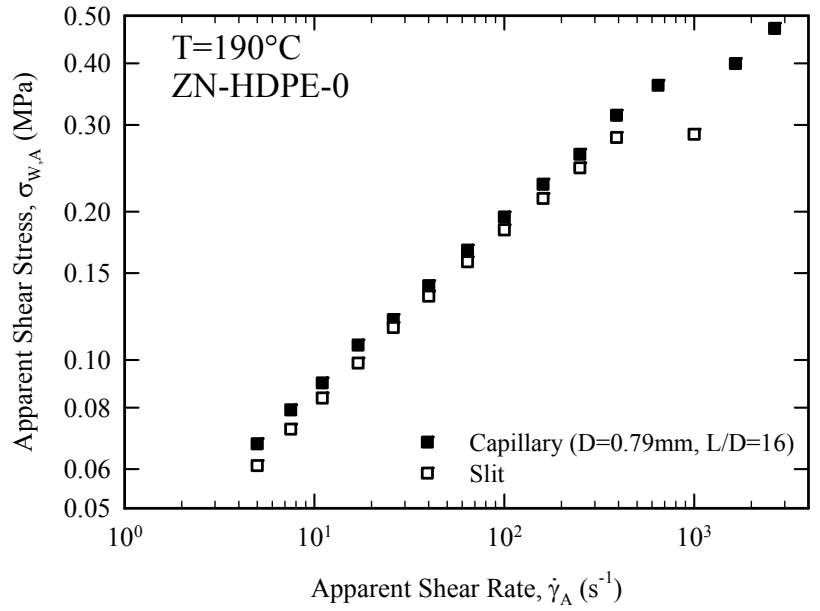

Figure 6.10b. *Flow curves of the resin ZN-HDPE-0 for different die types at T=190°C.*

First the flow curves of the slit die lie above those obtain from the other dies. Once all corrections (Bagley, Rabinowitsch and slip) are applied these flow curves are expected to superpose at least over the low shear rate range. Similar observations have been reported by Delgadillo et al [6].

Tables 6.3a and 6.3b list the critical shear rates and stresses for all types of die geometries used for resins m-HDPE-1 and ZN-HDPE-0, respectively. For the case of capillary dies both the Bagley corrected and uncorrected critical stresses are reported (typical Bagley correction results are presented in Appendix C.2). They differ by roughly 10%.

Table 6.3a. *Critical apparent shear rates and shear stress values or the onset of sharkskin for m-HDPE-1 resin at different temperatures and different types of die.*

Temperature	***Capillary***		***Slit***		***Annular***	
(°C)	$\dot{\gamma}_{A,cr}$ (s^{-1})	$\sigma_{A,cr}$*(MPa)*	$\dot{\gamma}_{A,cr}$ (s^{-1})	$\sigma_{A,cr}$*(MPa)*	$\dot{\gamma}_{A,cr}$ (s^{-1})	$\sigma_{A,cr}$*(MPa)*
140	3.9	0.11	3.9	0.08	-	-
150	6.1	0.11	6.1	0.10	-	-
160	13.7	0.12	13.7	0.10	-	-
170	13.7	0.12–0.11*	13.7	0.10	-	-
190	13.7	0.11–0.10 *	16	0.09	50.6	0.13
210	21.0	0.11–0.10*	21	0.09	80	0.13
230	32.2	0.12	32.2	0.09	-	-

** Bagley Corrected*

Table 6.3b. *Critical apparent shear rates and shear stress values or the onset of sharkskin for ZN-HDPE-0 resin at different temperatures and different types of die.*

Temperature	***Capillary***		***Slit***	
(°C)	$\dot{\gamma}_{A,cr}$ (s^{-1})	$\sigma_{A,cr}$ *(MPa)*	$\dot{\gamma}_{A,cr}$ (s^{-1})	$\sigma_{A,cr}$ *(MPa)*
140	3.8	0.09	2.4	0.06
150	21	0.15 – 0.14*	32.2	0.16
160	50	0.19	160	0.24
170	50	0.18	250	0.28
190	312	0.29 – 0.23*	312	0.26
210	312	0.28	501	0.27
230	501	0.28 – 0.23*	501	0.26

** Bagley Corrected*

For the case of metallocene resin, there is no clear difference in its processing in capillary and slit dies, but a considerable improvement in its processability has been achieved in the annular die. Slit over capillary die also causes a small improvement in the processing of ZN-HDPE-0 compared to capillary die. The higher critical shear rates and stresses obtained in annular dies is believed to be due to the fact the extrudates at the exit possess a higher surface area to volume aspect ratio. This provides the ability of flow to have a 3D spiraling movement that provides additional degrees of freedom for the stress concentration at the die exit to be relieved as it is opposed in the case of capillary where the stress can be relieved only in one direction [6].

6.3.3 Effect of Die Entrance Angle

Fig. 6.11 depicts the flow curves for resin m-HDPE-1 at relatively low temperature T=160°C in capillary dies with different entrance angles namely 15°, 45° and 90° (data for 30° and 60° were obtained but not plotted for the sake of clarity. Other data are plotted in Appendix C.1.2). As it was discussed before with reference to Fig. 6.2a, this resin exhibits FIC at high rates with the effect to be more dominant for extensional flows. The same effect can be inferred from Fig. 6.11. The effect is mitigated by decreasing the entrance angle simply due to a decrease in the average Hencky strain rate in the entry region of the die.

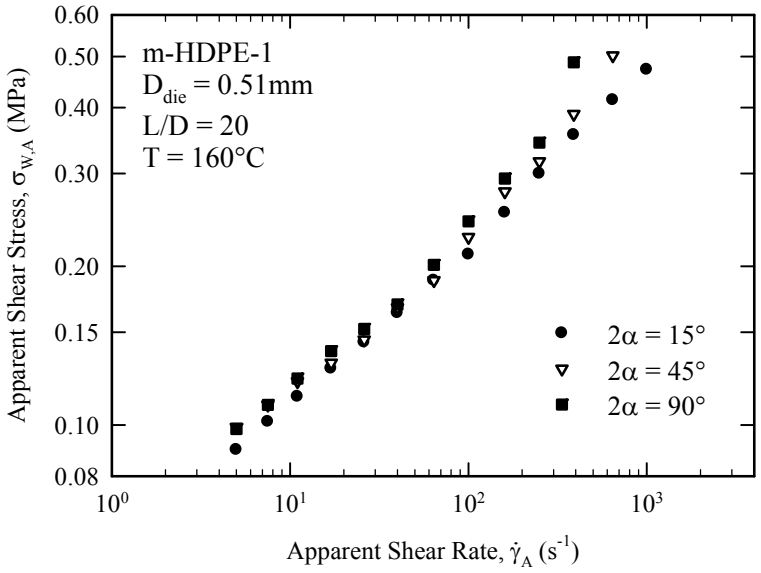

Figure 6.11. *The effect of die entrance angle on the flow curve and processing of resin m-HDPE-1 at T=160°C.*

Table 6.4 lists the critical apparent shear rate and shear stress values for the onset of sharkskin for resin m-HDPE-1 extruded through dies having different entrance angles. It appears that use of a low contraction angle die improves processing significantly (see Table 6.4). There are a few studies on the effect of die entrance angle on the sharkskin and most of them not systematic although they appear to support the findings of the present work [3, 69]. According to Moynihan et al [55] for the case of fully developed flows (L/D > 10) [7], sharkskin is influenced by stresses encountered by the melt in the upstream area. Since a low contraction angle keeps extensional stresses to lower levels compared with those at larger contraction angles, a relative improvement is expected.

Table 6.4. *The critical apparent shear rate and shear stress values for the onset of sharkskin in capillary extrusion with dies having different entrance angles for resin m-HDPE-1 at two different temperatures.*

Die Entrance Angle (°)	*T=190°C*		*T=160°C*	
	$\dot{\gamma}_{A,cr}$ (s^{-1})	$\sigma_{A,cr}$ (*MPa*)	$\dot{\gamma}_{A,cr}$ (s^{-1})	$\sigma_{A,cr}$ (*MPa*)
15	50.6	0.13	20.0	0.14
30	32.2	0.12	13.7	0.14
45	32.2	0.10	13.7	0.13
60	21.0	0.10	13.7	0.11
90	21.0	0.10	9.1	0.11

6.3.4 Effect of Processing Aid

In order to overcome sharkskin and to render the processes economically feasible, polymer processing aids (PPAs) are frequently used. PPAs can eliminate the sharkskin and the stick-slip or postpone them to higher flow rates. The end result is an increase of the productivity as well as an energy cost reduction, while high product quality is maintained. The additives mostly used for polyolefin extrusion processes are fluoropolymers [92-94]. Amos et al [185] and Achilleos et al [96] have reviewed the formulation, applications and performance of various processing aids. The fluoropolymer particles in the melt flowing next to the solid wall gradually coat the die wall thus providing a layer for polyethylene to slip [4, 94, 186].

Figs. 6.12a and 6.12b illustrate the effect of adding 0.1 wt% of a fluoropolymer (referred as PPA) on the flow curves of m-HDPE-1 and ZN-HDPE-0, respectively. The PPA has no significant effect on the flow curve of m-HDPE-1 in terms of both decreasing the pressure drop needed for flow and the processability. On the contrary it appears to be more effective for the case of ZN-HDPE-0. Mavridis and Fronek [187] have reported that PPA efficiency increases for the broader MWD resins. While this is true for ZN-HDPE-0, it is not for the m-HDPE-1. It will be shown in the next chapter that the m-HDPE-1 slips significantly on the die wall. Hence, addition of PPA does not cause further slippage. However, in the case of ZN-HDPE-0, the slip in the presence of PPA is significant as the pure melt does not slip at all. Therefore a large reduction in the pressure drop is expected. This pressure (or shear stress) reduction causes the significant improvement in the processability of ZN-HDPE-0 in the presence of PPA.

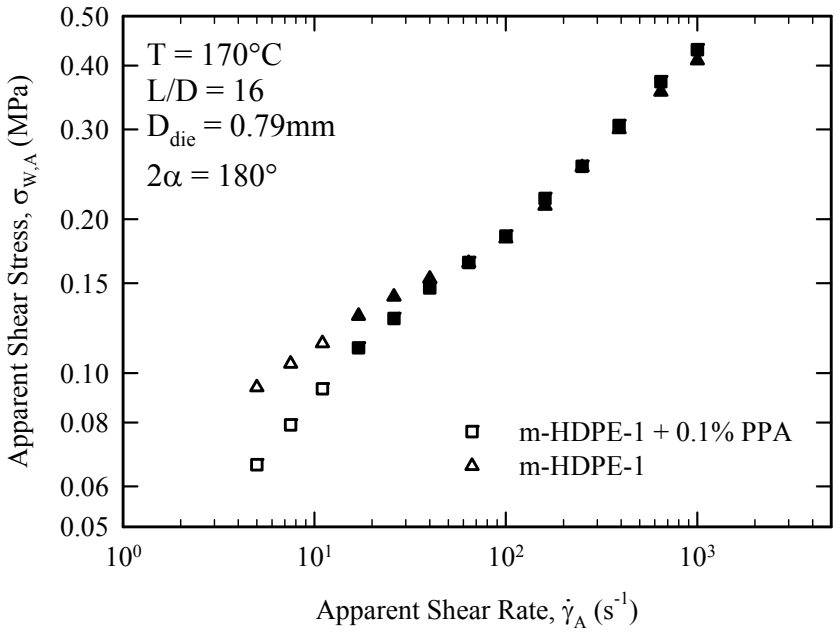

Figure 6.12a. *The effect of 0.1% PPA on the flow curve of m-HDPE-1 at T= 170°C. The open and closed symbols represent smooth and rough extrudates, respectively.*

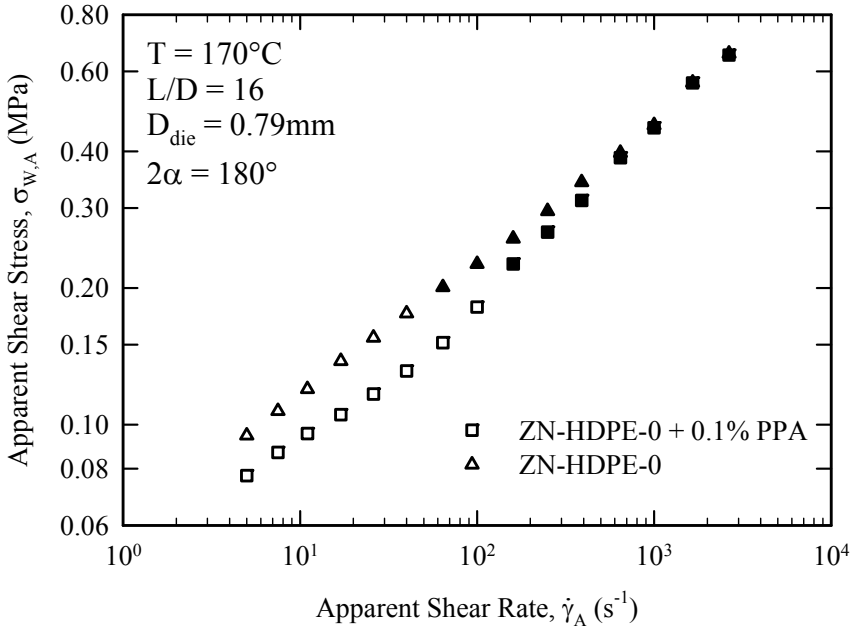

Figure 6.12b. *The effect of 0.1% PPA on the flow curve of ZN-HDPE-0 at T= 170°C. The open and closed symbols represent smooth and rough extrudates, respectively.*

6.4 Correlations for Critical Stresses

Using a development for the critical shear stress for the onset of sharkskin proposed by Graessley [39] and data reported in the literature for m-HDPEs [109, 188-190], Allal et al [90] derived Eq. 6.5 to correlate the critical shear rate for the onset of sharkskin with molecular parameters:

$$1/\dot{\gamma}_c = (0.16\tau_0 M_e^{1.5}/M_0^2)(M_w/M_e)^{4.3} \tag{6.5}$$

Where $\dot{\gamma}_c$ is the critical shear rate for the onset of sharkskin, τ_0 is an elementary characteristic time independent of molecular weight, which includes the effects of temperature and chain microstructure [191] and M_0, M_e and M_w are monomer molecular weight, average molecular weight between entanglements and weight average molecular weight, respectively. In Eq. 6.5, except M_w, all the other parameters in the right hand side are independent of molecular weight. Therefore, by rearranging Eq. 6.5, the following correlation can be easily derived:

$$\dot{\gamma}_c \propto M_w^{-4.3} \tag{6.6}$$

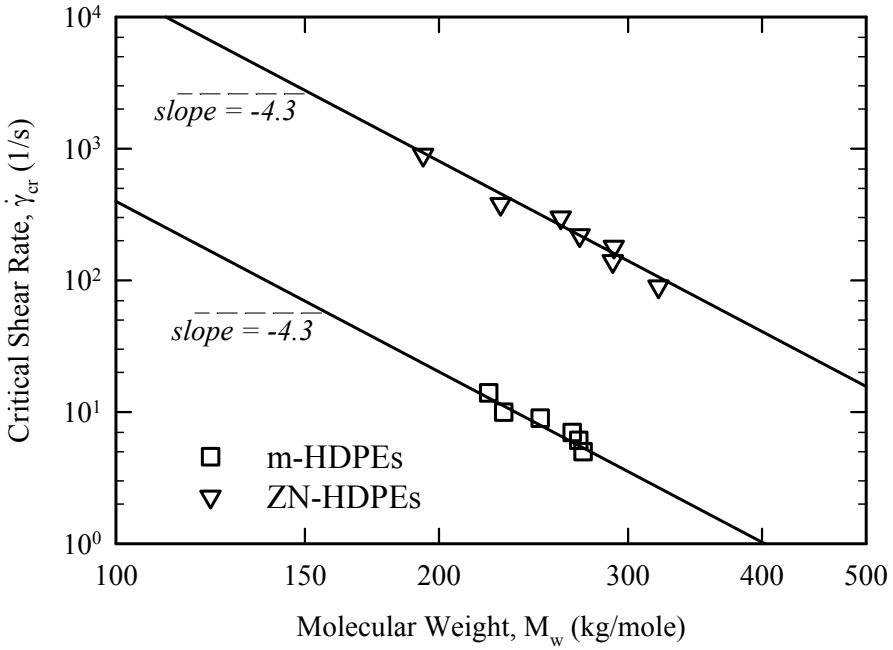

Figure 6.13. *Correlation between critical shear rate for the onset of sharkskin and weight average molecular weights of m-HDPEs according to Eq. 6.6.*

Fig. 6.13 depicts such a scaling for the cases of the m-HDPEs and ZN-HDPEs resins. Although both groups follow the same scaling, the pre-factors for the Eq. 6.5 are different. The critical shear rates for the onset of sharkskin for the ZN-HDPEs appear to be one order of magnitude higher than those for the m-HDPEs.

The critical shear stress for the onset of sharkskin, σ_{c1}, can be correlated with the molecular weight distribution parameters as is illustrated in Fig. 6.14. This correlation can be written as below:

$$\sigma_{c1} = \frac{PI_w^{0.5}}{4 \times PI_z \times (M_z/877{,}000)} \tag{6.7}$$

Where $PI_z \equiv M_z/M_w$ and the number 877,000 is used as a reference M_z value.

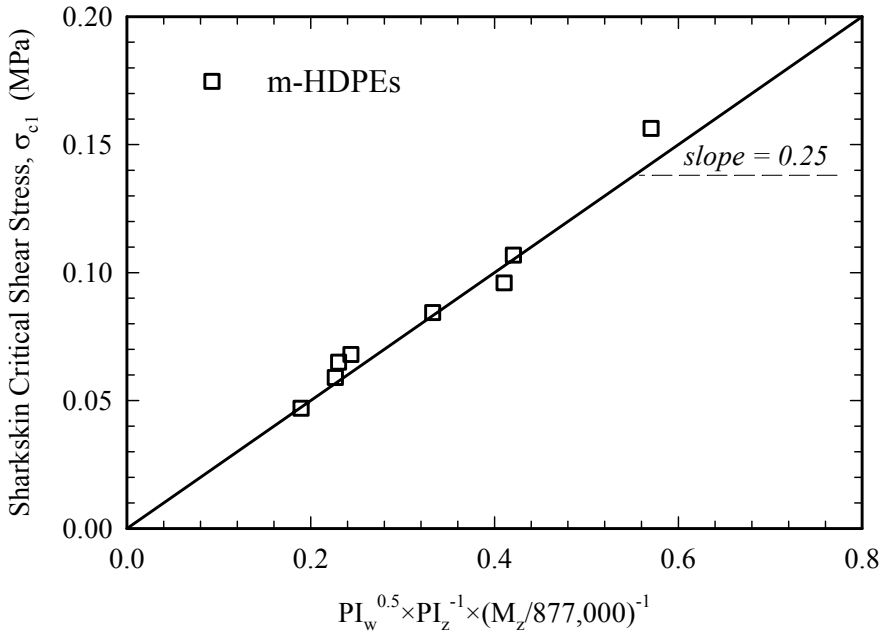

Figure 6.14. *Linear correlation between critical shear stress for the onset of sharkskin and molecular weight distribution parameters for m-HDPEs according to the Eq. 6.7.*

The values of the critical stress for the onset of gross melt fracture for the HDPEs with PDI<19 are in the range of 0.20-0.32 MPa which is in agreement with the reported values for HDPEs [3, 8, 58, 63, 100, 112]. However, these values for the case of m-HDPEs with PDI>19 are well below the values reported in the literature.

Regarding the critical shear stress, σ_{c2}, for the onset of stick-slip transition, based on the cohesive failure molecular mechanism (disentanglement), it has been shown that $\sigma_{c2} \propto M_w^{-0.5}$ [65, 108]. This correlation appears to hold as demonstrated in Fig. 6.15 where data from the present study as well as from other studies on HDPEs are plotted. The continuous line in Fig. 6.15 is:

$$\sigma_{c2} = \sigma_{cr}(M_w/56{,}000)^{-0.5} \tag{6.8}$$

where σ_{cr} is a critical reference stress equal to 0.71 MPa and 56,000 is a normalization molecular weight in g/mol.

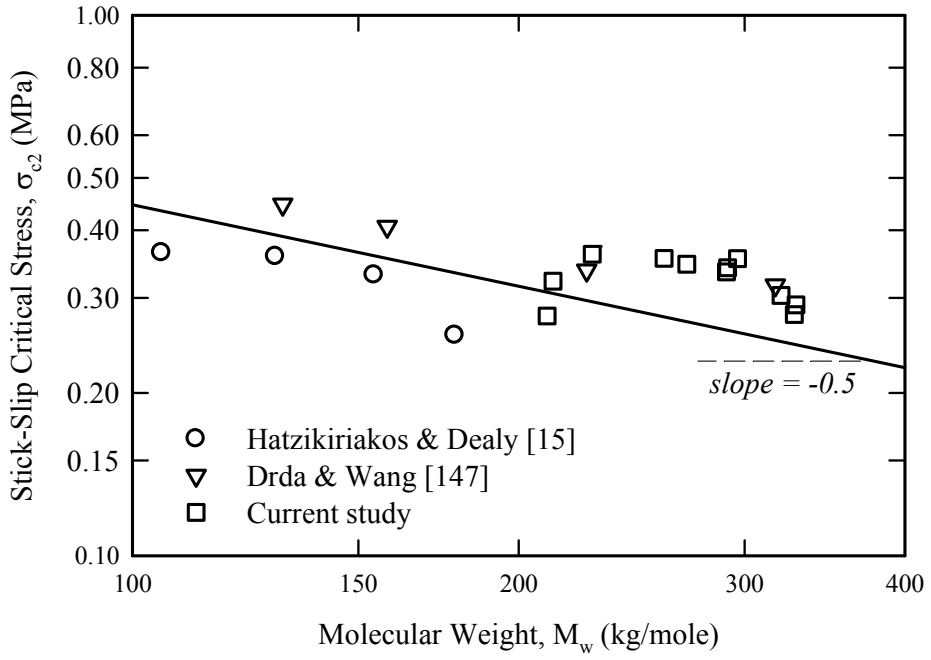

Figure 6.15. *The relation between critical shear stress for the onset of stick-slip with weight average molecular weight for different HDPEs at T=190°C.*

Moreover, as it has been reported in previous studies [3, 100, 112, 148], the critical shear rate for the onset of stick-slip instability is an increasing function of temperature, while the σ_{c2} is practically a weak function of temperature and about equal to 0.3 MPa. This value is in the range of 0.22-0.50 MPa reported by Hatzikiriakos and Dealy [8] for HDPEs of various molecular characteristics. These observations are also in agreement with present experimental results.

For a polymer of known molecular weight, M_w, σ_{c2} can be calculated from Eq. 6.8. Then to complete the prediction of the transition from weak to strong slip an equation for σ_{c3} is needed. Such an expression was proposed by Hatzikiriakos [143]. It was assumed that after the sudden disentanglement at the critical shear stress of σ_{c2}, the stress relaxes exponentially from σ_{c2} to σ_{c3} for the reestablishment of entanglements with a characteristic time proportional to the longest relaxation time. As zero shear viscosity is also proportional to the longest relaxation time, the following expression can be readily derived:

$$log(\sigma_{c2}/\sigma_{c3}) = \eta_0/\eta_R \tag{6.9}$$

Where η_R is some reference viscosity (a constant) equal to 20 Pa.s. Fig. 6.16 plots $log(\sigma_{c2}/\sigma_{c3})$ as a function of zero shear viscosity for high-density polyethylenes studied by Hatzikiriakos and Dealy [15] and data from the present work. The continuous line represents Eq. 6.9.

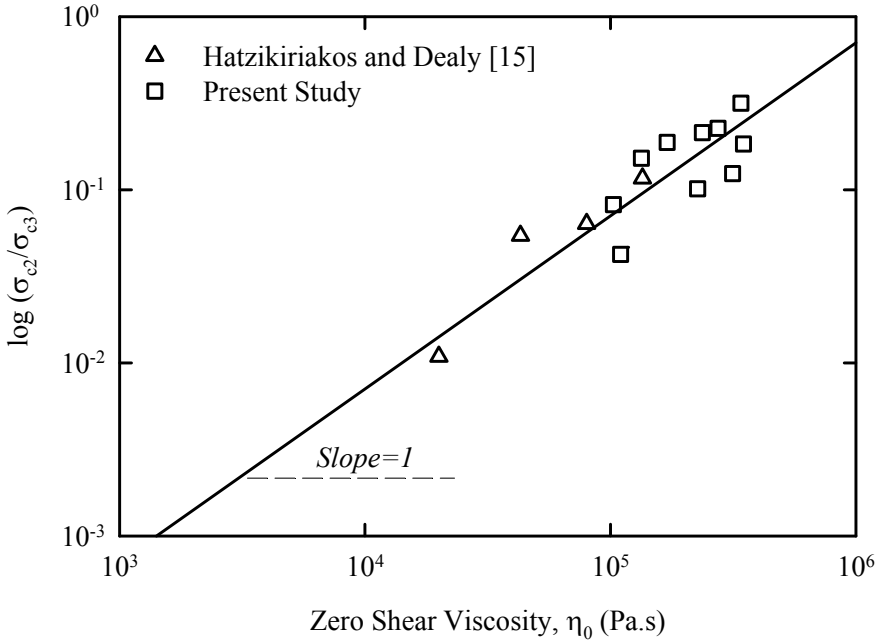

Figure 6.16. *Scaling of the ratio of the critical shear stresses for the onset of stick-slip transition and the critical shear stress for the onset of gross melt fracture with zero shear viscosity for high-density polyethylenes.*

6.5 Summary

In this chapter, the effects of processing conditions and molecular parameters on the melt fracture of broad molecular weight ZN-HDPEs and m-HDPEs have been discussed. The results showed that although these resins exhibited similar rheology both in shear and extension, they exhibited markedly different melt fracture behaviour. In contrast with previous studies, the m-HDPEs which had a broader molecular weight distribution, showed markedly worse processing properties compared to their ZN counterparts.

According to the experimental results, the critical shear stresses for different modes of melt fracture were almost insensitive to the temperature, but the critical shear rates shift to the higher values with temperature. The type of die has also been shown to affect the processing properties of the resins, i.e. better processability was found by switching from capillary dies to slit dies and much better in the case of annular dies. Based on the findings of this work, it can be concluded that the die entrance angle has a significant effect on the processability of HDPEs particularly at low entrance angles of 15 to 30°. Regarding the effect of PPA, it was shown that it is not effective in the case of m-HDPE resins, and it works better for the case of ZN-HDPEs. This is due to the significant slip of m-HDPEs which is the subject of study of chapter 7.

It was also found that the HDPEs with PDI<19 exhibit stick-slip instability, however, this is not the case for the m-HDPEs with PDI>19. A molecular mechanism was discussed that describes this behaviour quite well i.e. a criterion was derived for the occurrence of the stick-slip transition. Therefore based on these findings, resins with polydispersity in the range 9<PDI<19 exhibit superior processability compared to those with relatively narrow (PDI<9) and those of very broad MWD (PDI>19).

Finally, some interesting correlations were derived between the critical shear stress and shear rate for the onsets of sharkskin, stick-slip transition and gross melt fracture and molecular parameters. These correlations have been verified by experimental findings.

7 WALL SLIP OF HDPEs

Slip plays an important role in rheology and processing of polymers. In this chapter, the wall slip of Ziegler-Natta and metallocene HDPE resins is studied. The Cox-Merz rule for these resins is tested and possible origins of its failure are discussed. The Mooney analysis for slip is performed by using capillary data for dies having the same L/D and different diameters. The effects of molecular weight and molecular weight distribution on slip are also studied. Finally, slip models are proposed that can be used to completely predict the flow curves of HDPEs.

7.1 Cox-Merz Rule

The Cox-Merz rule is an empirical relationship stating that the shear viscosity is identical with complex viscosity at corresponding shear rates and angular frequencies [192]. This rule is practically important, because one may use it to predict shear viscosity using dynamic data (easier to measure). The Cox-Merz rule has been verified experimentally for many materials including PCLs [193], PEs [120], PSs [192, 194], metallic glasses [195] and many others. On the other hand, Venkatraman et al [196] and Vega et al [48] have reported that the Cox-Merz rule failed for HDPEs and m-HDPEs respectively and the origin of this failure remained unknown.

Figs. 7.1a and 7.1b plot the complex modulus $|G^*(\omega)|$ and the apparent wall shear stress, $\sigma_{W,A}(\dot{\gamma}_A)$, obtained from capillary rheometer for both ZN and m-HDPEs. For the sake of clarity each curve has been multiplied by a factor listed in Figs. 7.1a and 7.1b. It is clear that the Cox-Merz rule approximately applies for the case of ZN-HDPEs at all shear rates and frequencies. On the other hand, the Cox-Merz rule fails for all m-HDPEs. Capillary data for stresses greater than 200 s^{-1} where gross melt fracture effects are significant are not plotted. In addition the data have not been corrected for entrance pressure effects (Bagley correction) which are insignificant at these relatively small shear rates.

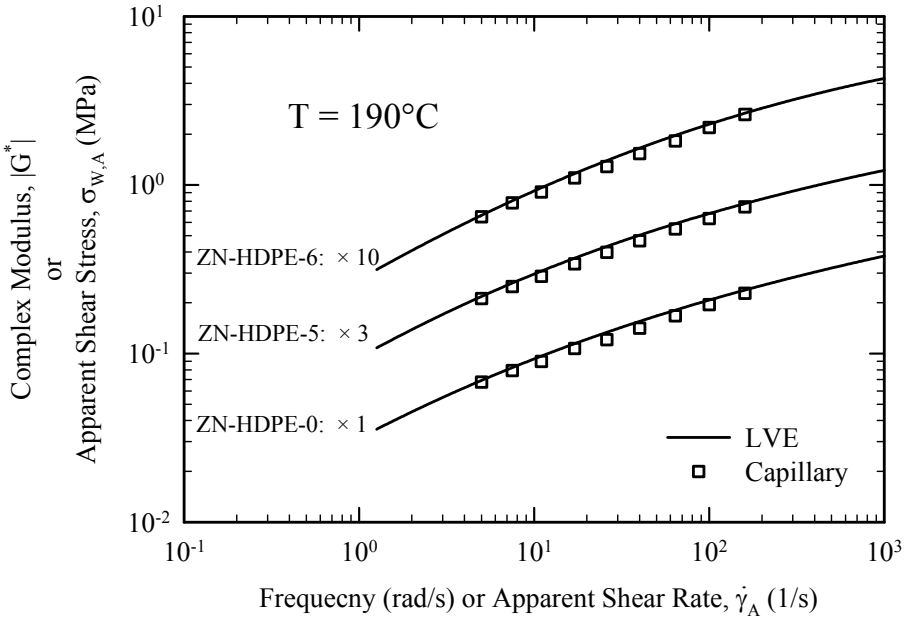

Figure 7.1a. *Testing the applicability of the Cox-Merz rule for a series of ZN-HDPEs at 190°C.*

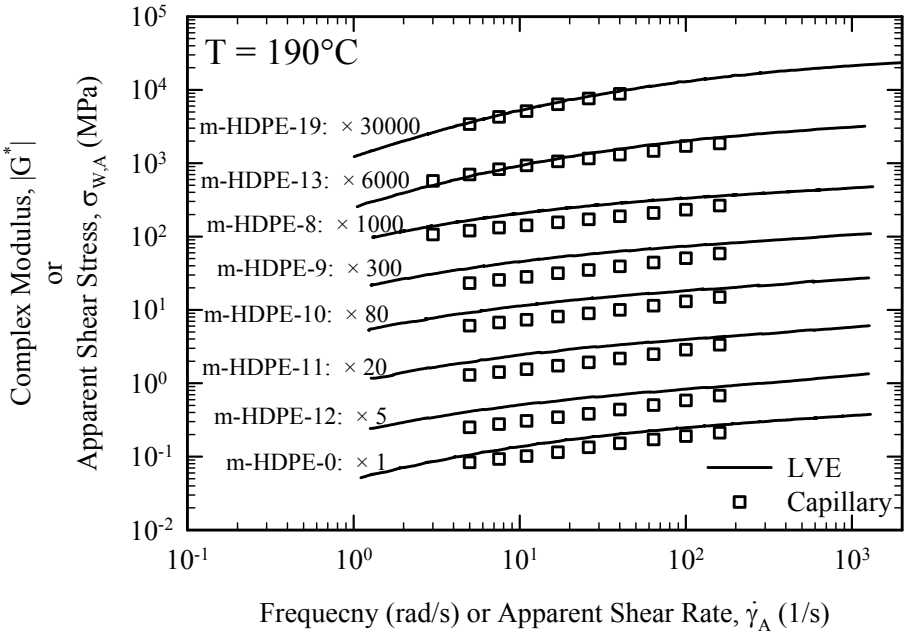

Figure 7.1b. *Testing the applicability of the Cox-Merz rule for a series of m-HDPEs at 190°C.*

The failure of the Cox-Merz rule might originate from a number of reasons which are examined next. First, when capillary experiments are performed at temperatures close to melting point, stress-induced crystallization originating at the entrance to the capillary where strong extensional effects apply, might cause an increase of $\eta(\dot{\gamma})$ compared to $|\eta^*(\omega)|$ (which is opposite to the failure of Cox-Merz rule we are familiar with). A similar effect ($\eta(\dot{\gamma}) > |\eta^*(\omega)|$) might exist due to a strong dependency of viscosity on pressure [11]. The $\eta(\dot{\gamma})$ should also be obtained at rates below those where instabilities such as stick-slip or oscillating melt fracture occurs.

Viscous heating effects might cause $\eta(\dot{\gamma})$ to be lower than $|\eta^*(\omega)|$ [37]. For HDPEs the effects of pressure and viscous heating on viscosity are not significant due to its low sensitivity to temperature and pressure [163].

Finally, failure of the Cox-Merz rule might be observed if the $\eta(\dot{\gamma})$ is not corrected for possible *slip effects* [149]. If this is the case, therefore, it is possible to calculate the slip velocities considering the deviation of flow curves from LVE data. This will be examined in the following sections.

7.2 Wall Slip Measurements

Fig. 7.2 depicts the diameter dependency of the flow curves for the m-HDPE-1 at T=190°C. The continuous line represents the LVE results presented in chapter 5 and Appendix A.1 plotted as flow curve ($|G^*(\omega)|$ versus ω). The diameter dependence of the flow curves is clear. This diameter dependence is consistent with the assumption of slip and the Mooney technique [3, 15, 36] can be used to determine the slip velocity as a function of shear stress by plotting $\dot{\gamma}_A$ versus $1/D$ (details for Mooney analysis are presented in Appendix E):

$$\dot{\gamma}_A = \dot{\gamma}_{A,S} + 8u_s/D \tag{7.1}$$

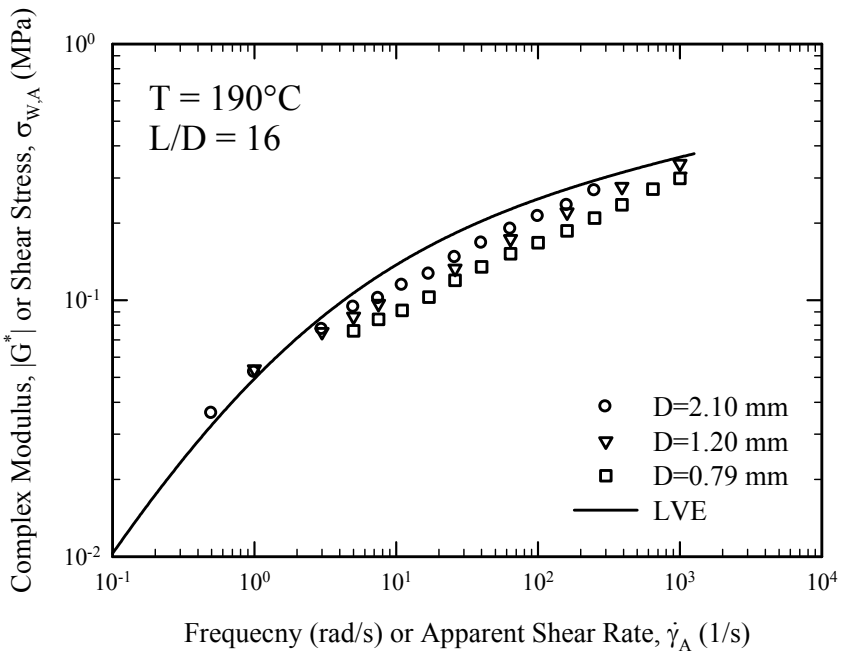

Figure 7.2. *The Bagley corrected flow curves of resin m-HDPE-1 at T=190°C for different diameters. The continuous line is LVE data.*

Moreover, the deviation of each flow curve of Fig. 7.2 that corresponds to a different diameters from the LVE curve can also be interpreted as wall slip by using $u_s = [\dot{\gamma}_A - (4n/3n+1)\omega] \times D/8$ at a given wall shear stress value that corresponds to the frequency, ω. If the assumption that Cox-Merz rule failure is mainly due to slippage, the slip velocities from the two methods should be the same.

Fig. 7.3 depicts slip velocity of m-HDPE-1 at T=190°C obtained from Mooney analysis along with the ones calculated from flow curves deviation of LVE data for different diameters. As it is clear from this figure, the data agree well which supports the previous assumption i.e. slippage is responsible for Cox-Merz failure.

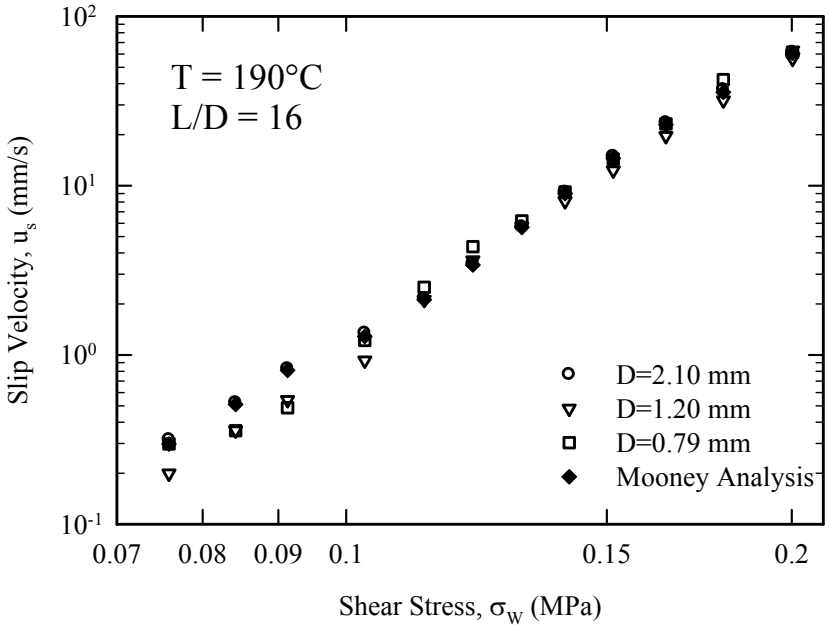

Figure 7.3. *Slip velocities of resin m-HDPE-1 at T=190°C. The open symbols are obtained from flow curves deviation of LVE data for different diameters.*

7.3 Slip Velocities

7.3.1 Effect of Temperature

Fig. 7.4a plots the slip velocities of resin m-HDPE-1 at different temperatures from 190°C to 230°C. The slip velocity increases with temperature consistent with the time-temperature superposition (TTS). It is noted that calculated slip velocities less than 1 mm/s have been neglected as insignificant (within experimental error). Using the values of the shift factors obtained from linear viscoelasticity, the slip velocity curves can be brought together to obtain a master slip velocity curve which implies a power law trend as, $a_T u_s = a\sigma_w^m$. This is shown in Fig. 7.4b where a reasonable superposition has been obtained.

Based on the slip velocity calculations, the HDPEs can be placed into two major groups: In the first group belong to these HDPEs of typically wide molecular weight distribution (PDI>19) that slip readily and significantly at relatively low values of the wall shear stress. These resins exhibit no stick-slip transition and the Cox-Merz rule typically fails due to significant slip. The second

group of resins exhibit stick-slip transition. The Cox-Merz rule is approximately obeyed for low polydispersity polymers, where the stick-slip is dominant and occurs over a wide range of apparent shear rates. For the second group of resins both their flow curve and slip velocity are subdivided into two distinct branches (double valued function over certain range of rates) [179].

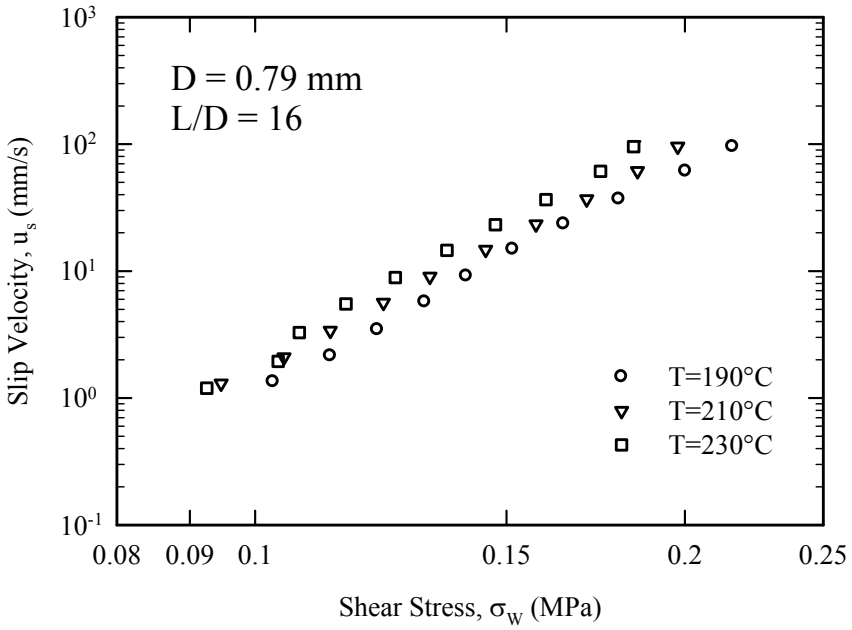

Figure 7.4a. *The slip velocity of m-HDPE-1 as a function of wall shear stress at different temperatures from 190°C to 230°C.*

7.3.2 Slip Velocity of Polymer Exhibiting Stick-slip ($M_w/M_e > \lambda \times PDI$)

Fig. 7.5 plots the slip velocities for some of the resins which show stick-slip instability. The slip velocities for the low-flow branch show that the magnitude of slip increases with increase of polydispersity. For the high-flow rate branch, the slip velocities are essentially of the order of plug flow and they seem to be independent of the molecular characteristics of the polymer [8]. The jumps from the lower branch to the upper and from the upper to the lower occur discontinuously in the oscillatory flow region, and are shown by the two arrows for ZN-HDPE-5 in Fig. 7.5. These jumps seem to scale with PDI, although molecular weight has an additional effect. Roughly as PDI decreases, the range of shear rates over which stick-slip flow increases and this also makes the magnitudes of the jump to increase [8].

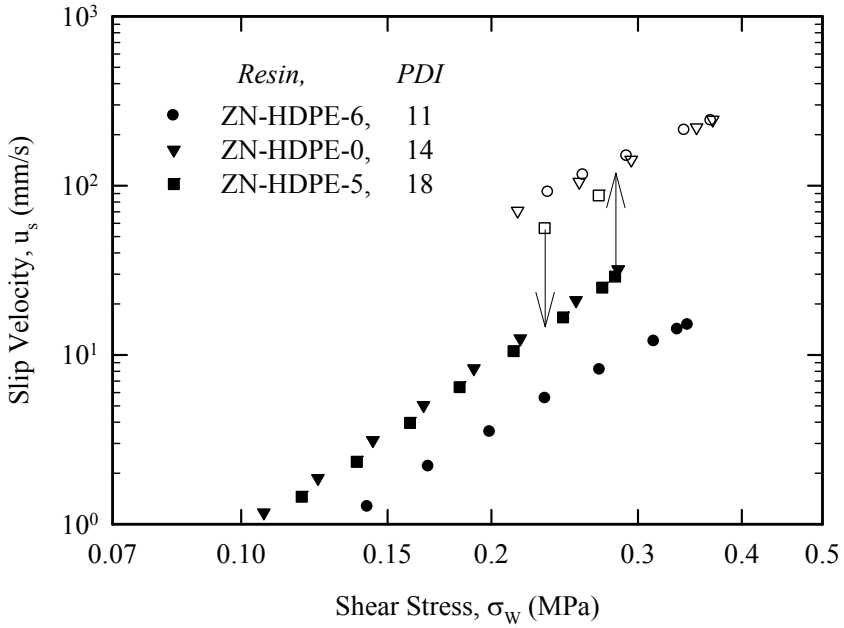

Figure 7.5. *The slip velocity of selected HDPEs which exhibit stick-slip as a function of wall shear stress at T=190°C. The arrows show transition from weak (closed symbols) to strong slip (open symbols) and vice versa for ZN-HDPE-5.*

It is interesting to examine how the slip velocity scales with molecular characteristics of the HDPEs. For this purpose we will also use the data reported by Hatzikiriakos and Dealy [15] for a series of HDPEs of various molecular weights and polydispersities.

Fig. 7.6 plots a master curve for the slip velocity for resins of low to moderate polydispersities up to 19 (HDPEs which obey $(M_w/M_e > \lambda \times PDI,$ see Fig. 6.8) including those reported by Hatzikiriakos and Dealy [15] shown as Resins A-F. An overall good superposition is obtained. It can be observed that the slip velocity increases with increase of polydispersity and decreases with increase of molecular weight. The numerical value of 56,000 is chosen as a convenient normalization value for the molecular weight. A slope of roughly 3 can be obtained from Fig. 7.6, which results in the following scaling for the slip velocity model for these polymers (straight line in Fig. 7.6):

$$a_T u_s = \alpha_{A,L}\left[\sigma_w PI_w/(M_w/56{,}000)^{2/3}\right]^3 \tag{7.2}$$

here $\alpha_{A,L} = 9.3 \times 10^{-3}\, m.MPa^{-3}.s^{-1}$ is the proportionality constant of the lower slip velocity branch for the first group of resins (A group) with PDI<19. The slip velocity for the upper branch is essentially nearly plug flow (as the flow mean velocity is about 90% of the slip velocity) slip velocity and it can be described by $a_T u_s = \alpha_{A,U}\sigma_w^3$ where $\alpha_{A,U} = 5.4 \times 10^{-3}\, m.MPa^{-3}.s^{-1}$ is the proportionality constant of the upper slip velocity branch for the first group of resins (A group) with PDI<19. This Equation can be transformed into a flow curve to describe the upper branch for all HDPE's by substituting u_s with $D\dot{\gamma}_A/8$. It is noted that the upper branch of the flow curve is of no importance as the polymers in this flow regime exhibit gross melt fracture and no process operates at such high shear rates. As also pointed out above at very high frequencies, the complex viscosities of the various resins converge, as well as their flow curves and thus their slip velocities become independent of molecular characteristics.

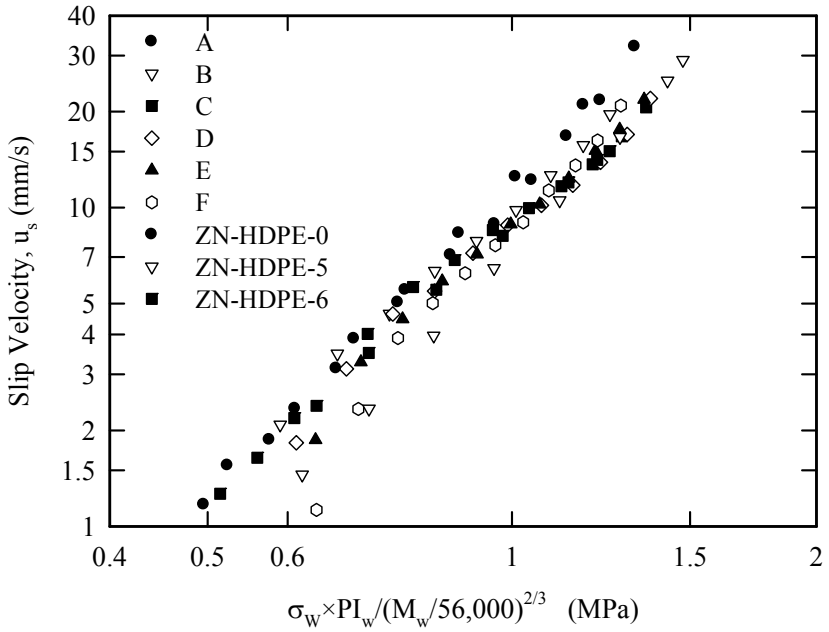

Figure 7.6. *Master curve for the slip velocity of HDPEs of the present study and those (resins A-F) studied by Hatzikiriakos and Dealy [15] at 190°C.*

As discussed above the increase of slip velocity with decrease of molecular weight has been observed for several nearly monodisperse systems, namely PSs [155, 156], PBs [149, 153, 154] and recently for PLAs [157]. The observation that the slip velocity increases with polydispersity is a new, although it is in order with the effects of polydispersity on the flow curves of HDPEs. As polydispersity increases from very low values, the size of the stick-slip transition (distance

between the two flow curves at the transition point) decreases (see Fig. 7.6). Moreover, the range of apparent shear rates over which stick-slip occurs decreases as can be seen to a certain extend from Fig 6.6 and as explained by Myerholtz [99].

7.3.3 Slip Velocity of Polymers with Continuous Flow Curve ($M_w/M_e < \lambda \times PDI$)

Fig. 7.7 plots the slip velocity of m-HDPEs at 190°C, those that do not exhibit stick-slip transition. The slip velocities were calculated based on the Mooney technique and based on the difference between the LVE master and the capillary flow curves. The slip velocities exhibit a power-law dependence on wall shear stress as also shown before [15]. On the same graph we have also plotted the slip velocities of the high flow rate branch of the HDPEs that exhibit stick-slip (plug flow slip velocities). It can be seen, the slip velocities of the m-HDPEs tend to attain almost plug flow at high enough levels of shear stress and that at these levels slip velocity becomes independent of molecular parameters.

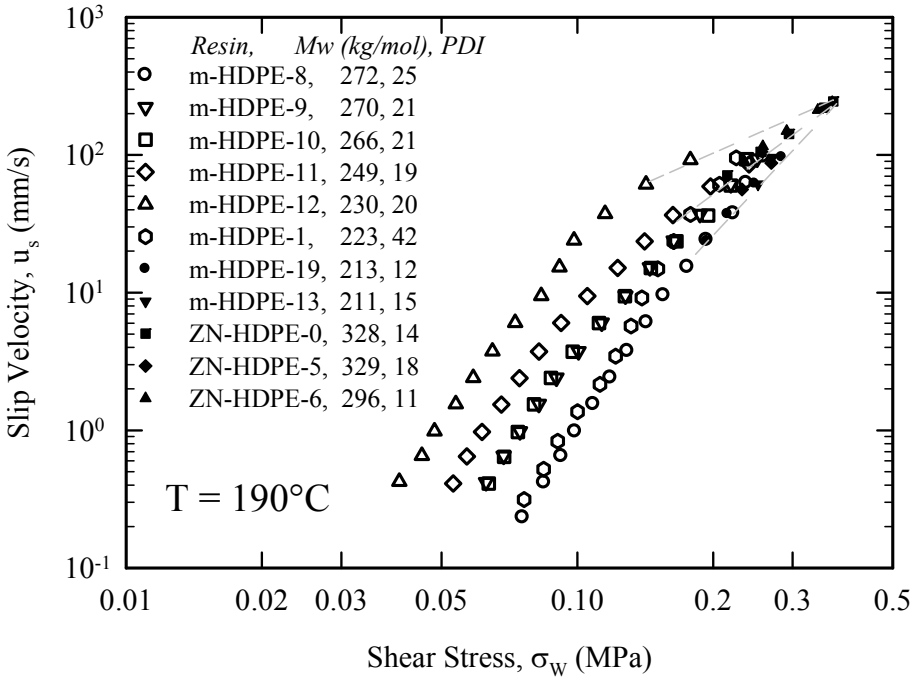

Figure 7.7. *The slip velocities versus wall shear stress for the all the HDPE resins at T=190°C. The open symbols correspond to the data after stick-slip phenomenon.*

The slip data for the m-HDPE resins can be brought into a master curve by normalizing the vertical and horizontal axis by appropriate molecular parameters. The superposition is satisfactory. As seen in Fig. 7.8 the slip velocity increases with molecular weight also found for the previous set of resins (stick-slip) although this time the dependence is much stronger. Surprisingly, the polydispersity for these resins have an effect opposite to what have been seen for the stick-slip HDPEs. The slip velocity decreases with increase of PDI. Apparently chains with molecular sizes far apart (high polydispersity) interact in a different manner as far as slip velocity concerns compared to molecular sizes that are much closer (low polydispersity). It appears that for a given molecular weight, there is a distribution that maximizes the slip velocity (around the point where the stick-slip transition occurs). A slope of roughly four can be obtained from Fig. 7.8, which results the following Equation for the slip velocity,

$$a_T u_s = \alpha_B [\sigma_w / PI_w \times (M_w/56{,}000)^{2.5}]^4 \tag{7.3}$$

Where $\alpha_B = 4.47 \times 10^{13}\ m.MPa^{-4}.s^{-1}$ is the proportionality constant of the slip velocity for the B group of resins with PDI>19. The power dependence of the slip velocity on wall shear stress is now 4 compared to 3 found before. Powers between 3 to 6 for the slip velocities of polyethylenes have been reported by various authors summarized by Hatzikiriakos [136]. The power of 10 for the molecular weight might seem unreasonable. For these wide molecular weight distribution resins, higher moments of molecular weight should play a role as these distributions are not typically symmetric i.e. normal distributions. However, the objective here was to find a scaling that involves the minimum number of molecular parameters. Another possible reason is that all these resins have molecular weights in the short range of 220,000 to 270,000 and possibly this causes the high exponent.

At any rate, this study appears to be the first to consider the combined effects of molecular weight and polydispersity on the slip velocity for several HDPEs of practical importance, namely HDPEs that exhibit stick –slip transition (low to moderate molecular weight distribution) and HDPEs which do not exhibit such transitions (wide molecular weight distribution and wide molecular weight distributions). Certainly more studies are welcome in the area as was recently stressed in a review article by Hatzikiriakos [136].

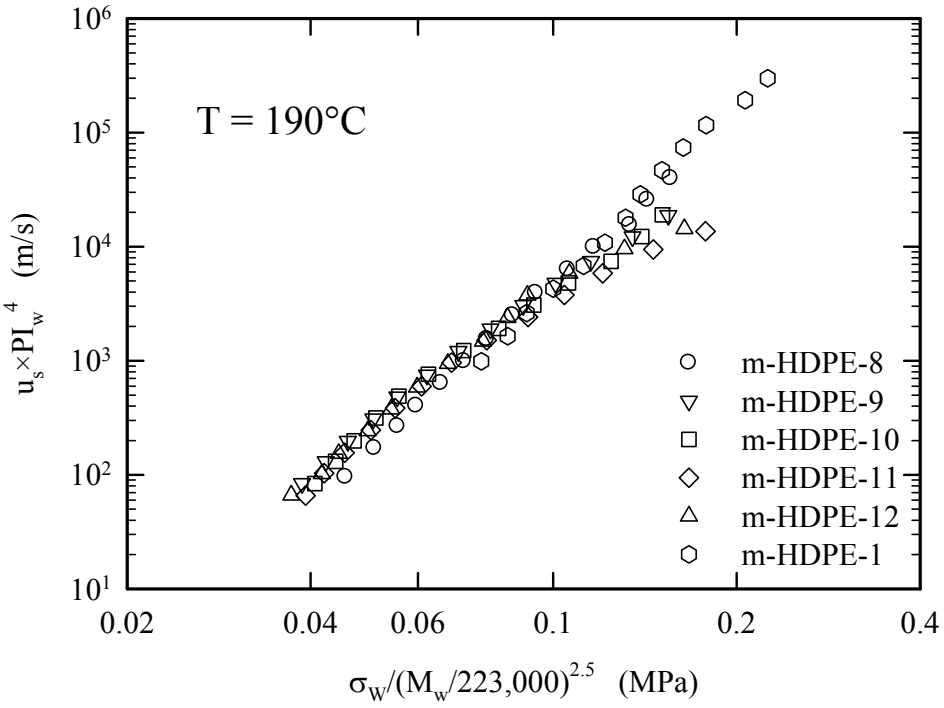

Figure 7.8. *Master curves for the slip velocities of m-HDPEs that do not exhibit stick-slip transition at T=190°C.*

7.4 Construction the Flow curves of HDPEs

Based on developments through this study, the flow curves of HDPEs can be constructed. An example is shown in Fig. 7.9 for ZN-HDPE-6 that exhibits stick-slip transition. Starting from its LVE behaviour, its low flow rate branch for a capillary die of a certain diameter, *D*, can be predicted by utilizing Eq. 7.2 for the slip velocity coupled with $u_s = [\dot{\gamma}_A - (4n/3n+1)\omega] \times D/8$. This part of the flow curve is stopped at σ_{c2}, which value can be determined by Eq. 6.8. The value of σ_{c3} can be calculated from Eq. 6.9 using the value of σ_{c2}. The approximate upper flow curve of the polymer can be calculated from $a_T u_s = a_{A,U}\sigma_w^3$ by replacing u_s with $D\dot{\gamma}_A/8$. As it can be seen from Fig. 7.9, the overall representation of the experimental flow curve is good. Similar results were obtained for all HDPEs studied in this work (more constructed flow curves can be found in Appendix F).

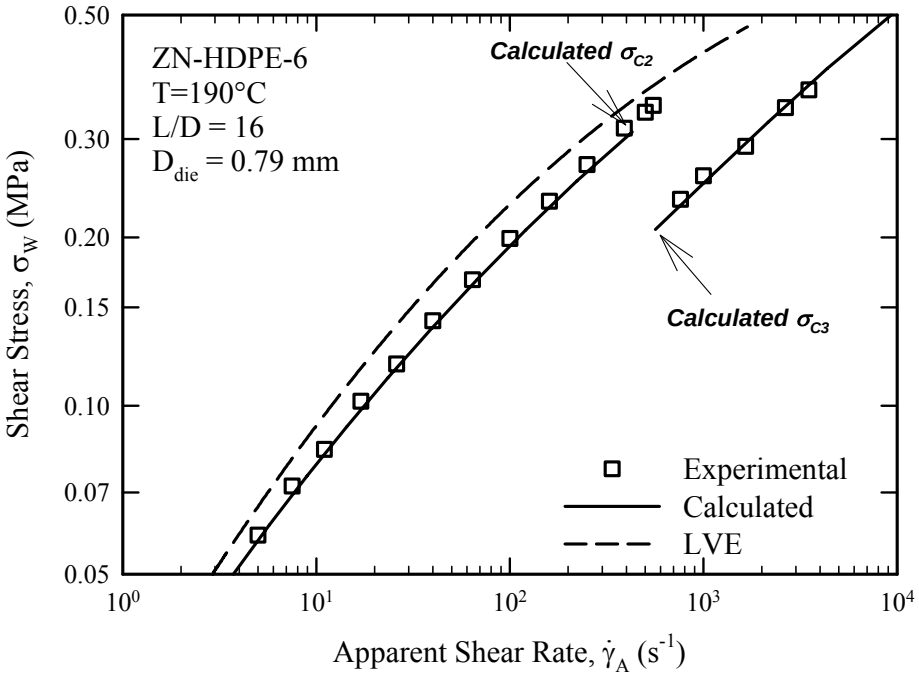

Figure 7.9. *Constructing the flow curve of ZN-HDPE-6 starting from LVE data.*

7.5 Summary

Wall slip of ZN-HDPEs and m-HDPEs was the subject of this chapter. Firstly, the validity of Cox-Merz rule for available resins was assessed and it failed for m-HDPE resins with PDI>19. To check the idea that slip is responsible for such a failure, slip velocities were calculated by means of Mooney analysis as well as the flow curves deviation from LVE data. The agreement of the calculated slip velocities from both methods supports the mentioned hypothesis.

The effects of molecular weight and molecular weight distribution were also studied. It was shown that for the resins which show stick-slip instability, there are two distinct slip regimes i.e. the weak and strong slip regimes attributed to the low and high branches of flow curve, respectively. The slip velocity in the strong mode is a plug/semi-plug flow and almost independent of molecular characteristics. However, the slip velocity in the weak regime was found to increase with decrease of molecular weight and polydispersity. Moreover, the gap size between these two regimes was found to increase with decrease of polydispersity.

Contrary to the ZN-HDPEs, the m-HDPEs with continuous flow curves exhibit a continuous slip velocity as a function of wall shear stress. Their slip velocity was also found to increase with decrease of molecular weight, but contrary to the stick-slip resins, increases with the polydispersity index.

Finally, starting from LVE results and based on the derived correlations, the flow curves of some stick-slip resins were constructed which were fairly in agreement with experimental results.

8 CONCLUSIONS AND CONTRIBUTIONS TO KNOWLEDGE

8.1 Conclusions

The rheological properties of ZN and m-HDPEs of broad molecular weight distribution have been investigated. The relation between the zero shear viscosity and the weight average molecular weight showed a power exponent which was initially found to be higher than the experimentally accepted value of 3.6 reported for linear PEs in the literature. However, taking into account the effect of broad molecular weight distribution and applying appropriate corrections the universal exponent was recovered. The steady state compliance showed a power-law dependence on M_z/M_w as expected. It was also a power-law function of $(M_{z+1}/M_w) \times (M_{z+1}/M_z)$ with power of 2.2, as previously found based on molecular theories. The crossover modulus has been found to exhibit a similar dependence on M_z/M_w.

The processing behaviors of these resins (two different series of Ziegler Natta and metallocene) have also been studied. Although these resins exhibited similar rheology both in shear and extension, they exhibited markedly different melt fracture behaviour. The ZN-HDPEs were found to fracture at significantly higher critical shear stresses exhibiting superior processability compared to the m-HDPEs. Based on the extensional results and slip analysis, it was found that the origin of these differences lie in the difference in the shape of broadness of MWD of these two polyethylenes. The type of die has also been shown to affect the processing properties of the resins. For example it was found that the critical stresses for the onset of sharkskin are higher in the case of a slit die and much higher in the case of an annular die, when compared with the values obtained in capillary extrusion. The enhanced processability in the case of an annular die is due to the high surface area to volume aspect ratio which provides degrees of freedom for the stress concentration to be relieved easier at the die exit. It has also been shown that the die entrance angle had a significant effect on the processability of high density polyethylenes particularly at low entrance angles of 15 to 30°. The validity of Cox-Merz rule was also tested for all HDPE resins. It was shown that this rule is approximately valid for ZN-HDPEs and apparently fails for m-HDPEs. However, wall slip measurements have shown that slip effects are present in m-HDPEs and this is the reason for the apparent failure. Once capillary data were

corrected for slip effects, the Cox-Merz rule was shown to be valid for the m-HDPEs as well. It was also shown that the PPA is not effective in the case of the m-HDPEs due to significant slippage of these polymers in their absence. Therefore, addition of PPA cannot further increase its slip which can cause a drop in the shear stress which in turn can improve their processability. On the other hand, the ZN-HDPEs did not slip in the absence of PPA or slip very little. Then PPA itself can cause significant slippage and drop in the shear stress that is the main reason for its effectiveness. Regarding the oscillation defect, the results showed that the HDPEs with PDI<19 exhibit a stick-slip transition and as a result their flow curve consists of two distinct branches, namely a low flow rate and a high flow rate. These resins exhibited significant slip in the high flow-rate branch where their slip approaches almost plug flow. The HDPEs with PDI>19 exhibited no stick-slip transition and a molecular mechanism was discussed to this effect that describes this behaviour quite well i.e. a criterion was derived for the occurrence of the stick-slip transition. Although the m-HDPEs had a broader molecular weight distribution compared to their ZN counterparts, their processing properties were much worse. Therefore based on these findings, resins with polydispersity in the range 9<PDI<19 exhibited superior processability compared to those with relatively narrow (PDI<9) and those of very broad MWD (PDI>19). Moreover, some interesting correlations were derived between the critical shear stress and shear rate for the onsets of sharkskin, stick-slip transition and gross melt fracture and molecular parameters. These correlations have been verified by experimental findings and have been proven to hold true.

The slip velocities of all available HDPEs were studied in an attempt to elucidate the effects of molecular weight and its distribution on their slip behaviour. Two distinctly different flow behaviors were observed. For HDPEs obeying the simple rule ($M_w/M_e > \lambda \times PDI$) which are essentially HDPEs of high molecular weight and low polydispersity, stick-slip transition occurs that subdivides both the flow curve and the slip velocity as a function of wall shear stress into two branches (essentially double-valued functions). For such HDPEs the slip velocity was found to increase with decrease of molecular weight and polydispersity. Moreover, the jump in terms of slip velocity was found to increase with decrease of polydispersity. The higher slip velocities obtained in the upper branch at high shear stress values were essentially plug flow and roughly independent of the molecular parameters of HDPEs. On the other hand, HDPEs obeying the

simple rule ($M_w/M_e > \lambda \times PDI$) essentially HDPEs of medium to high molecular weight and high polydispersity exhibited both a continuous flow curve and a continuous slip velocity as a function of the wall shear stress. These resins did not exhibit stick-slip transition. Their slip velocity was also found to increase with the decrease of molecular weight, although the effect of PDI was surprisingly found to be opposite to that PDI was found to have for the HDPEs exhibiting stick-slip transition. It is expected that as molecular weight decreases to sizes comparable to these of surface asperities, the slip velocity should start declining to zero. More studies are needed in this area to fully explore and understand the effects of molecular weight parameters such as molecular weight and its distribution on the slip behaviors, particularly for multimodal distribution polymers.

8.2 Contributions to Knowledge

The present work has yielded the following contribution to knowledge:

1- From the linear viscoelastic measurements, for m-HDPEs with very broad molecular weight distribution, the zero shear viscosity is not only a power-law function of molecular weight, but also molecular weight distribution (M_z/M_w). Based on our finding in this study, the universal exponent of 3.6 for the M_w dependence was confirmed, along with proposed linear dependence of viscosity on M_z/M_w. The new pre-factors for this correlation at different temperatures also have been found. Moreover, the available theoretical and experimental correlations of steady state compliance with different measures of molecular weight distribution were verified.

2- According to the results of this study, the processing properties of these two types of resins are completely different, while their rheological characteristics are almost similar. It was concluded that the shape of broadness of MWD is responsible for such an observation.

3- This study adds new contribution to the few available data in the literature regarding the effect of die type on the processing characteristics. The findings support previous observations that processability can be enhanced by using slit dies compared to capillary ones and can be enhanced much more for the case of annular dies. It was also shown that the processability would be better for low entrance angles capillary dies. New

correlations between critical shear rates and shear stresses with molecular characteristics and rheological properties for the onset of instabilities were also proposed.

4- Although the Cox-Merz rule is approximately valid for HDPEs of narrow to moderate MWD HDPEs, it fails for m-HDPEs with a wide MWD. It has been shown in this work that slip effects are present in m-HDPEs and this is the reason for the failure. Once capillary data are corrected for slip effects, the Cox-Merz rule is shown to be valid for the m-HDPEs as well. So it is found in this study that the failure of the empirical Cox-Merz rule is an indication of considerable slip. Therefore, it is proposed that slip velocity can be calculated from deviation from LVE results (Cox-Merz rule).

5- Although there is considerable number of reports on the effect of M_w on the stick-slip defect, there are a few on the effect of MWD. It was shown that by increasing the MWD, the stick-slip transition decreases in size until disappearing for HDPEs with a polydispersity (PDI) roughly greater than 19. The results of this project have shown to support the criterion for the occurrence of stick-slip transition developed by Allal and Vergnes [16] based on the hypothesis of disentanglement between tethered chains on the surface and molecules in the bulk.

6- It has been shown convincingly in this work that the slip velocity increases with increase of temperature and decrease in M_w. It has also been shown that the slip velocity decreases with increase of PDI for resins with PDI>19 (no stick-slip transition) and decrease of PDI for resins with PDI<19 (stick-slip). Possible reason for this change might be interaction between the long and short changes in the broad MWD HDPEs (possible phase separation phenomena).

8.3 Recommendations for Future Work

There are several aspects of this work that could be investigated in the future. Some suggestions and recommendations on future studies are as follows:

1- In capillary rheometry or in many polymer processes polymer melts flow through converging zones. In these zones the melts experience considerably high tensile stresses which may possibly lead to *flow induced crystallization* (FIC). It is proposed to study the role of FIC on the melt fracture phenomena which would be useful in order to shed more light on the origin of these instabilities.

2- Performing more systematic studies on the effect of MWD on the slip by using polymers with the same Mw and different polydispersity is greatly needed not only for HDPEs but also for other important polymers such as LLDPEs and PPs.

3- Study the effect of roughness of the die wall on slip of various HDPEs particularly those having broad MWDs (metallocene HDPEs).

4- Measurement of slip velocities by direct nonintrusive, optical methods such as Laser Doppler Velocimetry (LDV) to compare with measured ones in the present study. The flow velocity profiles measured inside the die may provide useful information regarding the mechanism of slippage.

BIBLIOGRAPHY

1. Benham, E. and M. McDaniel, *"Polyethylene, High Density"*, in *Kirk-Othmer Encyclopedia of Chemical Technology***2000**, John Wiley & Sons, Inc.

2. Cho, H.S., K.H. Choi, D.J. Choi, and W.Y. Lee, *"Control of molecular weight distribution (MWD) for polyethylene catalyzed over Ziegler-Natta/Metallocene hybrid catalysts".* Korean Journal of Chemical Engineering, **2000**. 17(2): p. 205-09.

3. Ramamurthy, A.V., *"Wall Slip in Viscous Fluids and Influence of Materials of Construction".* Journal of Rheology, **1986**. 30(2): p. 337-57.

4. Hatzikiriakos, S.G. and J.M. Dealy, *"Effects of Interfacial Conditions on Wall Slip and Sharkskin Melt Fracture of Hdpe".* International Polymer Processing, **1993**. 8(1): p. 36-44.

5. Lee, H., D.H. Kim, and Y. Son, *"Anomalous rheological behavior of polyethylene melts in the gross melt fracture regime in the capillary extrusion".* Polymer, **2006**. 47(11): p. 3929-34.

6. Delgadillo-Velazquez, O., G. Georgiou, M. Sentmanat, and S.G. Hatzikiriakos, *"Sharkskin and oscillating and capillary dies and not welt fracture: Why in slit in annular dies?".* Polymer Engineering and Science, **2008**. 48(2): p. 405-14.

7. Hatzikiriakos, S.G. and K.B. Migler, eds. *"Polymer processing instabilities: control and understanding"*. Chemical industries**2005**, Marcel Dekker: New York. x, 470 p.

8. Hatzikiriakos, S.G. and J.M. Dealy, *"Role of Slip and Fracture in the Oscillating Flow of Hdpe in a Capillary".* Journal of Rheology, **1992**. 36(5): p. 845-84.

9. Dealy, J.M. and K.F. Wissbrun, *"Melt rheology and its role in plastics processing : theory and applications"***1990**, New York: Van Nostrand Reinhold. xix, 665 p.

10. Sentmanat, M.L. *"Dual windup extensional rheometer"*, **2003**: U.S.

11. Kazatchkov, I.B., S.G. Hatzikiriakos, and C.W. Stewart, *"Extrudate distortion in the capillary/slit extrusion of a molten polypropylene".* Polymer Engineering and Science, **1995**. 35(23): p. 1864-71.

12. Rosenbaum, E.E., S.G. Hatzikiriakos, and C.W. Stewart, *"Flow Implications in the Processing of Tetrafluoroethylene/Hexafluoropropylene Copolymers".* International Polymer Processing, **1995**. 10(3): p. 204-12.

13. Hatzikiriakos, S.G., I.B. Kazatchkov, and D. Vlassopoulos, *"Interfacial phenomena in the capillary extrusion of metallocene polyethylenes".* Journal of Rheology, **1997**. 41(6): p. 1299-316.

14. Goldstein, S., *"Modern developments in fluid dynamics: an account of theory and experiment relating to boundary layers, turbulent motion and wakes"*. Vol. 2. **1938**: The Clarendon Press. 702.

15. Hatzikiriakos, S.G. and J.M. Dealy, *"Wall Slip of Molten High-Density Polyethylenes .2. Capillary Rheometer Studies"*. Journal of Rheology, **1992**. 36(4): p. 703-41.

16. Allal, A. and B. Vergnes, *"Molecular interpretation of the "stick-slip" defect of linear polymers"*. Journal of Non-Newtonian Fluid Mechanics, **2009**. 164(1-3): p. 1-8.

17. Vasile, C. and M. Pascu, *"Practical Guide to Polyethylene"***2005**: Rapra Technology.

18. Liu, C.Y., J. Wang, and J.S. He, *"Rheological and thermal properties of m-LLDPE blends with m-HDPE and LDPE"*. Polymer, **2002**. 43(13): p. 3811-18.

19. Stadler, F.J., A. Nishioka, J. Stange, K. Koyama, and H. Munstedt, *"Comparison of the elongational behavior of various polyolefins in uniaxial and equibiaxial flows"*. Rheologica Acta, **2007**. 46(7): p. 1003-12.

20. Liang, R., *"Processing flow behavior and modeling of polyethylene melts"*. Journal of Central South University of Technology, **2007**. 14: p. 178-82.

21. Zhang, J. and G. Hsuan *"Experimental study of stress cracking in high density polyethylene pipes"*, **2005**, Drexel University, Drexel University: Philadelphia, Pa. p. xv, 164 leaves.

22. Harris, M.G. *"High density polyethylene melt blends for improved stress cracking resistance in pipe"*, **2003**: U.S.

23. Peacock, A.J., *"Handbook of polyethylene : structures, properties, and applications"*. Plastics engineering**2000**, New York: Marcel Dekker. vii, 534 p.

24. DesLauriers, P.J., M.P. Mcdaniel, D.C. Rohlfing, R.K. Krishnaswamy, S.J. Secora, E.A. Benham, P.L. Maeger, A.R. Wolfe, A.M. Sukhadia, and B.B. Beaulieu, *"A comparative study of multimodal vs. bimodal polyethylene pipe resins for PE-100 applications"*. Polymer Engineering and Science, **2005**. 45(9): p. 1203-13.

25. Doi, M., *"Introduction to polymer physics"*. Oxford science publications**1996**, Oxford New York: Clarendon Press ; Oxford University Press. ix, 120 p.

26. Cowie, J.M.G. and V. Arrighi, *"Polymers : chemistry and physics of modern materials"*. 3rd ed**2008**, Boca Raton: CRC Press/Taylor & Francis. 499 p.

27. Agarwal, P.K., *"Relationship between Steady-State Shear Compliance and Molecular-Weight Distribution"*. Macromolecules, **1979**. 12(2): p. 342-44.

28. Kurata, M., *"Effect of Molecular-Weight Distribution on Viscoelastic Properties of Polymers .2. Terminal Relaxation-Time and Steady-State Compliance"*. Macromolecules, **1984**. 17(4): p. 895-98.

29. Mills, N.J. and A. Nevin, *"Oscillatory Shear Measurements on Polystyrene Melts in Terminal Region"*. Journal of Polymer Science Part a-2-Polymer Physics, **1971**. 9(2): p. 267.

30. Dealy, J.M., *"Rheometers for molten plastics : a practical guide to testing and property measurement"***1982**, New York: Van Nostrand Reinhold. xviii, 302 p.

31. Sentmanat, M.L., *"Miniature universal testing platform: from extensional melt rheology to solid-state deformation behavior"*. Rheologica Acta, **2004**. 43(6): p. 657-69.

32. Sentmanat, M., B.N. Wang, and G.H. McKinley, *"Measuring the transient extensional rheology of polyethylene melts using the SER universal testing platform"*. Journal of Rheology, **2005**. 49(3): p. 585-606.

33. Patil, P.D., I. Ochoa, J.J. Feng, and S.G. Hatzikiriakos, *"Viscoelastic flow simulation of polytetrafluoroethylene (PTFE) paste extrusion"*. Journal of Non-Newtonian Fluid Mechanics, **2008**. 153(1): p. 25-33.

34. Delgadillo-Velazquez, O. and S.G. Hatzikiriakos, *"Processability of LLDPE/LDPE blends: Capillary extrusion studies"*. Polymer Engineering and Science, **2007**. 47(9): p. 1317-26.

35. Wang, Y.Y. and S.Q. Wang, *"From elastic deformation to terminal flow of a monodisperse entangled melt in uniaxial extension"*. Journal of Rheology, **2008**. 52(6): p. 1275-90.

36. Mooney, M., *"Explicit Formulas for Slip and Fluidity"*. Journal of Rheology, **1931**. 2(2): p. 210-22.

37. Rosenbaum, E.E. and S.G. Hatzikiriakos, *"Wall slip in the capillary flow of molten polymers subject to viscous heating"*. Aiche Journal, **1997**. 43(3): p. 598-608.

38. Yeow, Y.L., H.L. Lee, A.R. Melvani, and G.C. Mifsud, *"A new method of processing capillary viscometry data in the presence of wall slip"*. Journal of Rheology, **2003**. 47(2): p. 337-48.

39. Graessley, W.W., *"Effect of Long Branches on the Temperature-Dependence of Viscoelastic Properties in Polymer Melts"*. Macromolecules, **1982**. 15(4): p. 1164-67.

40. Carella, J.M., J.T. Gotro, and W.W. Graessley, *"Thermorheological Effects of Long-Chain Branching in Entangled Polymer Melts"*. Macromolecules, **1986**. 19(3): p. 659-67.

41. Hatzikiriakos, S.G., *"Long chain branching and polydispersity effects on the rheological properties of polyethylenes"*. Polymer Engineering and Science, **2000**. 40(11): p. 2279-87.

42. Dealy, J.M. and R.G. Larson, *"Structure and rheology of molten polymers : from structure to flow behavior and back again"***2006**, Munich Cincinnati: Hanser Publishers ; Hanser Gardner Publications. xiv, 516 p.

43. Wasserman, S.H. and W.W. Graessley, *"Prediction of linear viscoelastic response for entangled polyolefin melts from molecular weight distribution"*. Polymer Engineering and Science, **1996**. 36(6): p. 852-61.

44. Garcia-Franco, C.A. and D.W. Mead, *"Rheological and molecular characterization of linear backbone flexible polymers with the Cole-Cole model relaxation spectrum"*. Rheologica Acta, **1999**. 38(1): p. 34-47.

45. Kazatchkov, I.B., N. Bohnet, S.K. Goyal, and S.G. Hatzikiriakos, *"Influence of molecular structure on the rheological and processing behavior of polyethylene resins"*. Polymer Engineering and Science, **1999**. 39(4): p. 804-15.

46. Pattamaprom, C. and R.G. Larson, *"Predicting the linear viscoelastic properties of monodisperse and polydisperse polystyrenes and polyethylenes"*. Rheologica Acta, **2001**. 40(6): p. 516-32.

47. Munoz-Escalona, A., P. Lafuente, J.F. Vega, and A. Santamaria, *"Rheology of metallocene-catalyzed monomodal and bimodal polyethylenes"*. Polymer Engineering and Science, **1999**. 39(11): p. 2292-303.

48. Vega, J.F., A. MunozEscalona, A. Santamaria, M.E. Munoz, and P. Lafuente, *"Comparison of the rheological properties of metallocene-catalyzed and conventional high-density polyethylenes"*. Macromolecules, **1996**. 29(3): p. 960-65.

49. Carella, J.M., *"Comparison of the rheological properties of metallocene-catalyzed and conventional high-density polyethylenes - Comment"*. Macromolecules, **1996**. 29(25): p. 8280-81.

50. Raju, V.R., G.G. Smith, G. Marin, J.R. Knox, and W.W. Graessley, *"Properties of Amorphous and Crystallizable Hydrocarbon Polymers .1. Melt Rheology of Fractions of Linear Polyethylene"*. Journal of Polymer Science Part B-Polymer Physics, **1979**. 17(7): p. 1183-95.

51. Raju, V.R., H. Rachapudy, and W.W. Graessley, *"Properties of Amorphous and Crystallizable Hydrocarbon Polymers .4. Melt Rheology of Linear and Star-Branched Hydrogenated Polybutadiene"*. Journal of Polymer Science Part B-Polymer Physics, **1979**. 17(7): p. 1223-35.

52. Wood-Adams, P.M., J.M. Dealy, A.W. deGroot, and O.D. Redwine, *"Effect of molecular structure on the linear viscoelastic behavior of polyethylene"*. Macromolecules, **2000**. 33(20): p. 7489-99.

53. Vega, J.F., J. Otegui, J. Ramos, and J. Martinez-Salazar, *"Effect of molecular weight distribution on Newtonian viscosity of linear polyethylene"*. Rheologica Acta, **2012**. 51(1): p. 81-87.

54. Tordella, J.P., *"Fracture in the Extrusion of Amorphous Polymers through Capillaries"*. Journal of Applied Physics, **1956**. 27(5): p. 454-58.

55. Moynihan, R.H., D.G. Baird, and R. Ramanathan, *"Additional Observations on the Surface Melt Fracture-Behavior of Linear Low-Density Polyethylene"*. Journal of Non-Newtonian Fluid Mechanics, **1990**. 36: p. 255-63.

56. Garvey, B.S., M.H. Whitlock, and J.A. Freese, *"Processing characteristics of synthetic tire rubber"*. Industrial and Engineering Chemistry, **1942**. 34: p. 1309-12.

57. Larson, R.G., *"Instabilities in Viscoelastic Flows"*. Rheologica Acta, **1992**. 31(3): p. 213-63.

58. Denn, M.M., *"Extrusion instabilities and wall slip"*. Annual Review of Fluid Mechanics, **2001**. 33: p. 265-87.

59. Leonov, A.I. and A.N. Prokunin, *"Nonlinear phenomena in flows of viscoelastic polymer fluids"*. 1st ed**1994**, London ; New York: Chapman & Hall. xvi, 475 p.

60. Vinogradov, G.V., M.L. Friedman, B.V. Yarlykov, and A.Y.a. Malkin, *"Unsteady flow of polymer melts: Polypropylene"*. Rheologica Acta, **1970**. 9(3): p. 323-29.

61. Barone, J.R., N. Plucktaveesak, and S.Q. Wang, *"Interfacial molecular instability mechanism for sharkskin phenomenon in capillary extrusion of linear polyethylenes"*. Journal of Rheology, **1998**. 42(4): p. 813-32.

62. Barone, J.R., N. Plucktaveesak, and S.Q. Wang, *"Letter to the Editor: The mystery of the mechanism of sharkskin - Author's response"*. Journal of Rheology, **1999**. 43(1): p. 247-52.

63. Cogswell, F.N., *"Stretching Flow Instabilities at Exits of Extrusion Dies"*. Journal of Non-Newtonian Fluid Mechanics, **1977**. 2(1): p. 37-47.

64. Migler, K.B., Y. Son, F. Qiao, and K. Flynn, *"Extensional deformation, cohesive failure, and boundary conditions during sharkskin melt fracture"*. Journal of Rheology, **2002**. 46(2): p. 383-400.

65. Wang, S.Q., P.A. Drda, and Y.W. Inn, *"Exploring molecular origins of sharkskin, partial slip, and slope change in flow curves of linear low density polyethylene"*. Journal of Rheology, **1996**. 40(5): p. 875-98.

66. Venet, C. and B. Vergnes, *"Experimental characterization of sharkskin in polyethylenes"*. Journal of Rheology, **1997**. 41(4): p. 873-92.

67. Rutgers, R.P.G. and M.R. Mackley, *"The effect of channel geometry and wall boundary conditions on the formation of extrusion surface instabilities for LLDPE"*. Journal of Non-Newtonian Fluid Mechanics, **2001**. 98(2-3): p. 185-99.

68. Rutgers, R. and M. Mackley, *"The correlation of experimental surface extrusion instabilities with numerically predicted exit surface stress concentrations and melt strength for linear low density polyethylene"*. Journal of Rheology, **2000**. 44(6): p. 1319-34.

69. Howells, E.R. and J. Benbow, *"Flow defects in polymer melts"*. Transactions and Journal of the Plastics Institute, **1962**. 30: p. 240–53.

70. Rosenbaum, E.E., S.K. Randa, S.G. Hatzikiriakos, C.W. Stewart, D.L. Henry, and M. Buckmaster, *"Boron nitride as a processing aid for the extrusion of polyolefins and fluoropolymers"*. Polymer Engineering and Science, **2000**. 40(1): p. 179-90.

71. Rosenbaum, E.E. *"Rheology and Processability of FEP Teflon Resins for Wire Coating"*, in *Chemical and Biological Engineering*, **1998**, University of British Columbia.

72. Ansari, M., H.S. G., A.M. Sukhadia, and D.C. Rohlfing *"Melt Fracture of Linear Polyethylenes: Molecular Structure and Die Geometry Effects"*, in *ANTEC 2009 Plastics: Annual Technical Conference Proceedings*, **2009**, Society of Plastics Engineers: Chicago, IL. p. 9-13.

73. Vlachopoulos, J. and S. Lidorikis, *"Melt Fracture of Polystyrene"*. Polymer Engineering and Science, **1971**. 11(1): p. 1-&.

74. Baik, J.J. and C. Tzoganakis, *"A study of extrudate distortion in controlled-rheology polypropylenes"*. Polymer Engineering and Science, **1998**. 38(2): p. 274-81.

75. Miller, E. and J.P. Rothstein, *"Control of the sharkskin instability in the extrusion of polymer melts using induced temperature gradients"*. Rheologica Acta, **2004**. 44(2): p. 160-73.

76. Miller, E., S.J. Lee, and J.P. Rothstein, *"The effect of temperature gradients on the sharkskin surface instability in polymer extrusion through a slit die"*. Rheologica Acta, **2006**. 45(6): p. 943-50.

77. Waddon, A.J. and A. Keller, *"A Temperature Window of Extrudability and Reduced Flow Resistance in High-Molecular-Weight Polyethylene - Interpretation in Terms of Flow-Induced Mobile Hexagonal Phase"*. Journal of Polymer Science Part B-Polymer Physics, **1990**. 28(7): p. 1063-73.

78. Pudjijanto, S. and M.M. Denn, *"A Stable Island in the Slip-Stick Region of Linear Low-Density Polyethylene"*. Journal of Rheology, **1994**. 38(6): p. 1735-44.

79. Wang, S.Q. and P.A. Drda, *"Superfluid-like stick-slip transition in capillary flow of linear polyethylene melts .1. General features".* Macromolecules, **1996**. 29(7): p. 2627-32.

80. Santamaria, A., M. Fernandez, E. Sanz, P. Lafuente, and A. Munoz-Escalona, *"Postponing sharkskin of metallocene polyethylenes at low temperatures: the effect of molecular parameters".* Polymer, **2003**. 44(8): p. 2473-80.

81. Fujiyama, M. and H. Awaya, *"Relationship in Polypropylene Melt between Its Linear Viscoelasticity and Its Steady Capillary Flow Properties".* Journal of Applied Polymer Science, **1972**. 16(2): p. 275.

82. Vlachopoulos, J. and M. Alam, *"Critical Stress and Recoverable Shear for Polymer Melt Fracture".* Polymer Engineering and Science, **1972**. 12(3): p. 184.

83. Goyal, S.K., I.B. Kazatchkov, N. Bohnet, and S.G. Hatzikiriakos, *"Influence of molecular weight distribution on the rheological behavior of LLDP resins".* Antec'97 - Plastics Saving Planet Earth, Conference Proceedings, Vols 1 - 3, **1997**: p. 1076-80.

84. Fujiyama, M., Y. Kitajima, and H. Inata, *"Rheological properties of polypropylenes with different molecular weight distribution characteristics".* Journal of Applied Polymer Science, **2002**. 84(12): p. 2128-41.

85. Fujiyama, M. and H. Inata, *"Rheological properties of metallocene isotactic polypropylenes".* Journal of Applied Polymer Science, **2002**. 84(12): p. 2157-70.

86. Deeprasertkul, C., C. Rosenblatt, and S.Q. Wang, *"Molecular character of sharkskin phenomenon in metallocene linear low density polyethylenes".* Macromolecular Chemistry and Physics, **1998**. 199(10): p. 2113-18.

87. Mills, D.R., G.E. Moore, and D.W. Pugh, *"The Effect of Molecular Weight Distribution on the Flow Properties of Polyethylene".* Spe Transactions, **1961**. 1(1): p. 40-46.

88. Graessley, W.W. and L. Segal, *"Flow Behavior of Polystyrene Systems in Steady Shearing Flow".* Macromolecules, **1969**. 2(1): p. 49.

89. Yamaguchi, M., H. Miyata, V. Tan, and C.G. Gogos, *"Relation between molecular structure and flow instability for ethylene/alpha-olefin copolymers".* Polymer, **2002**. 43(19): p. 5249-55.

90. Allal, A., A. Lavernhe, B. Vergnes, and G. Marin, *"Relationships between molecular structure and sharkskin defect for linear polymers".* Journal of Non-Newtonian Fluid Mechanics, **2006**. 134(1-3): p. 127-35.

91. Allal, A. and B. Vergnes, *"Molecular design to eliminate sharkskin defect for linear polymers".* Journal of Non-Newtonian Fluid Mechanics, **2007**. 146(1-3): p. 45-50.

92. Rudin, A., S. Nam, A.T. Worm, and J.E. Blacklock *"Improvements in polyolefin processing with a fluorocarbon elastomer processing aid"*, in *ANTEC 1986 Plastics: Annual Technical Conference Proceedings*, **1986**: Boston, MA. p. 1154–57.

93. Priester, D.E., K.M. Stika, G.R. Chapman, R.S. Mcminn, and P. Ferrandez, *"Quality-Control Techniques for Processing Additives"*. Antec 93 : Be in That Number, Vols 1-3, **1993**. 39: p. 2528-33.

94. Kanu, R.C. and M.T. Shaw, *"Rheology of Polymer Blends - Simultaneous Slippage and Entrance Pressure Loss in the Ethylene-Propylene-Diene (Epdm) Viton System"*. Polymer Engineering and Science, **1982**. 22(8): p. 507-11.

95. Buckmaster, M.D., D.L. Henry, and S.K. Randa *"High speed extrusion"*, **1997**: U.S.

96. Achilleos, E.C., G. Georgiou, and S.G. Hatzikiriakos, *"Role of processing aids in the extrusion of molten polymers"*. Journal of Vinyl & Additive Technology, **2002**. 8(1): p. 7-24.

97. Bagley, E.B., I.M. Cabott, and D.C. West, *"DISCONTINUITY IN THE FLOW CURVE OF POLYETHYLENE"*. Journal of Applied Physics, **1958**. 29(1): p. 109-10.

98. Lupton, J.M. and H.W. Regester, *"Melt flow of polyethylene at high rates"*. Polymer Engineering & Science, **1965**. 5(4): p. 235-45.

99. Myerholtz, R.W., *"Oscillating Flow Behavior of High-Density Polyethylene Melts"*. Journal of Applied Polymer Science, **1967**. 11(5): p. 687.

100. Vinogradov, G.V., V.P. Protasov, and V.E. Dreval, *"The Rheological Behavior of Flexible-Chain Polymers in the Region of High Shear Rates and Stresses, the Critical Process of Spurting, and Supercritical Conditions of Their Movement at T Greater-Than Tg"*. Rheologica Acta, **1984**. 23(1): p. 46-61.

101. Vinogradov, G.V. and L.I. Ivanova, *"Viscous properties of polymer melts and elastomers exemplified by ethylene-propylene copolymer"*. Rheologica Acta, **1967**. 6(3): p. 209-22.

102. Weill, A., *"About the origin of sharkskin"*. Rheologica Acta, **1980**. 19(5): p. 623-32.

103. El Kissi, N., J.M. Piau, and F. Toussaint, *"Sharkskin and cracking of polymer melt extrudates"*. Journal of Non-Newtonian Fluid Mechanics, **1997**. 68(2-3): p. 271-90.

104. Wang, S.Q. and P.A. Drda, *"Stick slip transition in capillary flow of linear polyethylene .3. Surface conditions"*. Rheologica Acta, **1997**. 36(2): p. 128-34.

105. Durand, V., B. Vergnes, J.F. Agassant, E. Benoit, and R.J. Koopmans, *"Experimental study and modeling of oscillating flow of high density polyethylenes"*. Journal of Rheology, **1996**. 40(3): p. 383-94.

106. Sato, K. and A. Toda, *"Physical mechanism of stick-slip behavior in polymer melt extrusion: Temperature dependence of flow curve"*. Journal of the Physical Society of Japan, **2001**. 70(11): p. 3268-73.

107. Vergnes, B., S. Dhalewyn, and M.F. Boube, *"WALL SLIP AND INSTABILITIES IN THE FLOW OF EPDM COMPOUNDS"*. Theoretical and Applied Rheology, Vols 1 and 2, ed. P. Moldenaers and R. Keunings, **1992**, Amsterdam: Elsevier Science Publ B V. 399-401.

108. Wang, S.Q. and P.A. Drda, *"Stick-slip transition in capillary flow of polyethylene .2. Molecular weight dependence and low-temperature anomaly"*. Macromolecules, **1996**. 29(11): p. 4115-19.

109. Kalika, D.S. and M.M. Denn, *"Wall Slip and Extrudate Distortion in Linear Low-Density Polyethylene"*. Journal of Rheology, **1987**. 31(8): p. 815-34.

110. El Kissi, N. and J.M. Piau, *"The Different Capillary-Flow Regimes of Entangled Polydimethylsiloxane Polymers - Macroscopic Slip at the Wall, Hysteresis and Cork Flow"*. Journal of Non-Newtonian Fluid Mechanics, **1990**. 37(1): p. 55-94.

111. Robert, L., B. Vergnes, and Y. Demay, *"Complex transients in the capillary flow of linear polyethylene"*. Journal of Rheology, **2000**. 44(5): p. 1183-87.

112. Vinogradov, G.V., Y.G. Yanovski, B.V. Yarlykov, G.V. Berezhna, E.K. Borisenk, and A.Y. Malkin, *"Viscoelastic Properties and Flow of Narrow Distribution Polybutadienes and Polyisoprenes"*. Journal of Polymer Science Part a-2-Polymer Physics, **1972**. 10(6): p. 1061-&.

113. Uhland, E., *"ANOMALOUS FLOW BEHAVIOR OF HIGH-DENSITY POLYETHYLENE"*. Rheologica Acta, **1979**. 18(1): p. 1-24.

114. Yang, X.P., S.Q. Wang, A. Halasa, and H. Ishida, *"Fast flow behavior of highly entangled monodisperse polymers 1. Interfacial stick-slip transition of polybutadiene melts"*. Rheologica Acta, **1998**. 37(5): p. 415-23.

115. Blyler, L.L. and A.C. Hart, *"Capillary Flow Instability of Ethylene Polymer Melts"*. Polymer Engineering and Science, **1970**. 10(4): p. 193.

116. Durand, V., B. Vergnes, J.F. Agassant, and R.J. Koopmans, *"INFLUENCE OF THE MOLECULAR-WEIGHT ON THE OSCILLATING FLOW OF HDPE MELTS"*. Theoretical and Applied Rheology, Vols 1 and 2, ed. P. Moldenaers and R. Keunings, **1992**, Amsterdam: Elsevier Science Publ B V. 416-16.

117. Lim, F.J. and W.R. Schowalter, *"Wall Slip of Narrow Molecular-Weight Distribution Polybutadienes"*. Journal of Rheology, **1989**. 33(8): p. 1359-82.

118. Lin, Y.H., *"Explanation for Slip-Stick Melt Fracture in Terms of Molecular-Dynamics in Polymer Melts"*. Journal of Rheology, **1985**. 29(6): p. 605-37.

119. Lin, Y.H., *"Unified Molecular Theories of Linear and Nonlinear Viscoelasticity of Flexible Linear-Polymers - Explaining the 3.4 Power Law of the Zero-Shear Viscosity and the Slip Stick Melt Fracture Phenomenon".* Journal of Non-Newtonian Fluid Mechanics, **1987**. 23: p. 163-87.

120. Utracki, L.A. and R. Gendron, *"Pressure Oscillation during Extrusion of Polyethylenes .2.".* Journal of Rheology, **1984**. 28(5): p. 601-23.

121. Benbow, J.J. and P. Lamb, *"NEW ASPECTS OF MELT FRACTURE".* Spe Transactions, **1963**. 3(1): p. 7-17.

122. Kim, S. and J.M. Dealy, *"Gross melt fracture of polyethylene. I: A criterion based on tensile stress".* Polymer Engineering and Science, **2002**. 42(3): p. 482-94.

123. Tordella, J.P., in *Rheology: Theory and Applications*, F.R. Eirich, Editor **1969**, Academic Press, New York. p. 57–92.

124. Bergem, N. *"Visualization studies of polymer melt flow anomalies in extrusion"*, in *VIIth International Congress on Rheology*, **1976**, Swedish Society of Rheology: Gothenburg, Sweden. p. 50-55.

125. Vinogradov, G.V. and A.Y. Malkin, *"Rheology of polymers : viscoelasticity and flow of polymers"***1980**, Moscow Berlin: Mir Publishers ; Springer-Verlag. xii, 467 p.

126. Meller, M., A. Luciani, and J.A.E. Manson, *"Flow through a convergence. Part 2: Mixing of high viscosity ratio polymer blends".* Polymer Engineering and Science, **2002**. 42(3): p. 634-53.

127. Kazatchkov, I.B., F. Yip, and S.G. Hatzikiriakos, *"The effect of boron nitride on the rheology and processing of polyolefins".* Rheologica Acta, **2000**. 39(6): p. 583-94.

128. Mitsoulis, E., *"Secondary Flow Instabilities"*, in *Polymer processing instabilities: control and understanding*, S.G. Hatzikiriakos and K.B. Migler, Editors. **2005**, Marcel Dekker: New York. p. 43-71.

129. Carreras, E.S., N. El Kissi, J.M. Piau, F. Toussaint, and S. Nigen, *"Pressure effects on viscosity and flow stability of polyethylene melts during extrusion".* Rheologica Acta, **2006**. 45(3): p. 209-22.

130. Bagley, E.B. and H.P. Schreiber, *"Effect of Die Entry Geometry on Polymer Melt Fracture and Extrudate Distortion".* Transactions of the Society of Rheology, **1961**. 5: p. 341-53.

131. Piau, J.M., N. El Kissi, and B. Tremblay, *"Influence of Upstream Instabilities and Wall Slip on Melt Fracture and Sharkskin Phenomena during Silicones Extrusion through Orifice Dies".* Journal of Non-Newtonian Fluid Mechanics, **1990**. 34(2): p. 145-80.

132. Kim, S. and J.M. Dealy, *"Gross melt fracture of polyethylene. II: Effects of molecular structure"*. Polymer Engineering and Science, **2002**. 42(3): p. 495-503.

133. Maxwell, B. and J.C. Galt, *"Velocity Profiles for Polyethylene Melt in Tubes"*. Journal of Polymer Science, **1962**. 62(174): p. S50-&.

134. Hatzikiriakos, S.G. and J.M. Dealy, *"Wall Slip of Molten High-Density Polyethylene .1. Sliding Plate Rheometer Studies"*. Journal of Rheology, **1991**. 35(4): p. 497-523.

135. Archer, L.A., *"Wall Slip: measurement and Modelling Issues"*, in Polymer processing instabilities: control and understanding, S.G. Hatzikiriakos and K.B. Migler, Editors. **2005**, Marcel Dekker: New York. p. 73-120.

136. Hatzikiriakos, S.G., *"Wall slip of molten polymers"*. Progress in Polymer Science, **2012**. 37(4): p. 624-43.

137. Brochard-Wyart, F. and P.G. de Gennes, *"Shear-Dependent Slippage at a Polymer Solid Interface"*. Langmuir, **1992**. 8(12): p. 3033-37.

138. Migler, K.B., H. Hervet, and L. Leger, *"Slip Transition of a Polymer Melt under Shear-Stress"*. Physical Review Letters, **1993**. 70(3): p. 287-90.

139. Migler, K.B., G. Massey, H. Hervet, and L. Leger, *"The Slip Transition at the Polymer Solid Interface"*. Journal of Physics-Condensed Matter, **1994**. 6: p. A301-A04.

140. Anastasiadis, S.H. and S.G. Hatzikiriakos, *"The work of adhesion of polymer/wall interfaces and its association with the onset of wall slip"*. Journal of Rheology, **1998**. 42(4): p. 795-812.

141. Hill, D.A., T. Hasegawa, and M.M. Denn, *"On the Apparent Relation between Adhesive Failure and Melt Fracture"*. Journal of Rheology, **1990**. 34(6): p. 891-918.

142. Hill, D.A., *"Wall slip in polymer melts: A pseudo-chemical model"*. Journal of Rheology, **1998**. 42(3): p. 581-601.

143. Hatzikiriakos, S.G., *"Appropriate Boundary Conditions in the Flow of Molten Polymers"*. International Polymer Processing, **2010**. 25(1): p. 55-62.

144. Lau, H.C. and W.R. Schowalter, *"A Model for Adhesive Failure of Viscoelastic Fluids during Flow"*. Journal of Rheology, **1986**. 30(1): p. 193-206.

145. Munstedt, H., M. Schmidt, and E. Wassner, *"Stick and slip phenomena during extrusion of polyethylene melts as investigated by laser-Doppler velocimetry"*. Journal of Rheology, **2000**. 44(2): p. 413-27.

146. Robert, L., Y. Demay, and B. Vergnes, *"Stick-slip flow of high density polyethylene in a transparent slit die investigated by laser Doppler velocimetry"*. Rheologica Acta, **2004**. 43(1): p. 89-98.

147. Drda, P.P. and S.Q. Wang, *"Stick-Slip Transition at Polymer Melt/Solid Interfaces"*. Physical Review Letters, **1995**. 75(14): p. 2698-701.

148. Vinogradov, G.V., E.K. Borisenk, B.B. Boiko, and N.I. Insarova, *"Critical Regimes of Shear in Linear Polymers"*. Polymer Engineering and Science, **1972**. 12(5): p. 323.

149. Park, H.E., S.T. Lim, F. Smillo, J.M. Dealy, and C.G. Robertson, *"Wall slip and spurt flow of polybutadiene"*. Journal of Rheology, **2008**. 52(5): p. 1201-39.

150. Birinci, E. and D.M. Kalyon, *"Development of extrudate distortions in poly(dimethyl siloxane) and its suspensions with rigid particles"*. Journal of Rheology, **2006**. 50(3): p. 313-26.

151. Noroozi, N., J.A. Thomson, N. Noroozi, L.L. Schafer, and S.G. Hatzikiriakos, *"Viscoelastic behaviour and flow instabilities of biodegradable poly (epsilon-caprolactone) polyesters"*. Rheologica Acta, **2012**. 51(2): p. 179-92.

152. Worth, R.A., J. Parnaby, and H.A.A. Helmy, *"Wall Slip and Its Implications in Design of Single Screw Melt-Fed Extruders"*. Polymer Engineering and Science, **1977**. 17(4): p. 257-65.

153. Mhetar, V. and L.A. Archer, *"Slip in entangled polymer solutions"*. Macromolecules, **1998**. 31(19): p. 6639-49.

154. Mhetar, V. and L.A. Archer, *"Slip in entangled polymer melts. 1. General features"*. Macromolecules, **1998**. 31(24): p. 8607-16.

155. Awati, K.M., Y. Park, E. Weisser, and M.E. Mackay, *"Wall slip and shear stresses of polymer melts at high shear rates without pressure and viscous heating effects"*. Journal of Non-Newtonian Fluid Mechanics, **2000**. 89(1-2): p. 117-31.

156. Mackay, M.E. and D.J. Henson, *"The effect of molecular mass and temperature on the slip of polystyrene melts at low stress levels"*. Journal of Rheology, **1998**. 42(6): p. 1505-17.

157. Othman, N., B. Jazrawi, P. Mehrkhodavandi, and S.G. Hatzikiriakos, *"Wall slip and melt fracture of poly(lactides)"*. Rheologica Acta, **2012**. 51(4): p. 357-69.

158. Joshi, Y.M., A.K. Lele, and R.A. Mashelkar, *"Molecular model for wall slip: Role of convective constraint release"*. Macromolecules, **2001**. 34(10): p. 3412-20.

159. Utracki, L.A. and B. Schlund, *"Linear Low-Density Polyethylenes and Their Blends .4. Shear-Flow of Lldpe Blends with Lldpe and Ldpe"*. Polymer Engineering and Science, **1987**. 27(20): p. 1512-22.

160. Stadler, F.J. and H. Munstedt, *"Numerical description of shear viscosity functions of long-chain branched metallocene-catalyzed polyethylenes"*. Journal of Non-Newtonian Fluid Mechanics, **2008**. 151(1-3): p. 129-35.

161. Stadler, F.J., C. Piel, J. Kaschta, S. Rulhoff, W. Kaminsky, and H. Munstedt, *"Dependence of the zero shear-rate viscosity and the viscosity function of linear high-density polyethylenes on the mass-average molar mass and polydispersity".* Rheologica Acta, **2006**. 45(5): p. 755-64.

162. Mavridis, H. and R.N. Shroff, *"Temperature-Dependence of Polyolefin Melt Rheology".* Polymer Engineering and Science, **1992**. 32(23): p. 1778-91.

163. Krevelen, D.W.v., *"Properties of polymers : their correlation with chemical structure, their numerical estimation and prediction from additive group contributions".* 3rd, completely rev. ed **1990**, Amsterdam ; New York: Elsevier. xxii, 875 p.

164. den Doelder, J., *"Viscosity and compliance from molar mass distributions using double reptation models".* Rheologica Acta, **2006**. 46(2): p. 195-210.

165. Nobile, M.R. and F. Cocchini, *"Predictions of linear viscoelastic properties for polydisperse entangled polymers".* Rheologica Acta, **2000**. 39(2): p. 152-62.

166. Nobile, M.R. and F. Cocchini, *"A generalized relation between MWD and relaxation time spectrum".* Rheologica Acta, **2008**. 47(5-6): p. 509-19.

167. Cocchini, F. and M.R. Nobile, *"Constrained inversion of rheological data to molecular weight distribution for polymer melts".* Rheologica Acta, **2003**. 42(3): p. 232-42.

168. Mieras, H.J.M. and C.F.H. Vanrijn, *"Elastic Behaviour of Some Polymer Melts".* Nature, **1968**. 218(5144): p. 865.

169. Mills, N.J., *"Rheological Properties and Molecular Weight Distribution of Polydimethylsiloxane".* European Polymer Journal, **1969**. 5(5): p. 675-&.

170. Prest, W.M. and R.S. Porter, *"Rheological Properties of Poly(2,6-Dimethylphenylene Oxide- Polystyrene Blends".* Journal of Polymer Science Part a-2-Polymer Physics, **1972**. 10(9): p. 1639.

171. Onogi, S., T. Masuda, and K. Kitagawa, *"Rheological Properties of Anionic Polystyrenes. I. Dynamic Viscoelasticity of Narrow-Distribution Polystyrenes".* Macromolecules, **1970**. 3(2): p. 109-16.

172. Prest, W.M., *"Viscoelastic Properties of Blends of Entangled Polymers".* Journal of Polymer Science Part a-2-Polymer Physics, **1970**. 8(11): p. 1897.

173. Akovali, G., *"Viscoelastic Properties of Polystyrene".* Journal of Polymer Science Part a-2-Polymer Physics, **1967**. 5(5pa2): p. 875.

174. Mills, N.J., *"Elasticity of Polydimethylsiloxane Melts".* Nature, **1968**. 219(5160): p. 1249

175. Gabriel, C. and H. Munstedt, *"Influence of long-chain branches in polyethylenes on linear viscoelastic flow properties in shear".* Rheologica Acta, **2002**. 41(3): p. 232-44.

176. Resch, J.A., F.J. Stadler, J. Kaschta, and H. Munstedt, *"Temperature Dependence of the Linear Steady-State Shear Compliance of Linear and Long-Chain Branched Polyethylenes"*. Macromolecules, **2009**. 42(15): p. 5676-83.

177. Baumgaertel, M. and H.H. Winter, *"Determination of Discrete Relaxation and Retardation Time Spectra from Dynamic Mechanical Data"*. Rheologica Acta, **1989**. 28(6): p. 511-19.

178. Baumgaertel, M., A. Schausberger, and H.H. Winter, *"The Relaxation of Polymers with Linear Flexible Chains of Uniform Length"*. Rheologica Acta, **1990**. 29(5): p. 400-08.

179. Georgiou, G., *"Stick-slip Instability"*, in Polymer processing instabilities: control and understanding, S.G. Hatzikiriakos and K.B. Migler, Editors. **2005**, Marcel Dekker: New York. p. 161-206.

180. Joseph, D.D., *"Steep wave fronts on extrudates of polymer melts and solutions: Lubrication layers and boundary lubrication"*. Journal of Non-Newtonian Fluid Mechanics, **1997**. 70(3): p. 187-203.

181. Wang, X., X.Y. Wang, Z.B. Wang, J.H. Lee, P. Kalappa, and S.K. Kim, *"Sharkskin mechanism of LDPE and the dispersion of inorganic fillers in flow"*. Journal of Macromolecular Science Part B-Physics, **2006**. 45(5): p. 777-88.

182. Ansari, M., S.G. Hatzikiriakos, A.M. Sukhadia, and D.C. Rohlfing, *"Rheology of Ziegler-Natta and metallocene high-density polyethylenes: broad molecular weight distribution effects"*. Rheologica Acta, **2011**. 50(1): p. 17-27.

183. Vlachopoulos, J. and T.W. Chan, *"Comparison of Melt Fracture Initiation Conditions in Capillaries and Slits"*. Journal of Applied Polymer Science, **1977**. 21(5): p. 1177-87.

184. Bird, R.B. and O. Hassager, *"Dynamics of Polymeric Liquids: Fluid mechanics"*. Vol. 1. **1987**: Wiley. 672.

185. Amos, S.E., G.M. Giacoletto, J.H. Horns, C. Lavallée, and S.S. Woods *"'Polymer processing aids (PPA).'"*, in *Plastic Additives* **2001**: Hanser, Munich.

186. Shih, C.K., *"Rheological Properties of Incompatible Blends of 2 Elastomers"*. Polymer Engineering and Science, **1976**. 16(11): p. 742-46.

187. Mavridis, H. and K. Fronek, *"Effect of MWD on the amount of polymer process aid required to suppress sharkskin melt fracture in LLDPE"*. Journal of Plastic Film & Sheeting, **2002**. 18(1): p. 45-57.

188. MunozEscalona, A., P. Lafuente, J.F. Vega, M.E. Munoz, and A. Santamaria, *"Rheological behaviour of metallocene catalysed high density polytheylene blends"*. Polymer, **1997**. 38(3): p. 589-94.

189. Hong, Y., S.J. Coombs, J.J. Cooper-White, M.E. Mackay, C.J. Hawker, E. Malmstrom, and N. Rehnberg, *"Film blowing of linear low-density polyethylene blended with a novel hyperbranched polymer processing aid"*. Polymer, **2000**. 41(21): p. 7705-13.

190. Peon, J., M. Aguilar, J.F. Vega, B. del Amo, and J. Martinez-Salazar, *"On the processability of metallocene-catalysed polyethylene: effects of blending with ethylene-vinyl acetate copolymer"*. Polymer, **2003**. 44(5): p. 1589-94.

191. Leonardi, F., J.C. Majeste, A. Allal, and G. Marin, *"Rheological models based on the double reptation mixing rule: The effects of a polydisperse environment"*. Journal of Rheology, **2000**. 44(4): p. 675-92.

192. Cox, W.P. and E.H. Merz, *"Correlation of Dynamic and Steady Flow Viscosities"*. Journal of Polymer Science, **1958**. 28(118): p. 619-22.

193. Kanev, D., E. Takacs, and J. Vlachopoulos, *"Rheological evaluation and observations of extrusion instabilities of biodegradable polyesters"*. International Polymer Processing, **2007**. 22(5): p. 395-401.

194. Winter, H.H., *"Three views of viscoelasticity for Cox-Merz materials"*. Rheologica Acta, **2009**. 48(3): p. 241-43.

195. Kato, H., T. Ichitsubo, H. Igarashi, and A. Inoue, *"Correlation of dynamic and quasistatic relaxations: The Cox-Merz rule for metallic glass"*. Applied Physics Letters, **2009**. 95(23).

196. Venkatraman, S., M. Okano, and A. Nixon, *"A Comparison of Torsional and Capillary Rheometry for Polymer Melts - the Cox-Merz Rule Revisited"*. Polymer Engineering and Science, **1990**. 30(5): p. 308-13.

APPENDIX A – LINEAR VISCOELASTICITY

A.1. Master Curves

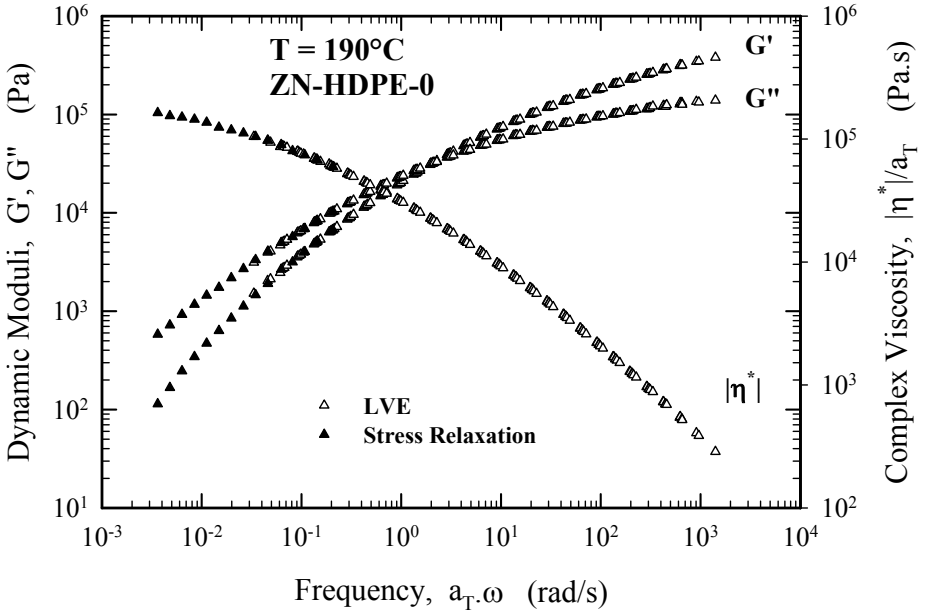

Figure A.1. *Master curves of storage and loss moduli for resin ZN-HDPE-0 at T_{ref} = 190°C. Data were obtained from frequency sweep linear viscoelastic measurements (LVE) and stress relaxation.*

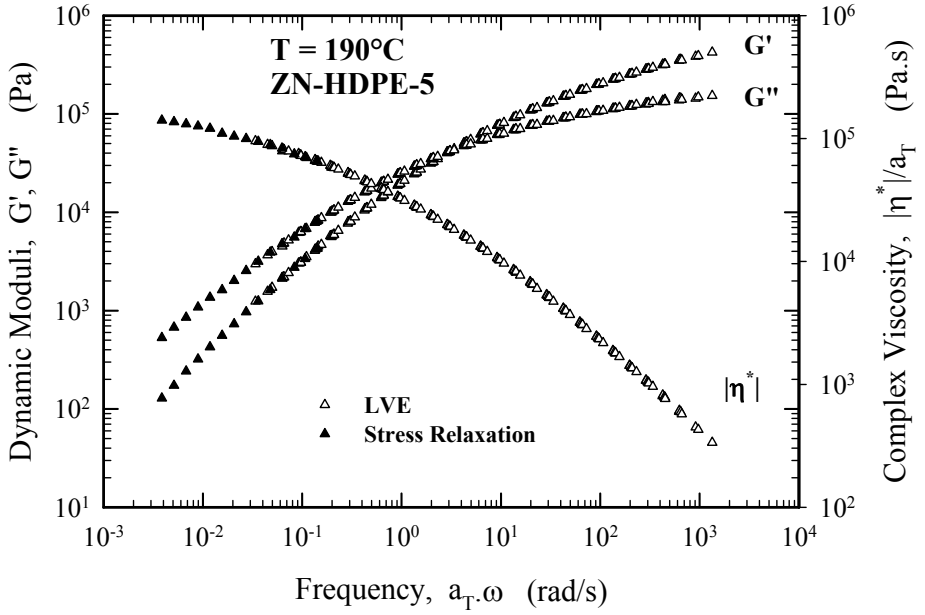

Figure A.2. *Master curves of storage and loss moduli for resin ZN-HDPE-5 at T_{ref} = 190°C. Data were obtained from frequency sweep linear viscoelastic measurements (LVE) and stress relaxation.*

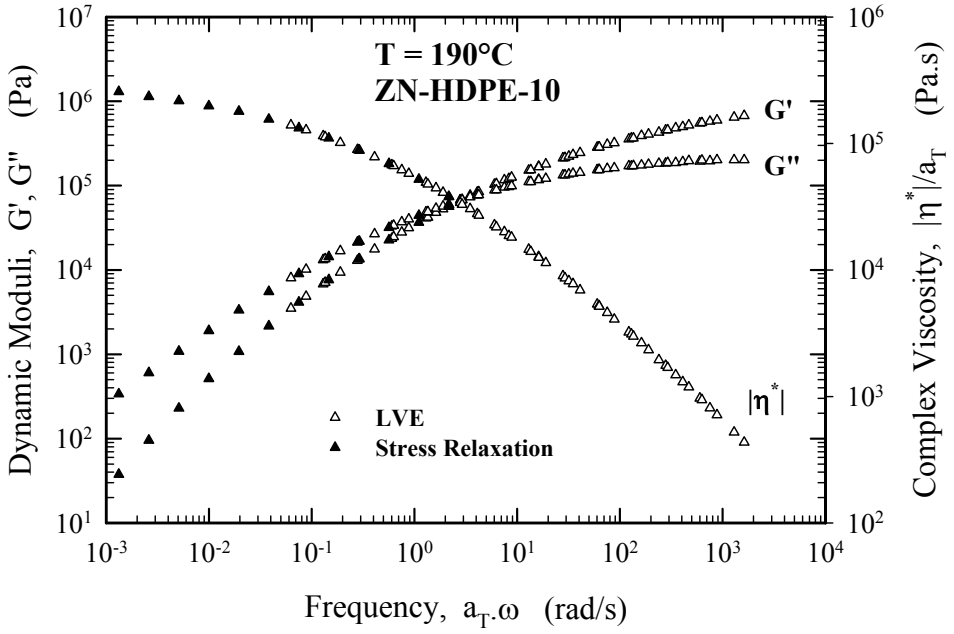

Figure A.3. *Master curves of storage and loss moduli for resin ZN-HDPE-10 at T_{ref} = 190°C. Data were obtained from frequency sweep linear viscoelastic measurements (LVE) and stress relaxation.*

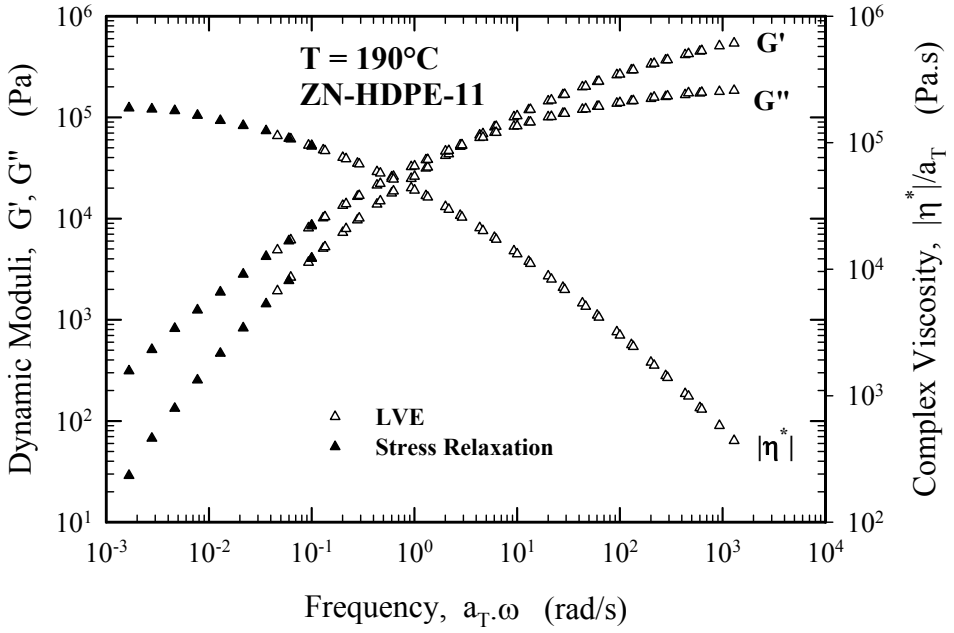

Figure A.4. *Master curves of storage and loss moduli for resin ZN-HDPE-11 at T_{ref} = 190°C. Data were obtained from frequency sweep linear viscoelastic measurements (LVE) and stress relaxation.*

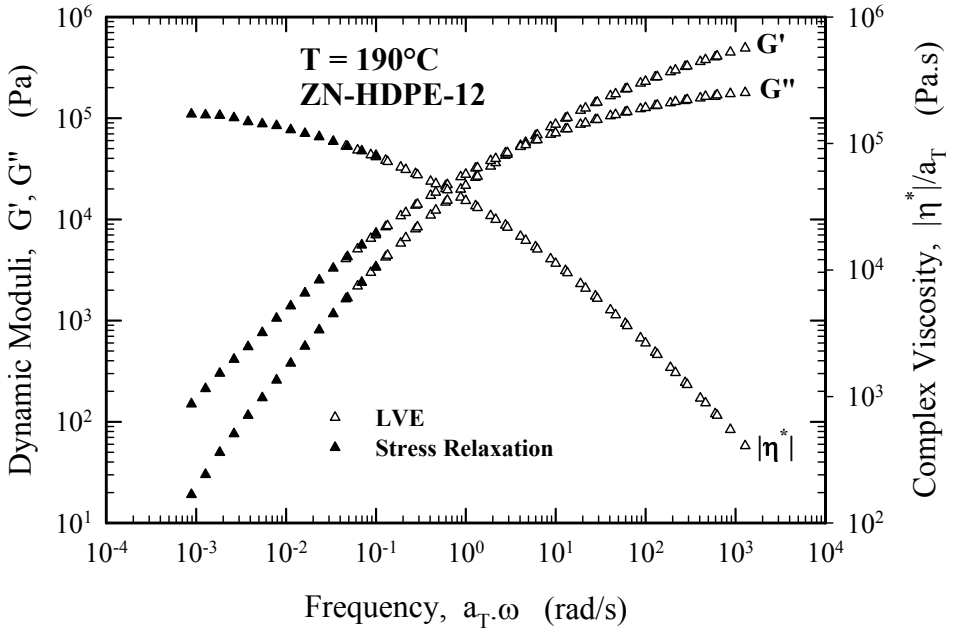

Figure A.5. *Master curves of storage and loss moduli for resin ZN-HDPE-12 at T_{ref} = 190°C. Data were obtained from frequency sweep linear viscoelastic measurements (LVE) and stress relaxation.*

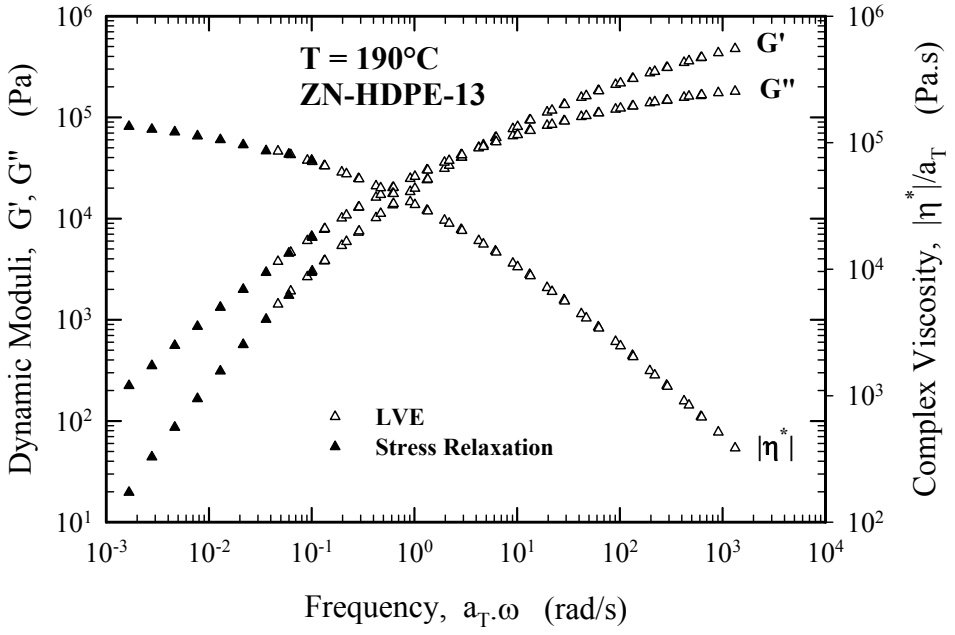

Figure A.6. *Master curves of storage and loss moduli for resin ZN-HDPE-13 at T_{ref} = 190°C. Data were obtained from frequency sweep linear viscoelastic measurements (LVE) and stress relaxation.*

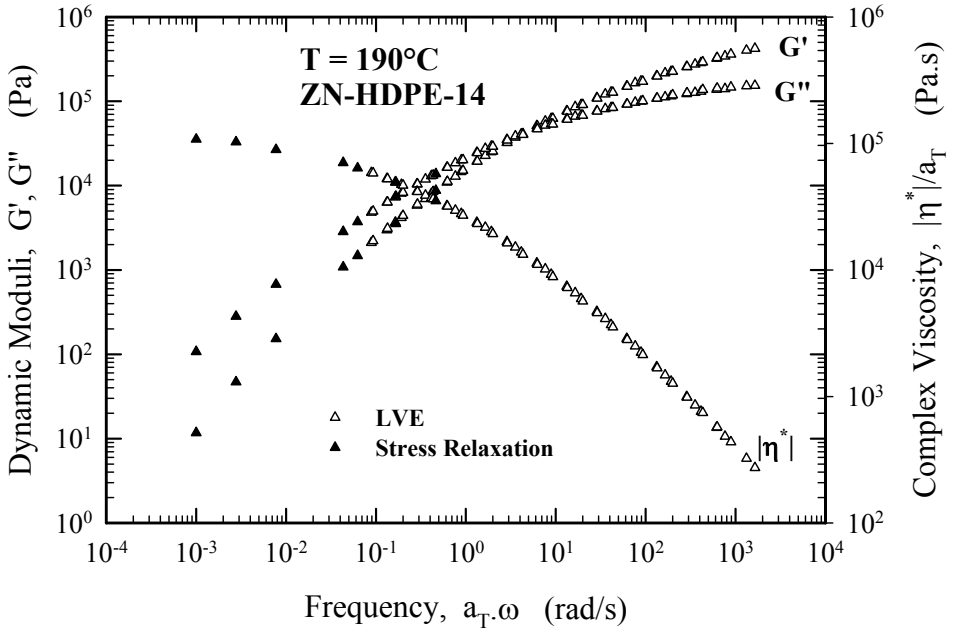

Figure A.7. *Master curves of storage and loss moduli for resin ZN-HDPE-14 at T_{ref} = 190°C. Data were obtained from frequency sweep linear viscoelastic measurements (LVE) and stress relaxation.*

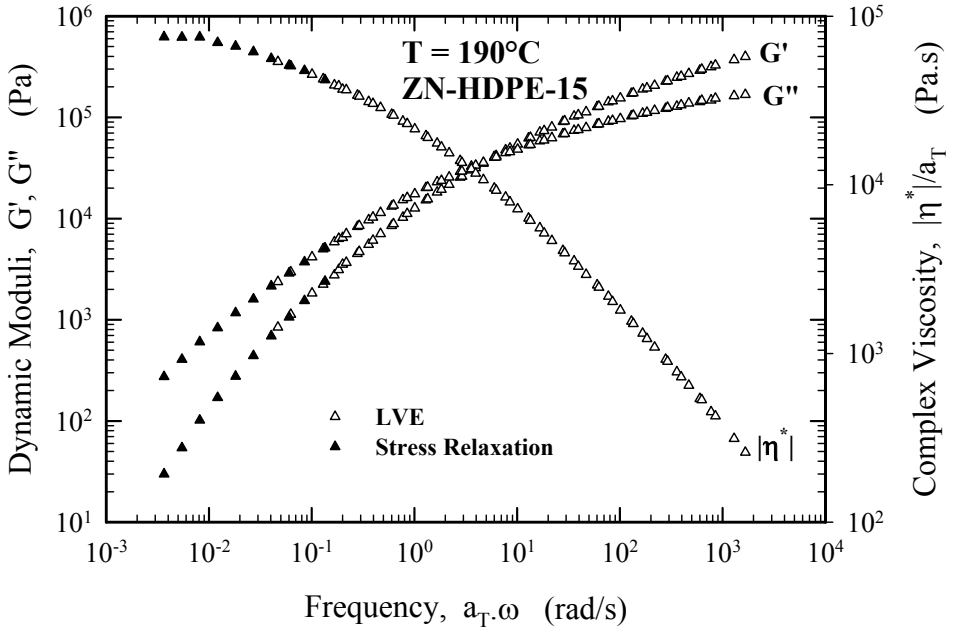

Figure A.8. *Master curves of storage and loss moduli for resin ZN-HDPE-15 at T_{ref} = 190°C. Data were obtained from frequency sweep linear viscoelastic measurements (LVE) and stress relaxation.*

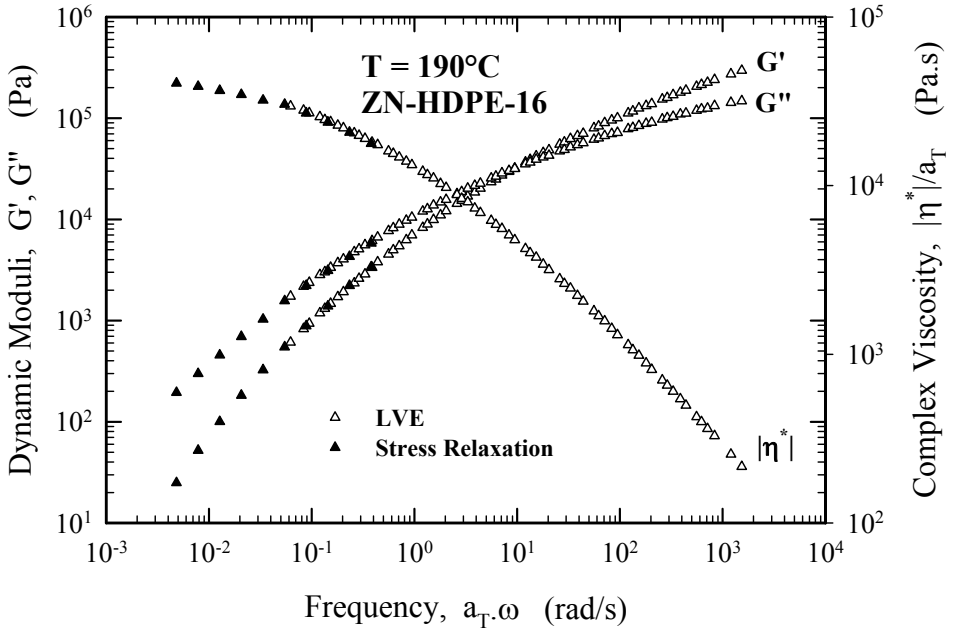

Figure A.9. *Master curves of storage and loss moduli for resin ZN-HDPE-16 at T_{ref} = 190°C. Data were obtained from frequency sweep linear viscoelastic measurements (LVE) and stress relaxation.*

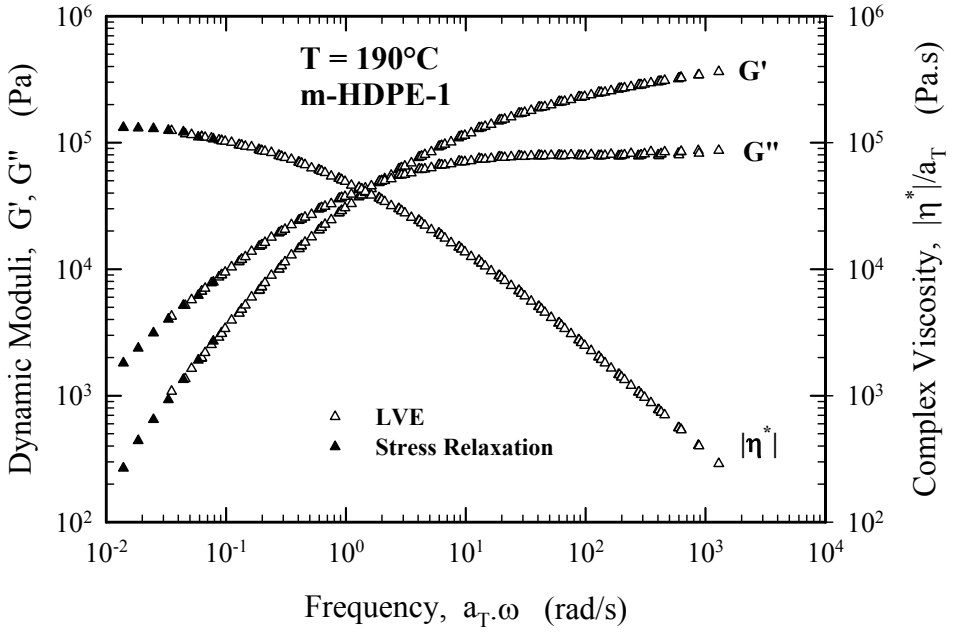

Figure A.10. *Master curves of storage and loss moduli for resin m-HDPE-1 at T_{ref} = 190°C. Data were obtained from frequency sweep linear viscoelastic measurements (LVE) and stress relaxation.*

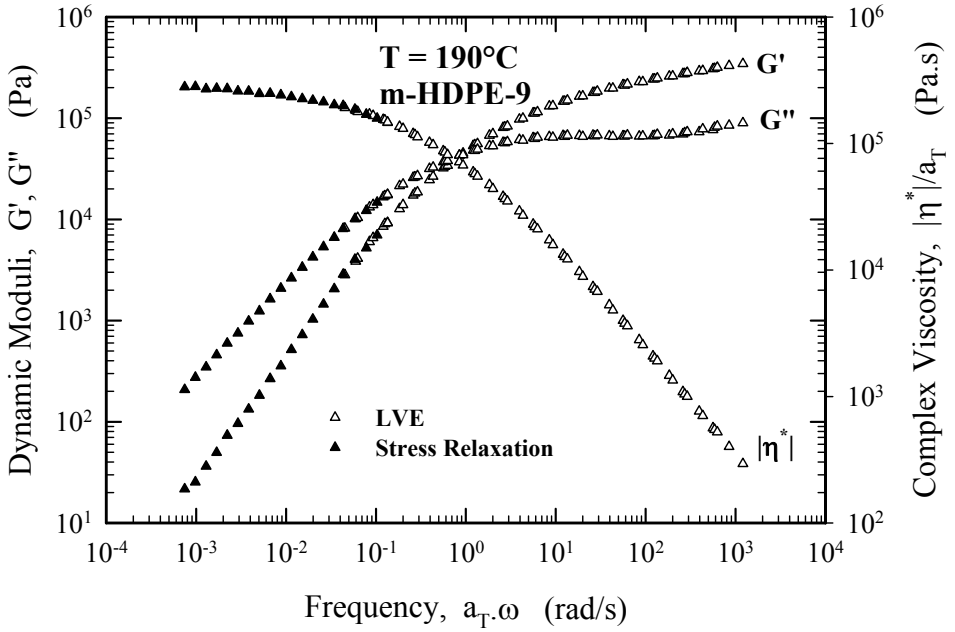

Figure A.11. *Master curves of storage and loss moduli for resin m-HDPE-9 at T_{ref} = 190°C. Data were obtained from frequency sweep linear viscoelastic measurements (LVE) and stress relaxation.*

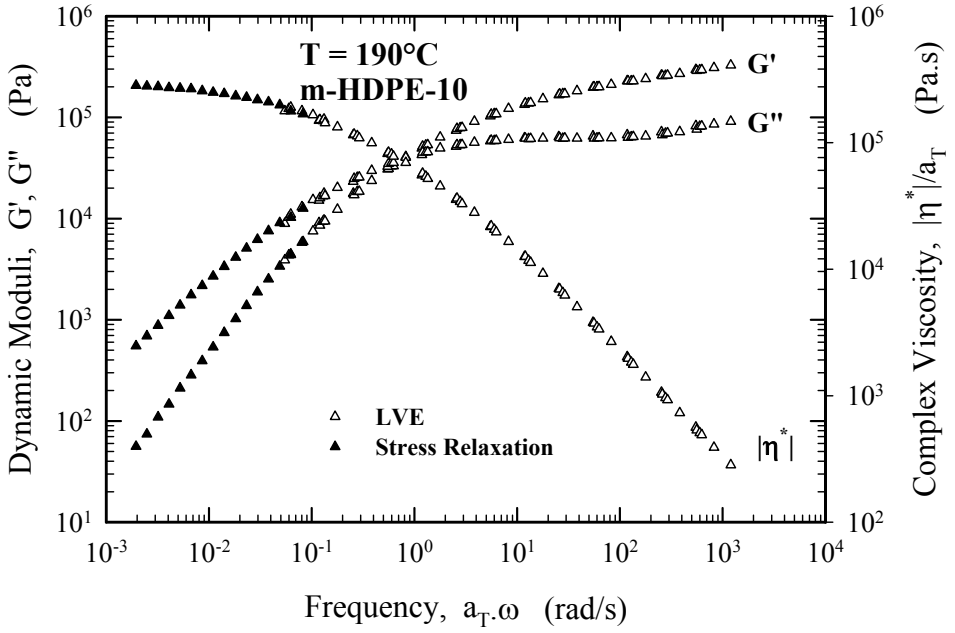

Figure A.12. *Master curves of storage and loss moduli for resin m-HDPE-10 at T_{ref} = 190°C. Data were obtained from frequency sweep linear viscoelastic measurements (LVE) and stress relaxation.*

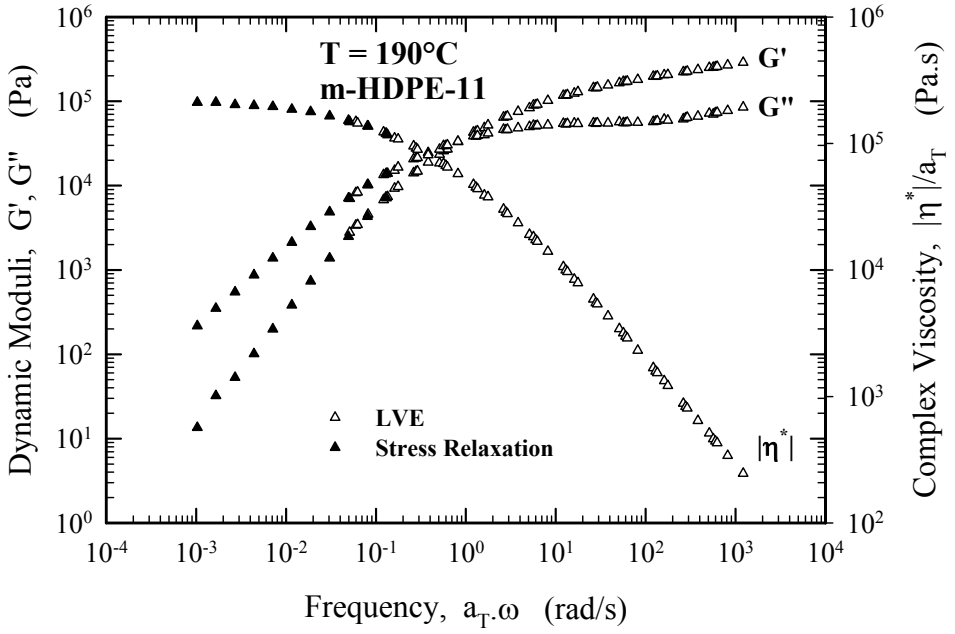

Figure A.13. *Master curves of storage and loss moduli for resin m-HDPE-11 at T_{ref} = 190°C. Data were obtained from frequency sweep linear viscoelastic measurements (LVE) and stress relaxation.*

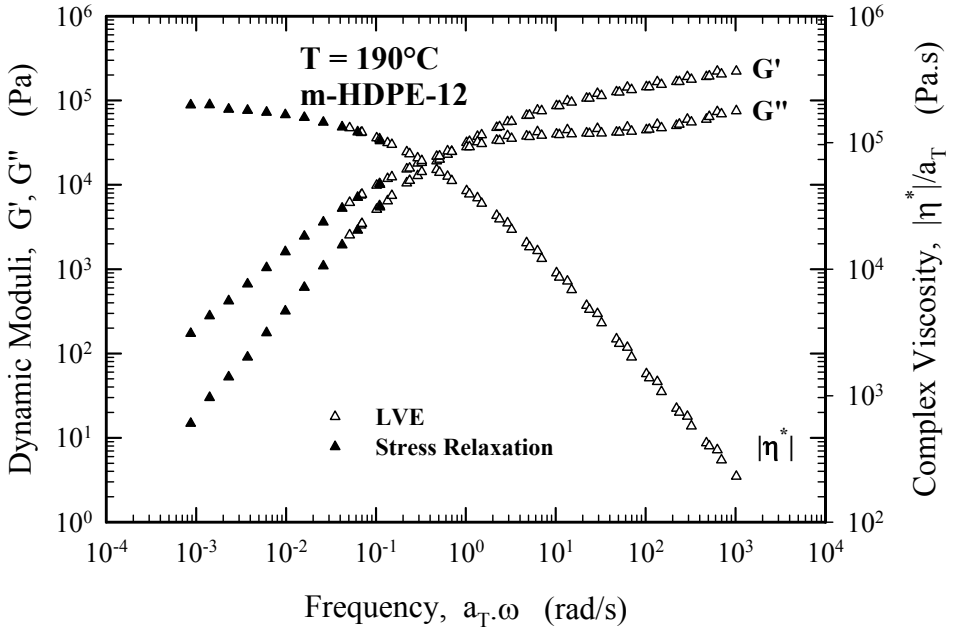

Figure A.14. *Master curves of storage and loss moduli for resin m-HDPE-12 at T_{ref} = 190°C. Data were obtained from frequency sweep linear viscoelastic measurements (LVE) and stress relaxation.*

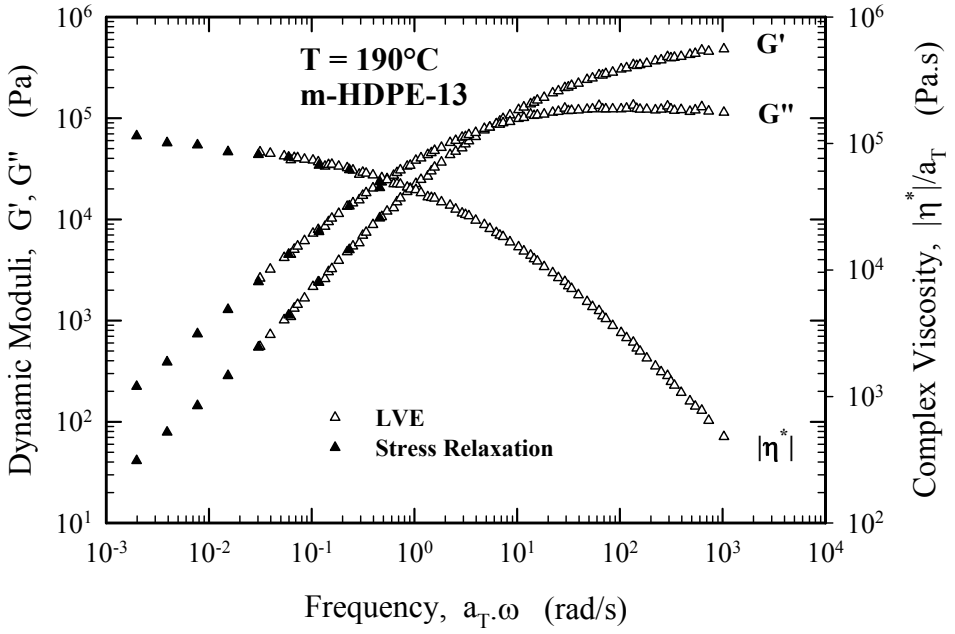

Figure A.15. *Master curves of storage and loss moduli for resin m-HDPE-13 at T_{ref} = 190°C. Data were obtained from frequency sweep linear viscoelastic measurements (LVE) and stress relaxation.*

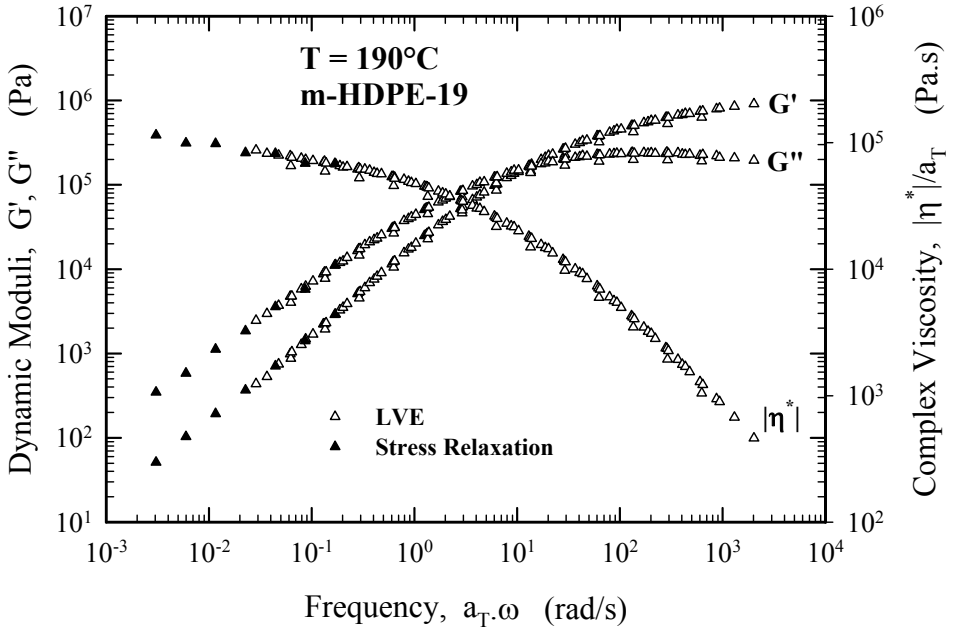

Figure A.16. *Master curves of storage and loss moduli for resin m-HDPE-19 at T_{ref} = 190°C. Data were obtained from frequency sweep linear viscoelastic measurements (LVE) and stress relaxation.*

A.2. Shift Factors

Table A.1. *Horizontal shift factors and activation energies for constructing master curve.*

Resin	Horizontal Shift Factor, a_T					E_a
	T=150°C	*T=170°C*	*T=190°C*	*T=210°C*	*T=230°C*	*(kcal/mole)*
ZN-HDPE-0	2.17	1.40	1.00	0.71	0.51	7.56
ZN-HDPE-5	2.08	1.50	1.00	0.69	0.52	7.46
ZN-HDPE-6	2.27	1.59	1.00	0.75	0.59	7.29
ZN-HDPE-10	2.06	1.40	1.00	0.74	-	6.93
ZN-HDPE-11	2.07	1.49	1.00	0.74	-	7.04
ZN-HDPE-12	2.05	1.40	1.00	0.74	-	6.89
ZN-HDPE-13	2.12	1.45	1.00	0.75	-	7.07
ZN-HDPE-14	2.13	1.43	1.00	0.69	-	7.56
ZN-HDPE-15	2.07	1.36	1.00	0.75	-	6.84
ZN-HDPE-16	1.94	1.34	1.00	0.71	-	6.73
m-HDPE-1	2.06	1.39	1.00	0.73	0.56	6.90
m-HDPE-8	2.13	1.43	1.00	0.77	-	6.90
m-HDPE-9	2.07	1.45	1.00	0.74	-	7.03
m-HDPE-10	2.01	1.38	1.00	0.92	-	5.49
m-HDPE-11	2.03	1.37	1.00	0.85	-	5.98
m-HDPE-12	2.0	1.37	1.00	0.87	-	5.72
m-HDPE-13	1.91	1.35	1.00	0.73	0.58	6.34
m-HDPE-19	2.03	1.37	1.00	0.75	0.57	6.75

A.3. Parsimonious Relaxation Spectra

Table A.2. *Parsimonious Relaxation Spectra for all the resins.*

Mode	*ZN-HDPE-0*		*ZN-HDPE-5*		*ZN-HDPE-6*		*ZN-HDPE-10*	
	λ_i *(s)*	G_i *(Pa)*	λ_i *(s)*	G_i *(Pa)*	λ_i *(s)*	G_i *(Pa)*	λ_i *(s)*	G_i *(Pa)*
1	0.000679	236375.7	0.000745	256309.2	0.000657	295177.1	0.000711	342347.9
2	0.004687	119993.9	0.005228	133955.3	0.004628	155683.5	0.005364	217558.1
3	0.025803	83941.61	0.029119	92935.65	0.025754	102084.6	0.033395	159770.3
4	0.136957	51196.86	0.153983	55001.55	0.138294	54071.65	0.200159	88998.29
5	0.717454	24323.07	0.800486	24159.86	0.745673	21322.23	1.193298	35367.43
6	3.751479	8582.533	4.104464	7480.318	4.090299	6308.725	7.56262	8931.907
7	21.33558	2623.237	23.37502	1879.899	23.7603	1740.091	50.93401	1527.885
8	146.5475	424.0777	181.9244	320.7249	198.4493	370.9492	387.3278	138.0883

Mode	*ZN-HDPE-11*		*ZN-HDPE-12*		*ZN-HDPE-13*		*ZN-HDPE-14*	
	λ_i *(s)*	G_i *(Pa)*	λ_i *(s)*	G_i *(Pa)*	λ_i *(s)*	G_i *(Pa)*	λ_i *(s)*	G_i *(Pa)*
1	0.000789	310768.1	0.000847	309566.8	0.000744	310067.1	0.000629	262915.7
2	0.005772	178274.4	0.006807	166115.8	0.00557	158964.5	0.004589	137940.8
3	0.034286	124485.1	0.044399	106083.6	0.033504	103555.9	0.027792	90467.74
4	0.196429	68475.55	0.279046	51716.46	0.194462	54270.72	0.162565	48126.22
5	1.111369	27392.82	1.72403	17669.13	1.111972	20932.34	0.928967	18879.81
6	6.225188	7167.717	11.20091	4020.929	6.446502	5295.38	5.237733	5067.522
7	33.42536	1593.01	77.03012	591.025	34.14986	1067.25	38.25527	1008.886
8	231.4075	174.7466	593.3561	68.62508	257.8695	97.41813	463.1736	56.2897

Mode	*ZN-HDPE-15*		*ZN-HDPE-16*	
	λ_i *(s)*	G_i *(Pa)*	λ_i *(s)*	G_i *(Pa)*
1	0.000538	289612.6	0.00053	263501.3
2	0.003722	132123	0.003711	102779.5
3	0.020789	82917.65	0.020594	57984.49
4	0.112638	44992.76	0.1131	28470.74
5	0.598268	19071.13	0.605889	11209.88
6	3.111558	5790.563	3.149166	3163.732
7	16.92205	1402.951	16.30383	759.652
8	107.9036	165.1019	98.58297	102.9341

Mode	*m-HDPE-1*		*m-HDPE-8*		*m-HDPE-9*		*m-HDPE-10*	
	λ_i *(s)*	G_i *(Pa)*	λ_i *(s)*	G_i *(Pa)*	λ_i *(s)*	G_i *(Pa)*	λ_i *(s)*	G_i *(Pa)*
1	0.000652	138464.3	0.000781	173981.6	0.000915	157658.3	0.00083	161704.4
2	0.004062	76619.69	0.007566	108566.6	0.009964	82743.72	0.008412	74074.87
3	0.01966	80614.43	0.051275	124598.6	0.075295	88850.09	0.058835	78231.77
4	0.088475	76837.51	0.308882	106458.4	0.492641	69868.74	0.362638	67498.28
5	0.383417	52753.99	1.727492	51695.54	2.949796	29356.31	2.074226	34189.03
6	1.611592	22962.76	10.10858	11670.6	17.84629	5248.18	11.62367	8779.244
7	6.46897	6004.133	81.40472	703.4459	162.0862	289.8034	74.57821	857.4981
8	34.81225	1088.862	828.6629	37.62244	1597.216	26.00886	691.4772	54.14863

Mode	*m-HDPE-111*		*m-HDPE-12*		*m-HDPE-13*		*m-HDPE-19*	
	λ_i *(s)*	G_i *(Pa)*	λ_i *(s)*	G_i *(Pa)*	λ_i *(s)*	G_i *(Pa)*	λ_i *(s)*	G_i *(Pa)*
1	0.000692	151086.4	0.000877	138000.9	0.001216	190695.1	0.000632	321847.3
2	0.006232	64215.47	0.008623	50780.37	0.009128	151029.6	0.004626	283051
3	0.0413	65509.82	0.058747	49289.99	0.050401	137146.6	0.024851	247904.1
4	0.243975	60145.76	0.344953	43762.19	0.260753	73058.5	0.12211	133085.7
5	1.3339	35068.01	1.856976	23966.08	1.352669	20168.35	0.595997	38574.47
6	6.957693	10394.29	9.657726	6827.35	7.853792	3055.936	3.098442	6523.295
7	36.4237	1575.595	58.03224	831.1806	58.42575	354.1737	20.00976	885.5724
8	447.1503	62.85716	636.6833	51.33302	504.6236	71.9296	210.0838	155.0879

APPENDIX B – EXTENSIONAL RHEOLOGY

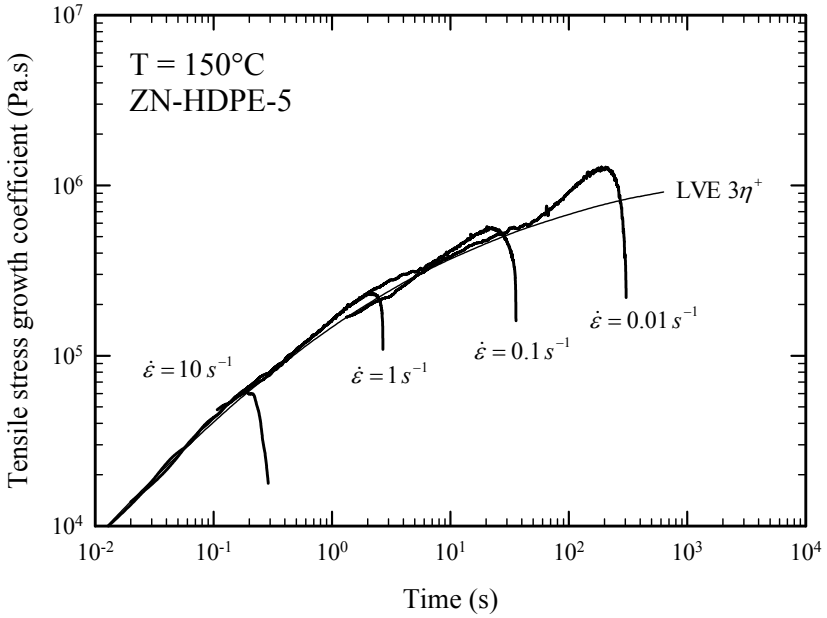

Figure B.1. *The tensile stress growth coefficient of resin ZN-HDPE-5 at several Hencky strain rates, at T=150°C. The line labeled as LVE* $3\eta^+$ *line has been calculated from fitting linear viscoelastic measurements with a parsimonious relaxation spectrum and use of Eq. 6.1.*

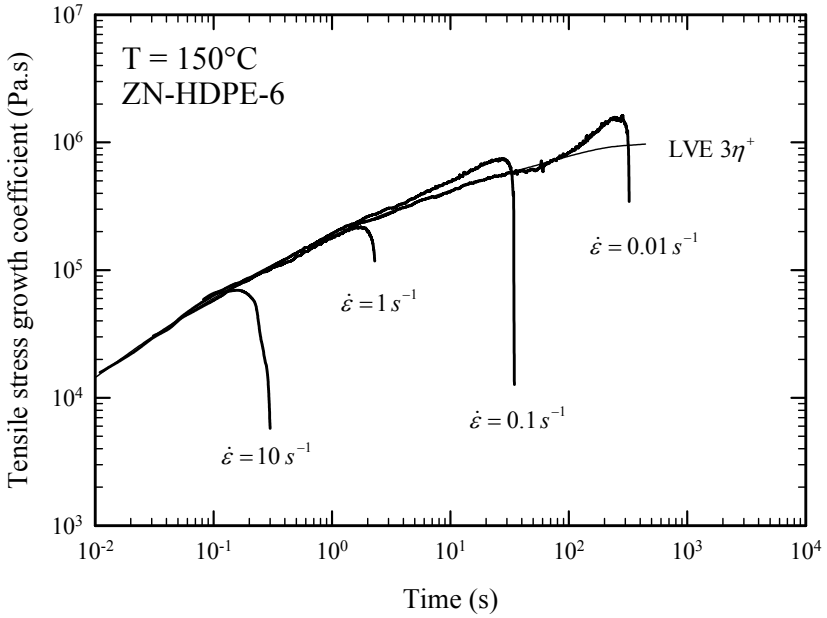

Figure B.2. *The tensile stress growth coefficient of resin ZN-HDPE-6 at several Hencky strain rates, at T=150°C. The line labeled as LVE* $3\eta^+$ *line has been calculated from fitting linear viscoelastic measurements with a parsimonious relaxation spectrum and use of Eq. 6.1.*

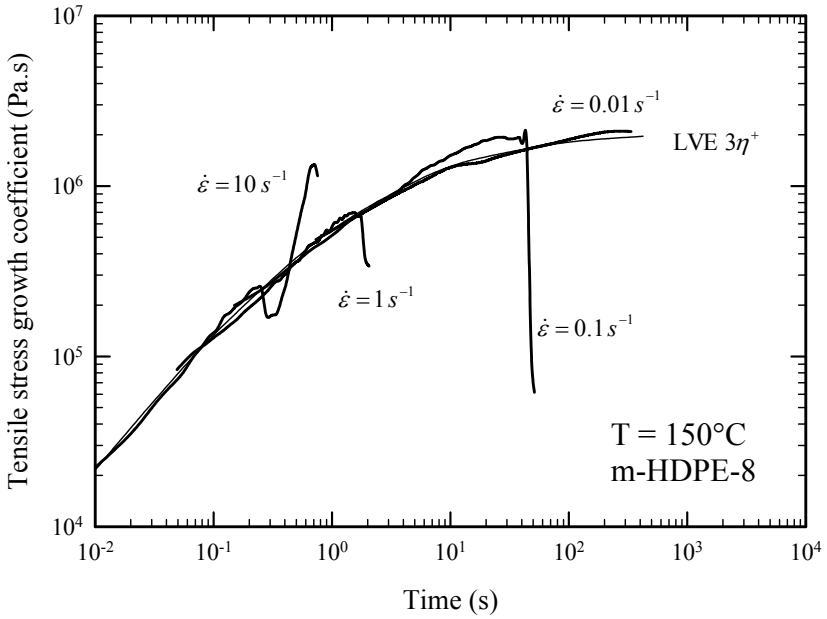

Figure B.3. *The tensile stress growth coefficient of resin m-HDPE-8 at several Hencky strain rates, at T=150°C. The line labeled as LVE* $3\eta^+$ *line has been calculated from fitting linear viscoelastic measurements with a parsimonious relaxation spectrum and use of Eq. 6.1.*

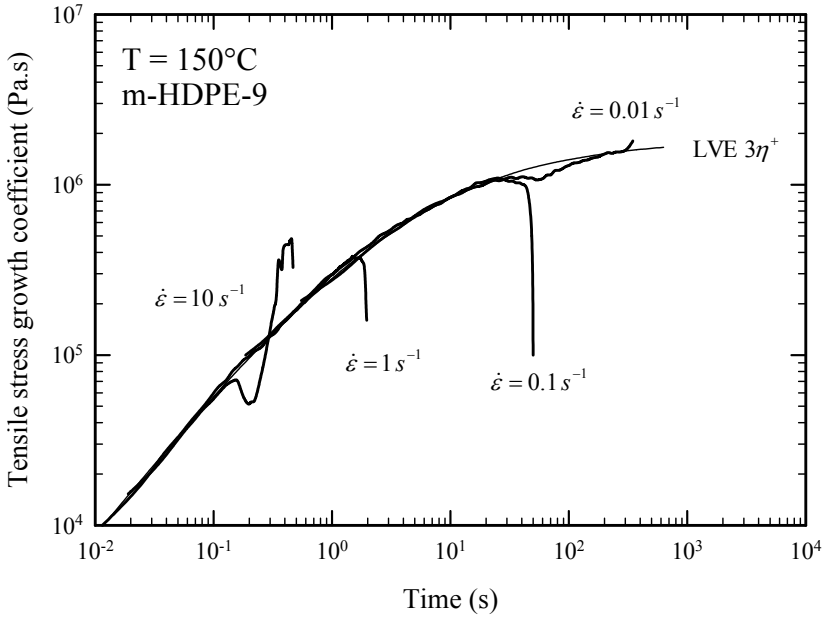

Figure B.4. *The tensile stress growth coefficient of resin m-HDPE-9 at several Hencky strain rates, at T=150°C. The line labeled as LVE* $3\eta^+$ *line has been calculated from fitting linear viscoelastic measurements with a parsimonious relaxation spectrum and use of Eq. 6.1.*

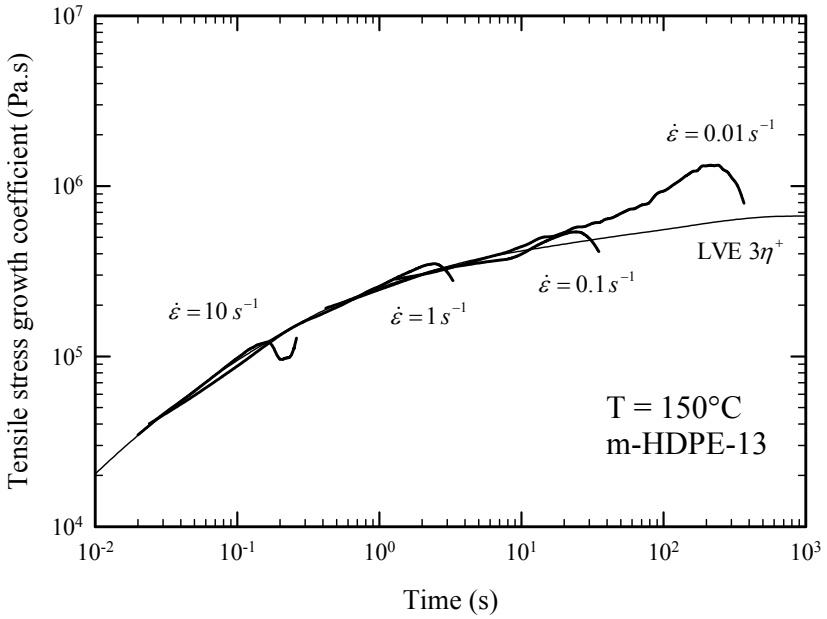

Figure B.5. *The tensile stress growth coefficient of resin m-HDPE-13 at several Hencky strain rates, at T=150°C. The line labeled as LVE* $3\eta^+$ *line has been calculated from fitting linear viscoelastic measurements with a parsimonious relaxation spectrum and use of Eq. 6.1.*

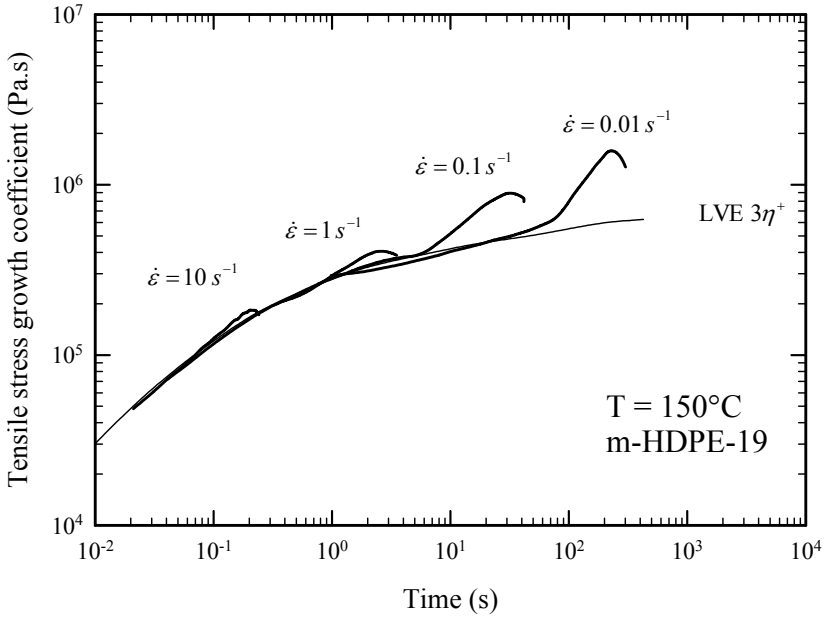

Figure B.6. *The tensile stress growth coefficient of resin m-HDPE-19 at several Hencky strain rates, at T=150°C. The line labeled as LVE* $3\eta^+$ *line has been calculated from fitting linear viscoelastic measurements with a parsimonious relaxation spectrum and use of Eq. 6.1.*

APPENDIX C – FLOW CURVES

C.1. Flow Curves

C.1.1. Effect of Temperature

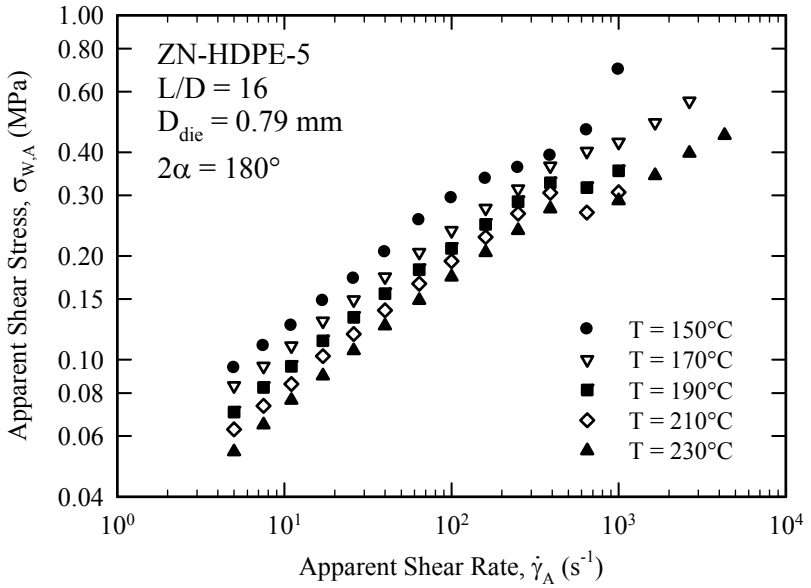

Figure C.1a. *The flow curves of resin ZN-HDPE-5 in capillary extrusion at different temperatures.*

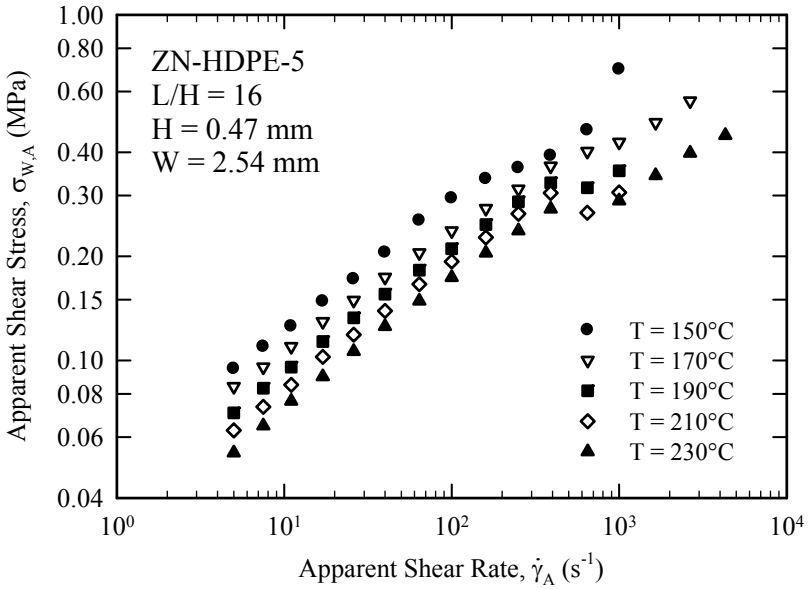

Figure C.1b. *The flow curves of resin ZN-HDPE-5 in slit extrusion at different temperatures.*

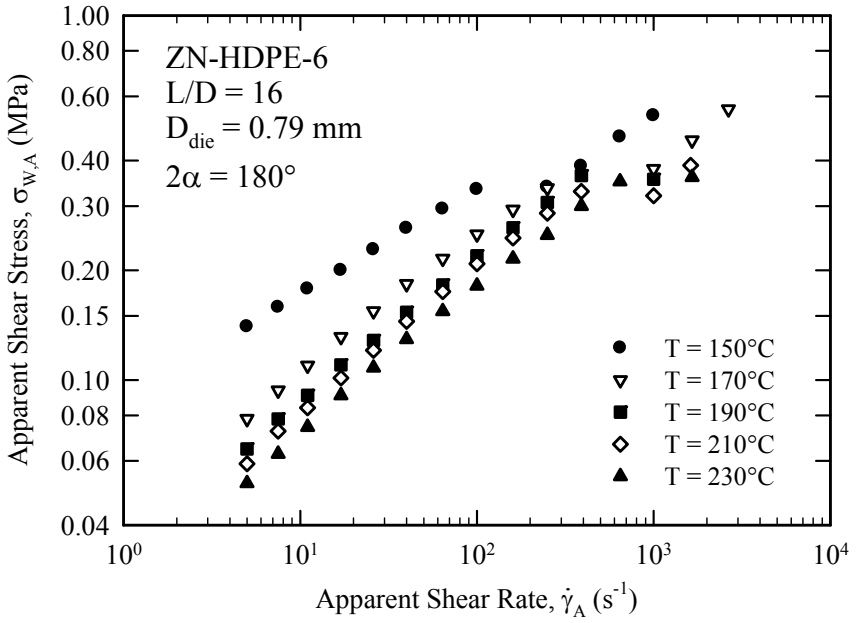

Figure C.2a. *The flow curves of resin ZN-HDPE-6 in capillary extrusion at different temperatures.*

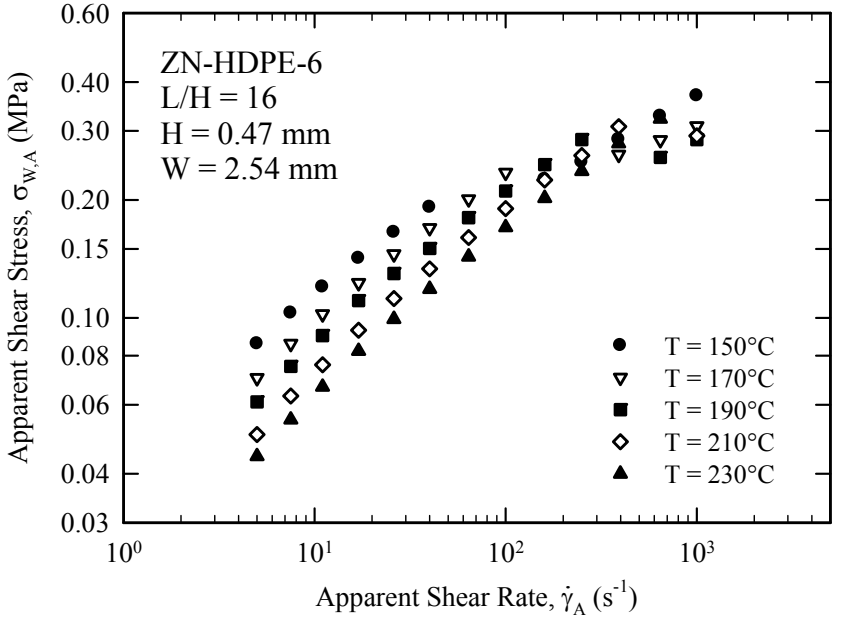

Figure C.2b. *The flow curves of resin ZN-HDPE-6 in slit extrusion at different temperatures.*

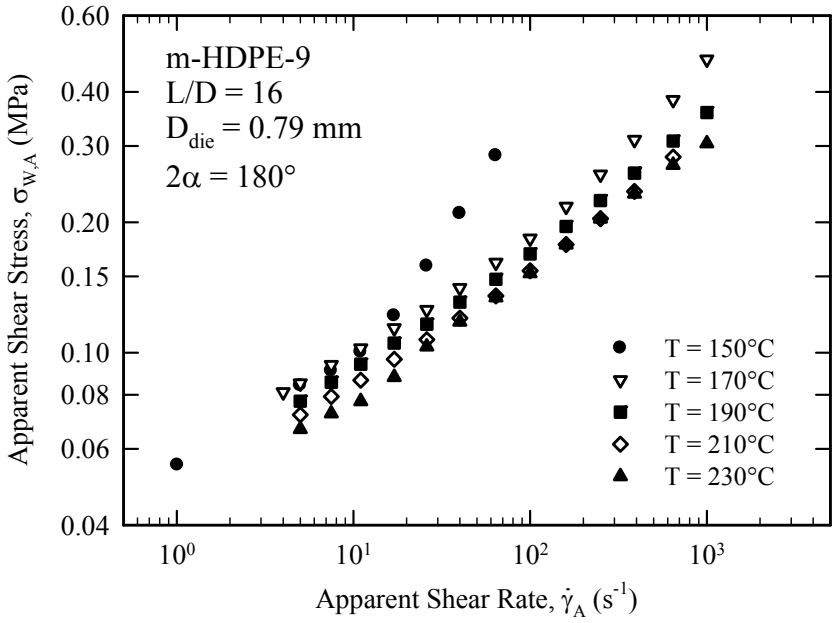

Figure C.3a. *The flow curves of resin m-HDPE-9 in capillary extrusion at different temperatures.*

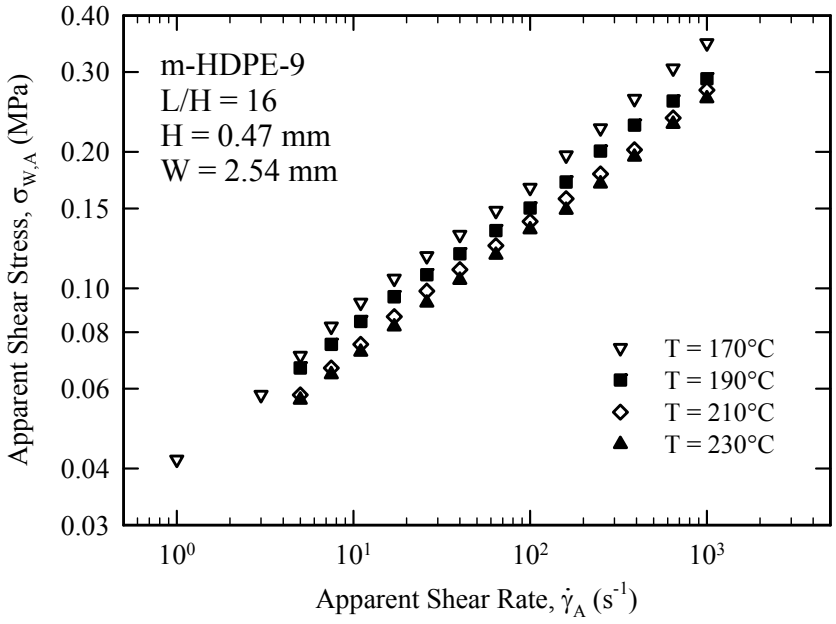

Figure C.3b. *The flow curves of resin m-HDPE-9 in slit extrusion at different temperatures.*

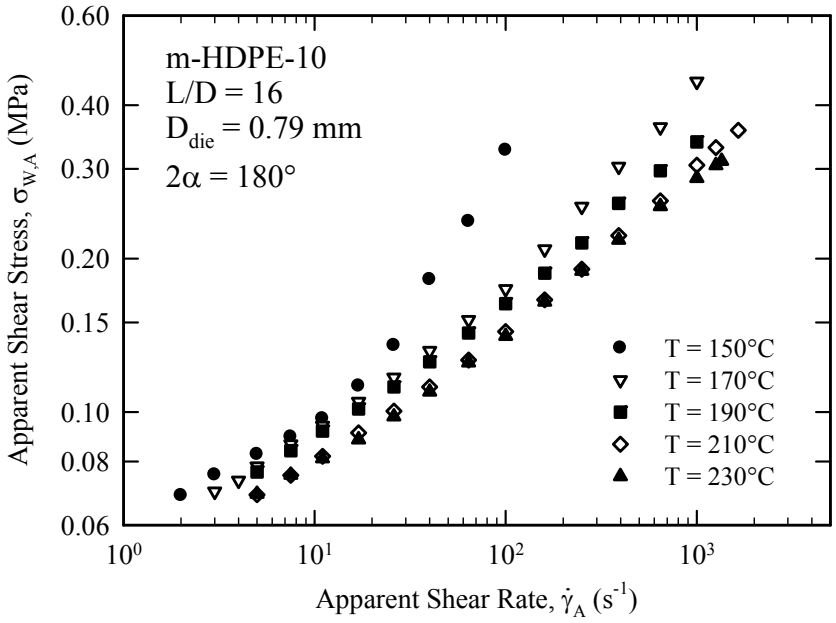

Figure C.4a. *The flow curves of resin m-HDPE-10 in capillary extrusion at different temperatures.*

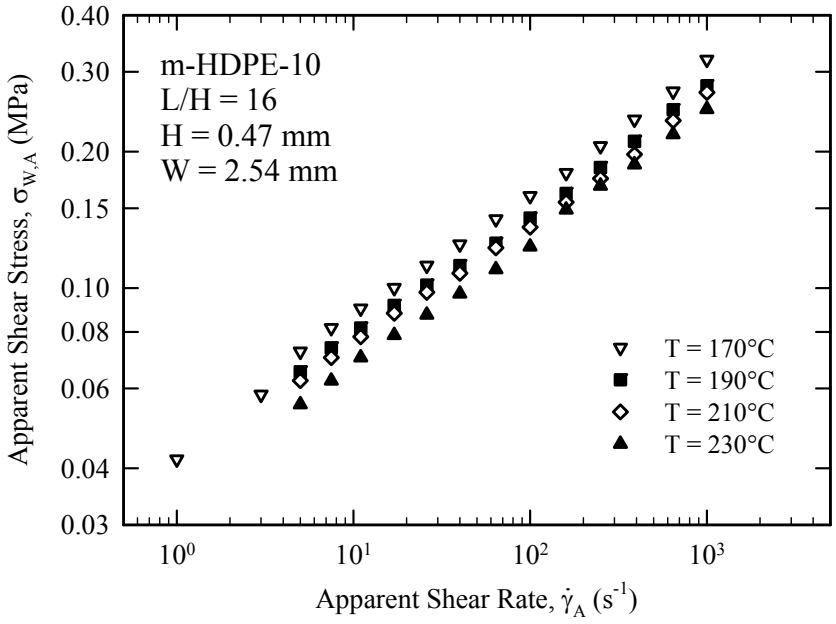

Figure C.4b. *The flow curves of resin m-HDPE-10 in slit extrusion at different temperatures.*

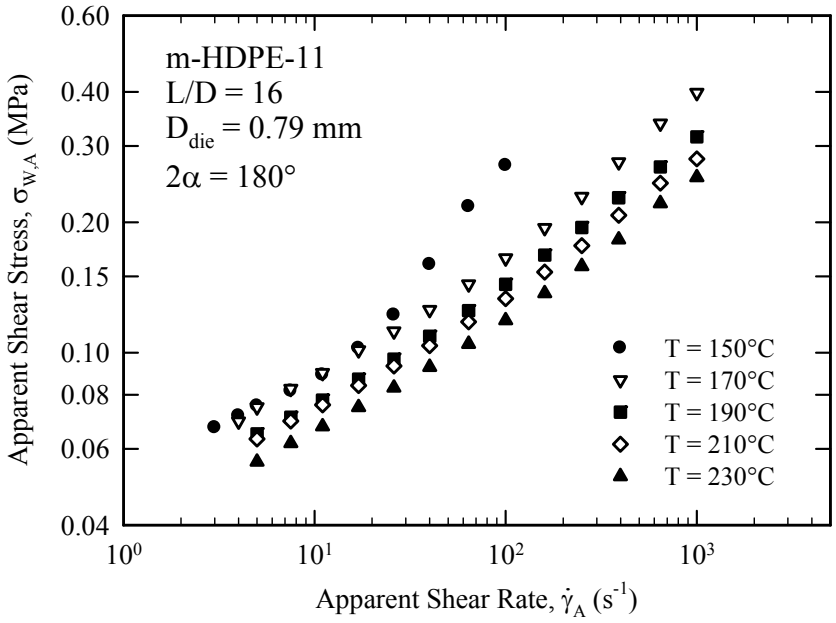

Figure C.5a. *The flow curves of resin m-HDPE-11 in capillary extrusion at different temperatures.*

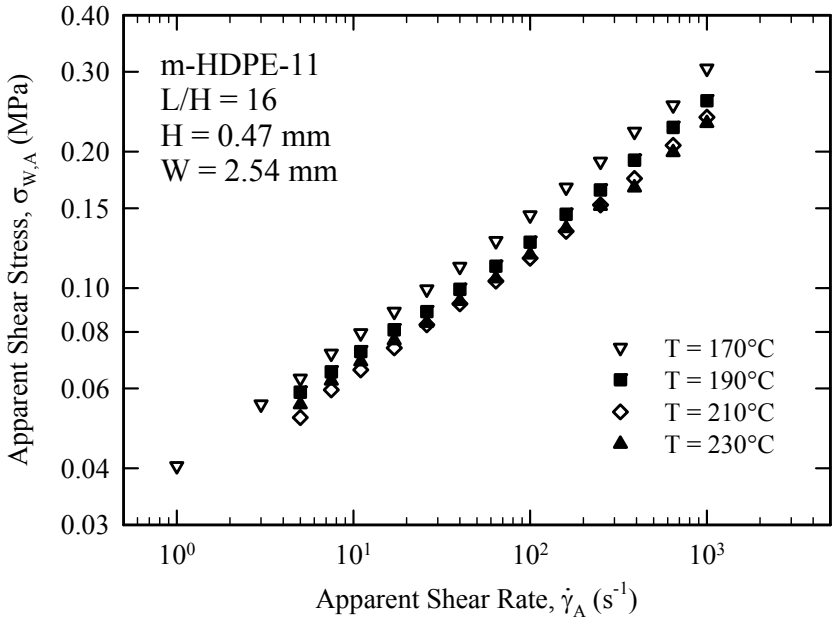

Figure C.5b. *The flow curves of resin m-HDPE-11 in slit extrusion at different temperatures.*

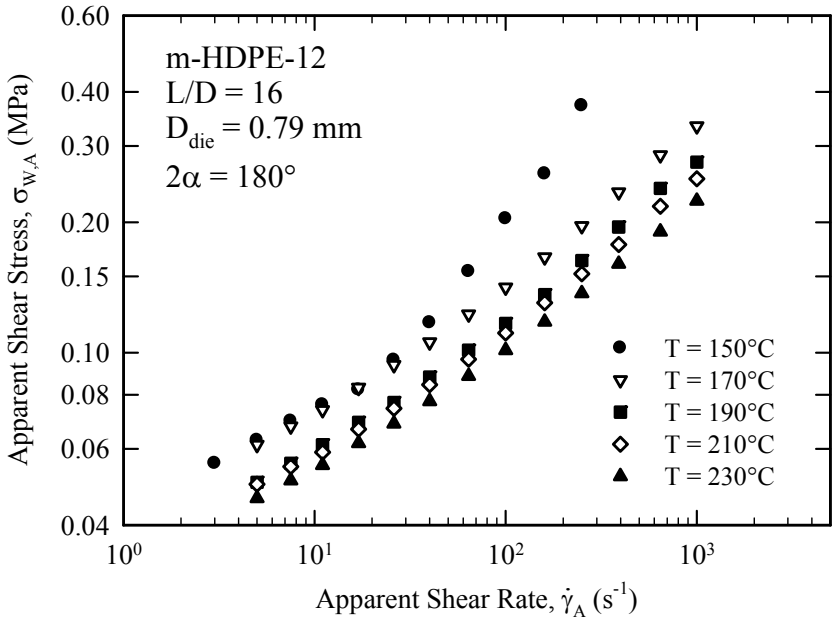

Figure C.6a. *The flow curves of resin m-HDPE-12 in capillary extrusion at different temperatures.*

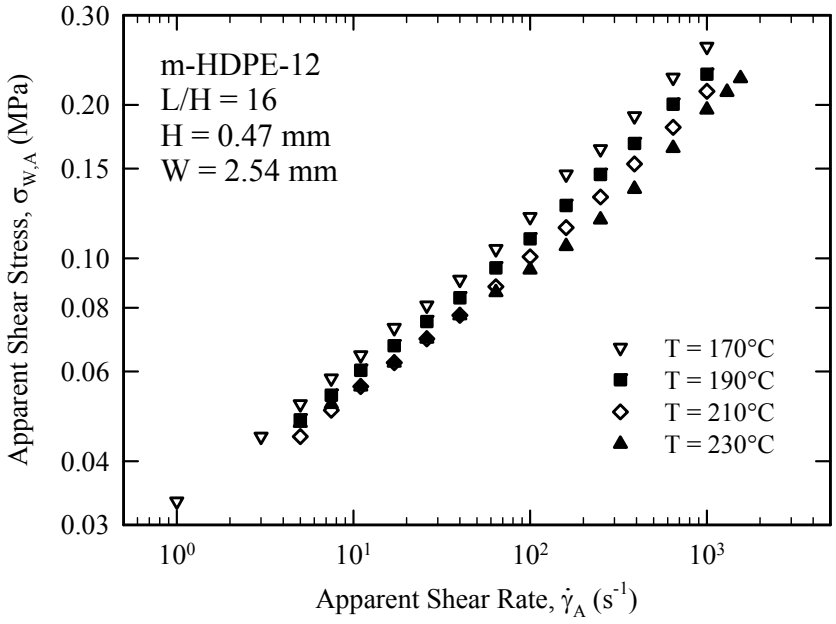

Figure C.6b. *The flow curves of resin m-HDPE-12 in slit extrusion at different temperatures.*

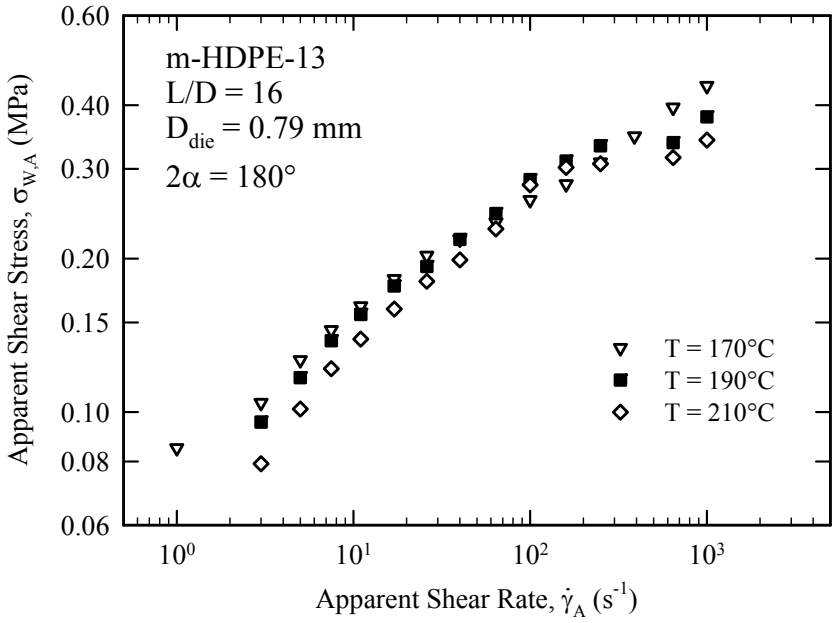

Figure C.7a. *The flow curves of resin m-HDPE-13 in capillary extrusion at different temperatures.*

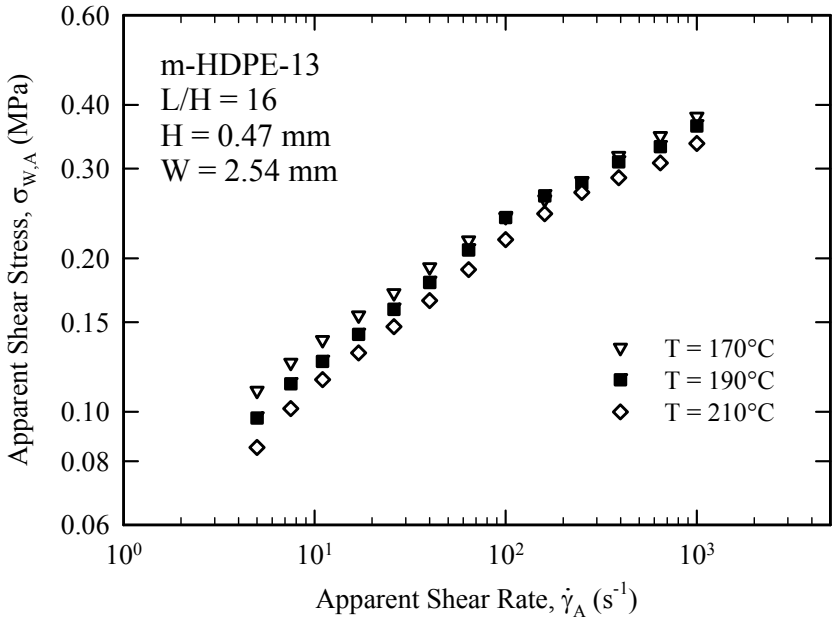

Figure C.7b. *The flow curves of resin m-HDPE-13 in slit extrusion at different temperatures.*

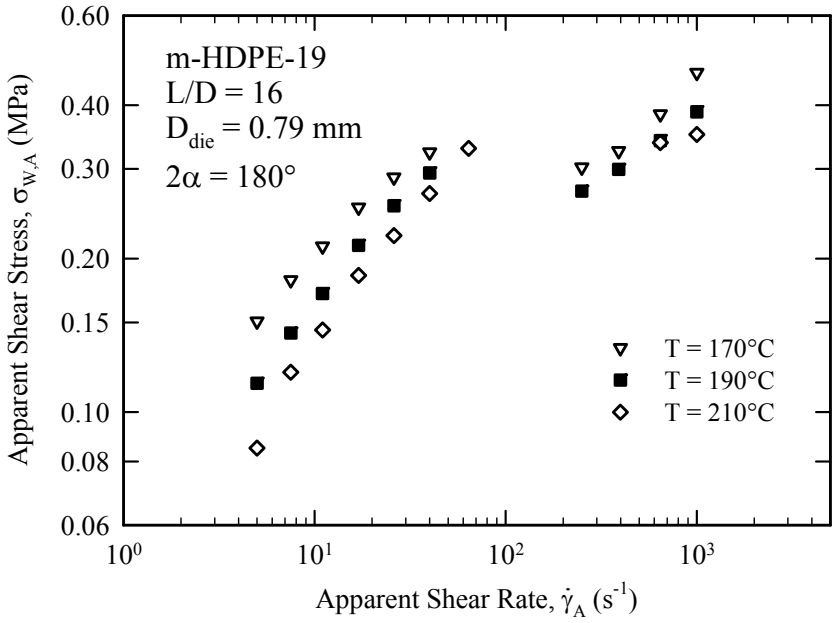

Figure C.8a. *The flow curves of resin m-HDPE-19 in capillary extrusion at different temperatures.*

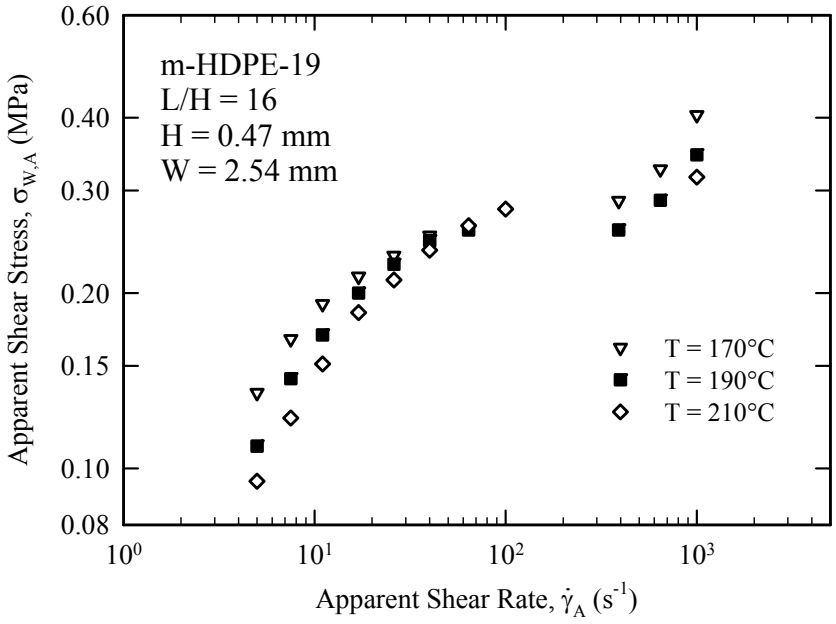

Figure C.8b. *The flow curves of resin m-HDPE-19 in slit extrusion at different temperatures.*

C.1.2. Effect of Die Entrance Angle

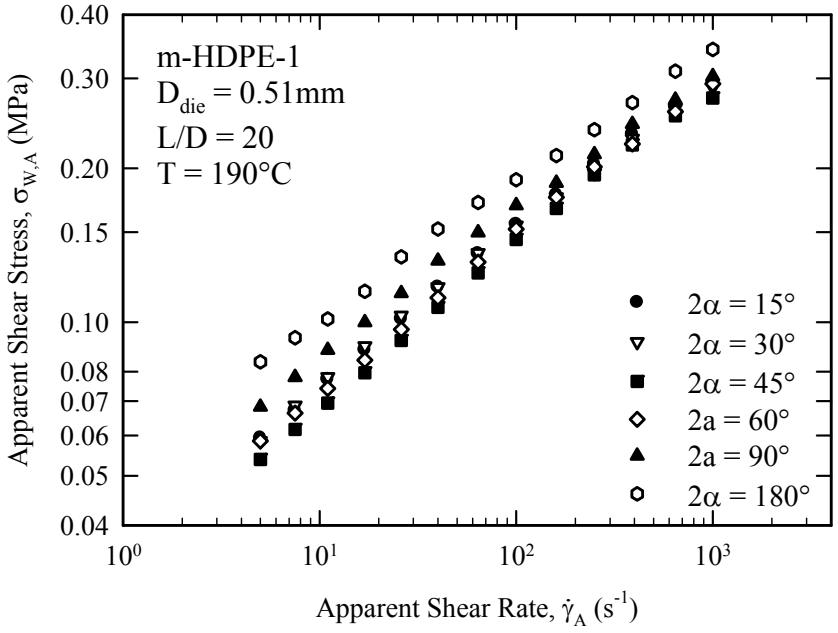

Figure C.9. *The effect of die entrance angle on the flow curve and processing of resin m-HDPE-1 at T=190°C*

C.2. Bagley Correction

As it has been noted in section 2.3.2.3, in order to perform Bagley correction, one should collect data for 3 different dies with the same diameter, but different length to diameter ratios. Then by plotting pressure drop values versus L/D at a given shear rate and extrapolate the data to the zero L/D, one can calculate the Bagley end pressure (Eq. 2.8). This procedure is shown below for one of the HDPE resins as an example.

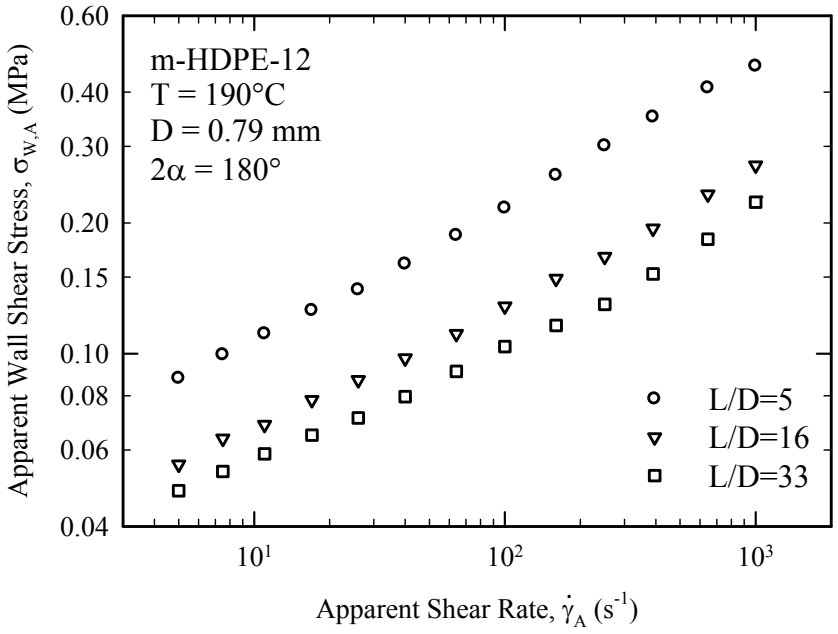

Figure C.10a. *The apparent flow curves of resin m-HDPE-12 at 190°C for various L/D ratios.*

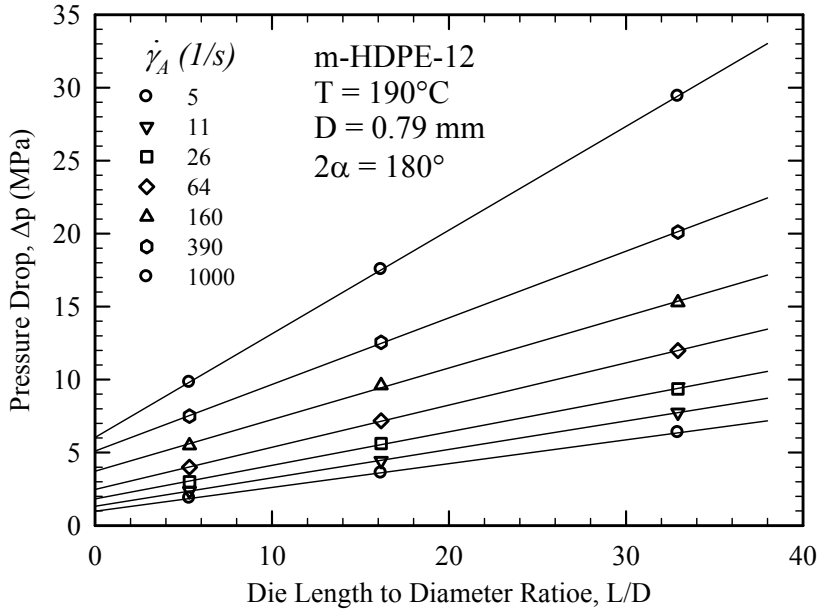

Figure C.10b. *The pressure drop for the capillary extrusion of the resin m-HDPE-12 at 190°C as a function of L/D for different values of the apparent shear rate (Bagley plot).*

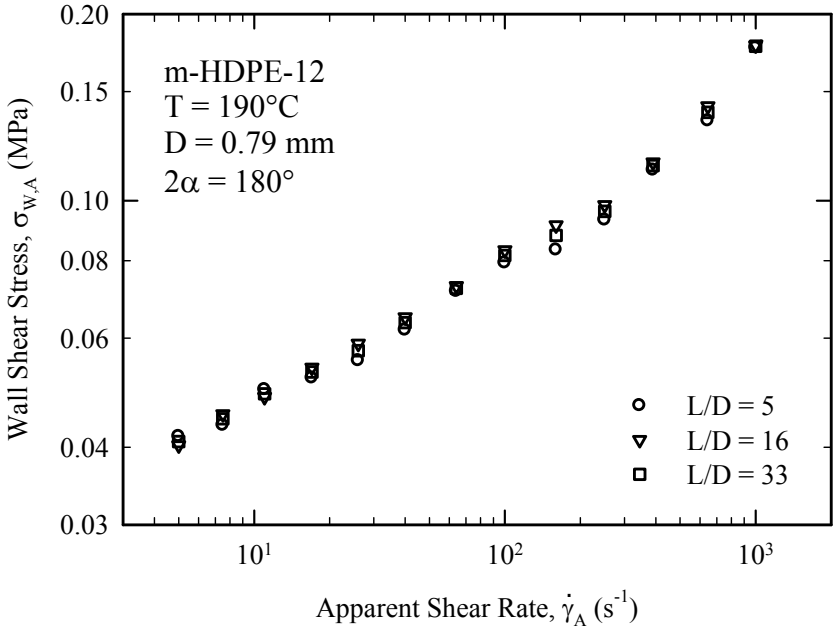

Figure C.10c. *The flow curves of resin m-HDPE-12 at 190°C as a function of the apparent shear rate for various L/D ratios corrected for the entrance effects. The data superpose well showing that the pressure effect of viscosity is negligible as expected for HDPE melts.*

APPENDIX D – PROCESSING MAPS

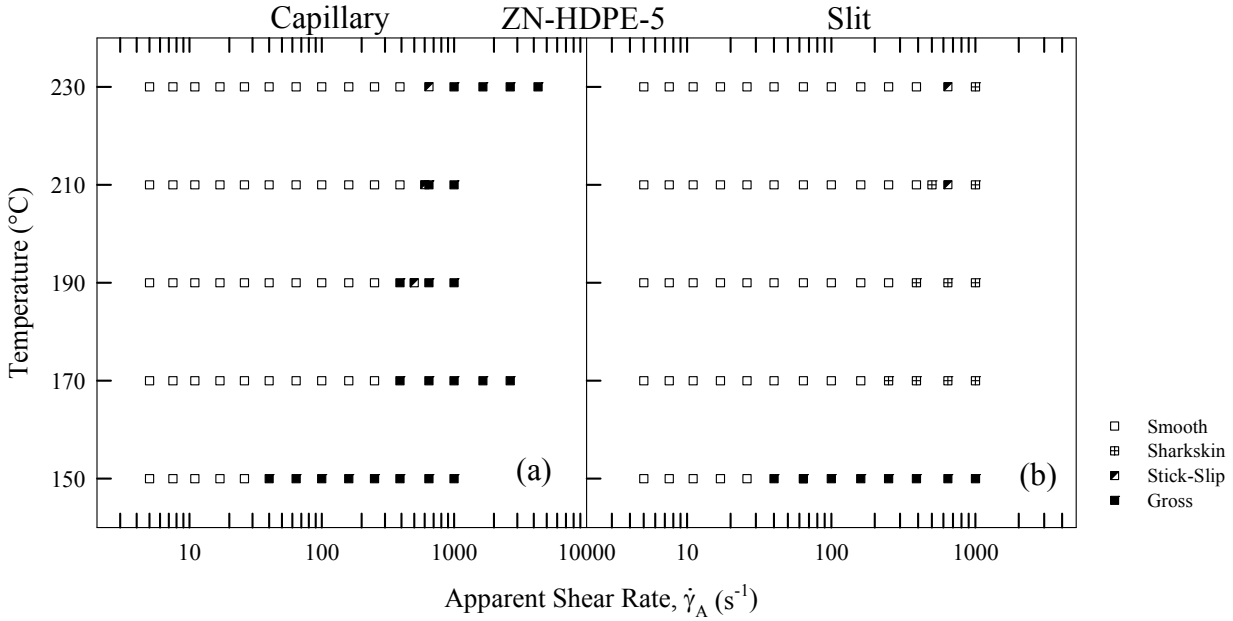

Figure D.1. *Processability map of resin ZN-HDPE-5 in extrusion through capillary and slit dies as a function of apparent shear rate and temperature.*

Table D.1. *Critical apparent shear rates and shear stresses for the onset of melt fracture in capillary and slit dies for resin ZN-HDPE-5 at different temperatures.*

Temperature (°C)	*Capillary*		*Slit*	
	$\dot{\gamma}_{A,cr}$ (s^{-1})	$\sigma_{A,cr}$(MPa)	$\dot{\gamma}_{A,cr}$ (s^{-1})	$\sigma_{A,cr}$(MPa)
150	32.2	0.19	32.2	0.17
170	312	0.34	200	0.26
190	312	0.31	312	0.26
210	501	0.34	442	0.28
230	630	0.33	610	0.31

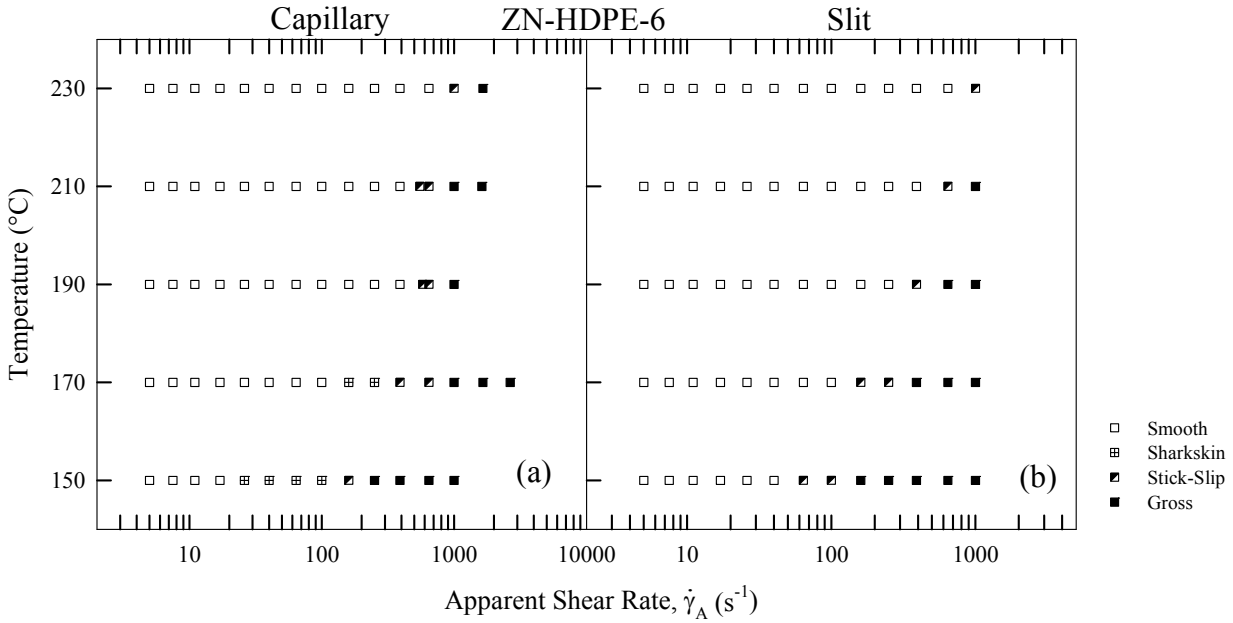

Figure D.2. *Processability map of resin ZN-HDPE-6 in extrusion through capillary and slit dies as a function of apparent shear rate and temperature.*

Table D.2. *Critical apparent shear rates and shear stresses for the onset of melt fracture in capillary and slit dies for resin ZN-HDPE-6 at different temperatures.*

Temperature (°C)	*Capillary*		*Slit*	
	$\dot{\gamma}_{A,cr}$ (s^{-1})	$\sigma_{A,cr}$(MPa)	$\dot{\gamma}_{A,cr}$ (s^{-1})	$\sigma_{A,cr}$(MPa)
150	21	0.21	55	0.21
170	126	0.27	140	0.27
190	550	0.41	305	0.31
210	530	0.36	490	0.33
230	860	0.4	670	0.33

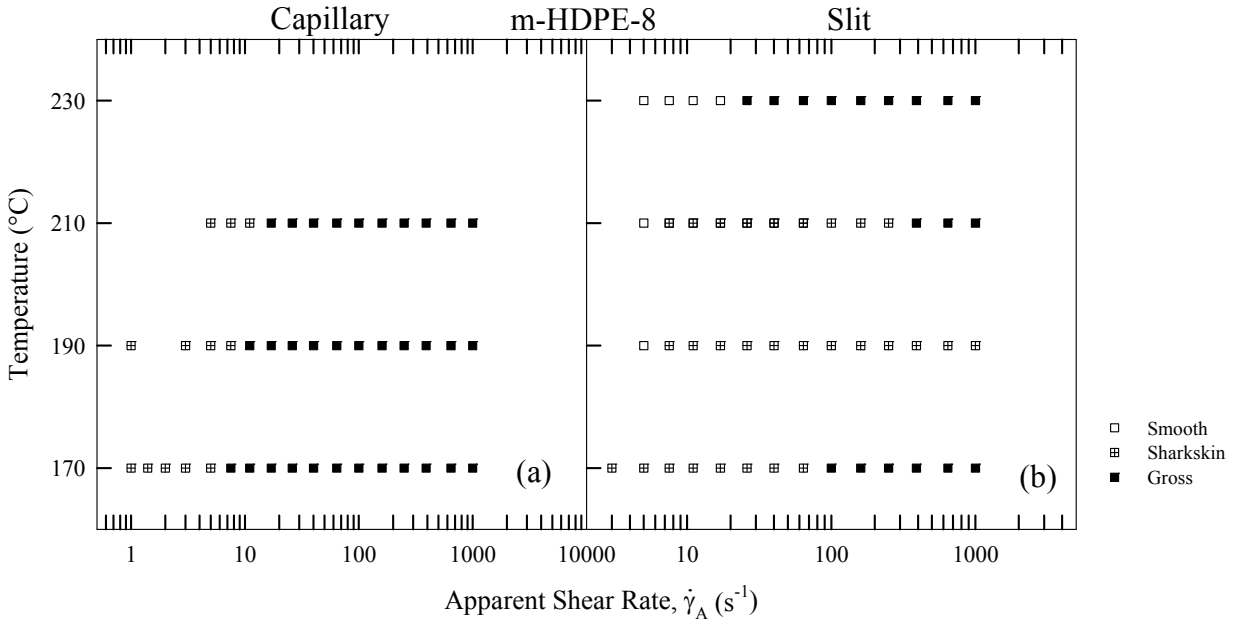

Figure D.3. *Processability map of resin m-HDPE-8 in extrusion through capillary and slit dies as a function of apparent shear rate and temperature.*

Table D.3. *Critical apparent shear rates and shear stresses for the onset of melt fracture in capillary and slit dies for resin m-HDPE-8 at different temperatures.*

Temperature (°C)	*Capillary*		*Slit*	
	$\dot{\gamma}_{A,cr}$ (s^{-1})	$\sigma_{A,cr}$(MPa)	$\dot{\gamma}_{A,cr}$ (s^{-1})	$\sigma_{A,cr}$(MPa)
170	No smooth extrudate got		1.73	0.08
190	No smooth extrudate got		6.12	0.10
210	No smooth extrudate got		13.67	0.12
230	No smooth extrudate got		21.02	0.13

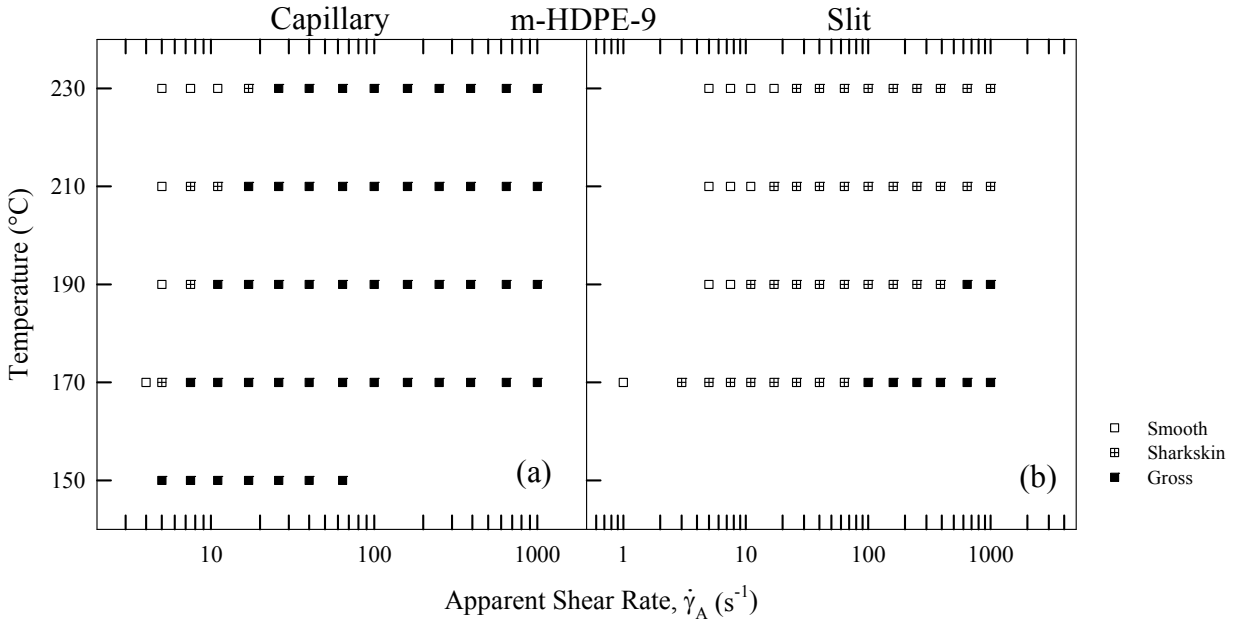

Figure D.4. *Processability map of resin m-HDPE-9 in extrusion through capillary and slit dies as a function of apparent shear rate and temperature.*

Table D.4. *Critical apparent shear rates and shear stresses for the onset of melt fracture in capillary and slit dies for resin m-HDPE-9 at different temperatures.*

Temperature (°C)	*Capillary*		*Slit*	
	$\dot{\gamma}_{A,cr}$ (s^{-1})	$\sigma_{A,cr}$(MPa)	$\dot{\gamma}_{A,cr}$ (s^{-1})	$\sigma_{A,cr}$(MPa)
150	2.25	0.07	Not Done	
170	4.47	0.08	1.73	0.05
190	6.12	0.08	9.08	0.08
210	6.12	0.08	13.7	0.08
230	13.7	0.08	21	0.09

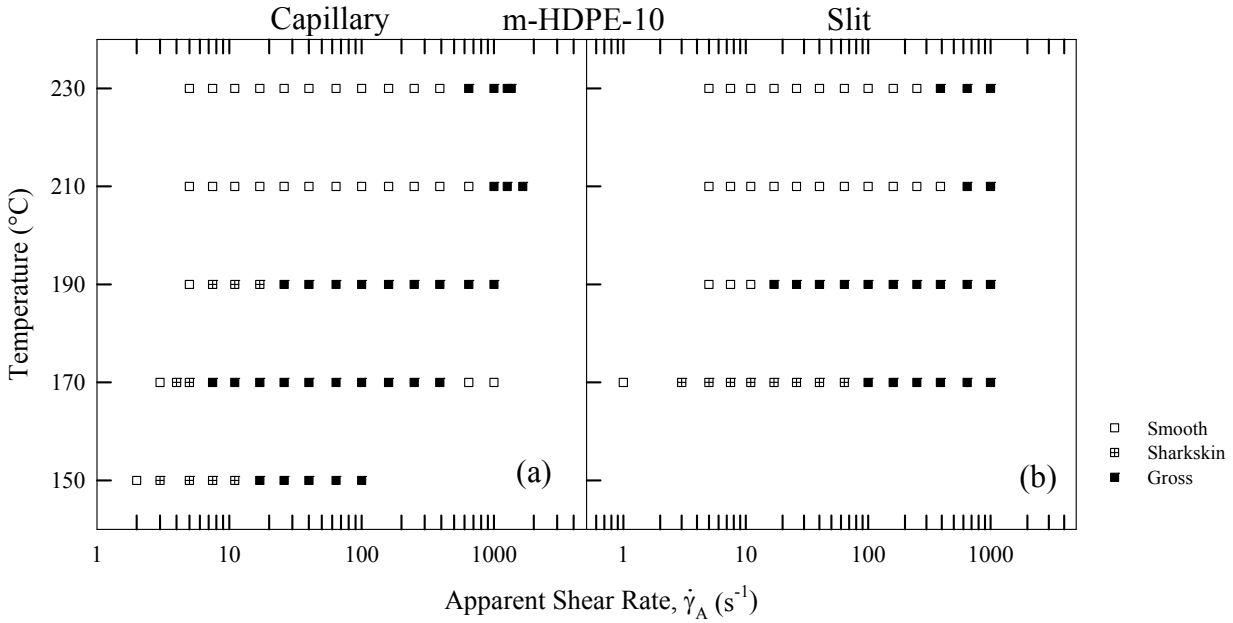

Figure D.5. *Processability map of resin m-HDPE-10 in extrusion through capillary and slit dies as a function of apparent shear rate and temperature.*

Table D.5. *Critical apparent shear rates and shear stresses for the onset of melt fracture in capillary and slit dies for resin m-HDPE-10 at different temperatures.*

Temperature (°C)	*Capillary*		*Slit*	
	$\dot{\gamma}_{A,cr}$ (s^{-1})	$\sigma_{A,cr}$(MPa)	$\dot{\gamma}_{A,cr}$ (s^{-1})	$\sigma_{A,cr}$(MPa)
150	2.45	0.07	Not Done	
170	3.46	0.07	1.73	0.05
190	6.12	0.08	13.7	0.09
210	803	0.28	502	0.21
230	502	0.23	312	0.18

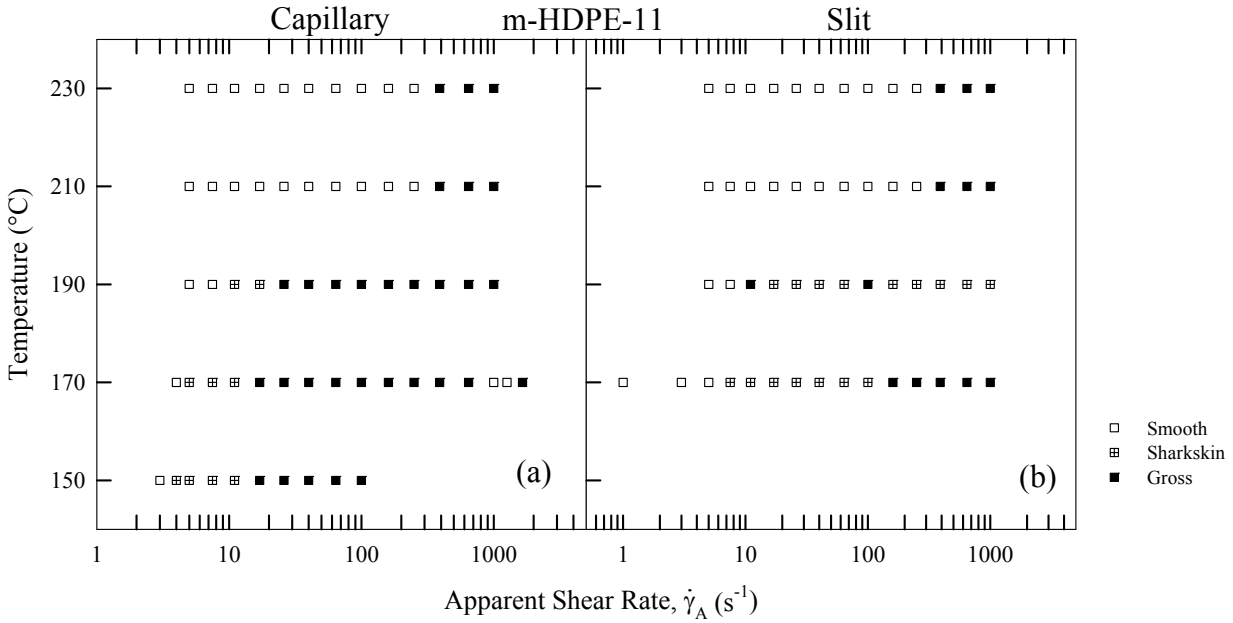

Figure D.6. *Processability map of resin m-HDPE-11 in extrusion through capillary and slit dies as a function of apparent shear rate and temperature.*

Table D.6. *Critical apparent shear rates and shear stresses for the onset of melt fracture in capillary and slit dies for resin m-HDPE-11 at different temperatures.*

Temperature (°C)	*Capillary*		*Slit*	
	$\dot{\gamma}_{A,cr}$ (s^{-1})	$\sigma_{A,cr}$(MPa)	$\dot{\gamma}_{A,cr}$ (s^{-1})	$\sigma_{A,cr}$(MPa)
150	3.46	0.07	Not Done	
170	4.47	0.07	6.12	0.07
190	9.08	0.07	9.08	0.07
210	312	0.19	312	0.16
230	312	0.17	312	0.16

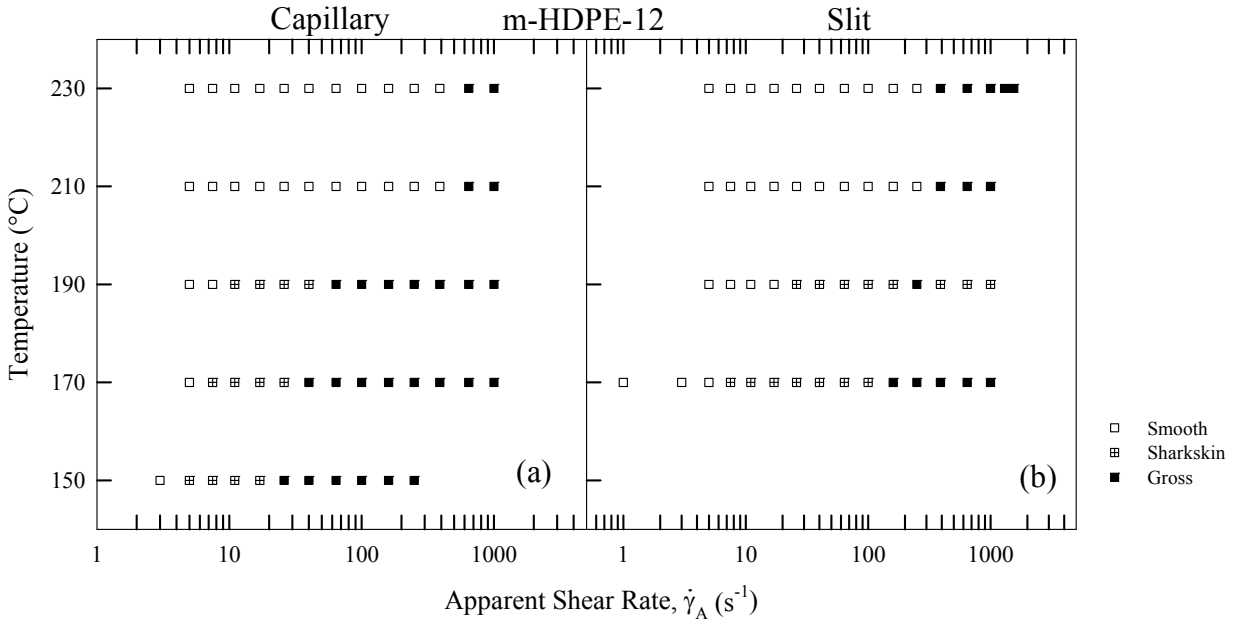

Figure D.7. *Processability map of resin m-HDPE-12 in extrusion through capillary and slit dies as a function of apparent shear rate and temperature.*

Table D.7. *Critical apparent shear rates and shear stresses for the onset of melt fracture in capillary and slit dies for resin m-HDPE-12 at different temperatures.*

Temperature (°C)	*Capillary*		*Slit*	
	$\dot{\gamma}_{A,cr}$ (s^{-1})	$\sigma_{A,cr}$(MPa)	$\dot{\gamma}_{A,cr}$ (s^{-1})	$\sigma_{A,cr}$(MPa)
150	3.87	0.06	Not Done	
170	6.12	0.06	6.12	0.05
190	9.08	0.06	9.08	0.06
210	502	0.20	312	0.14
230	502	0.17	312	0.13

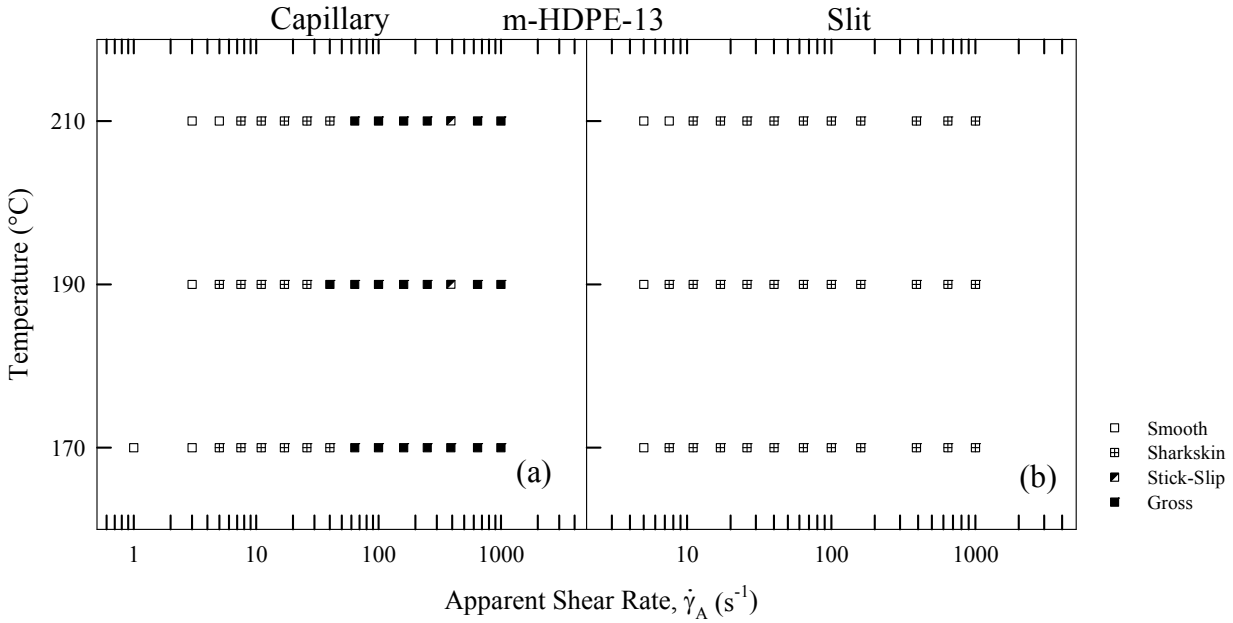

Figure D.8. *Processability map of resin m-HDPE-13 in extrusion through capillary and slit dies as a function of apparent shear rate and temperature.*

Table D.8. *Critical apparent shear rates and shear stresses for the onset of melt fracture in capillary and slit dies for resin m-HDPE-13 at different temperatures.*

Temperature (°C)	*Capillary*		*Slit*	
	$\dot{\gamma}_{A,cr}$ (s^{-1})	$\sigma_{A,cr}$(MPa)	$\dot{\gamma}_{A,cr}$ (s^{-1})	$\sigma_{A,cr}$(MPa)
170	3.87	0.11	6.12	0.12
190	3.87	0.11	6.12	0.11
210	6.12	0.11	9.08	0.11

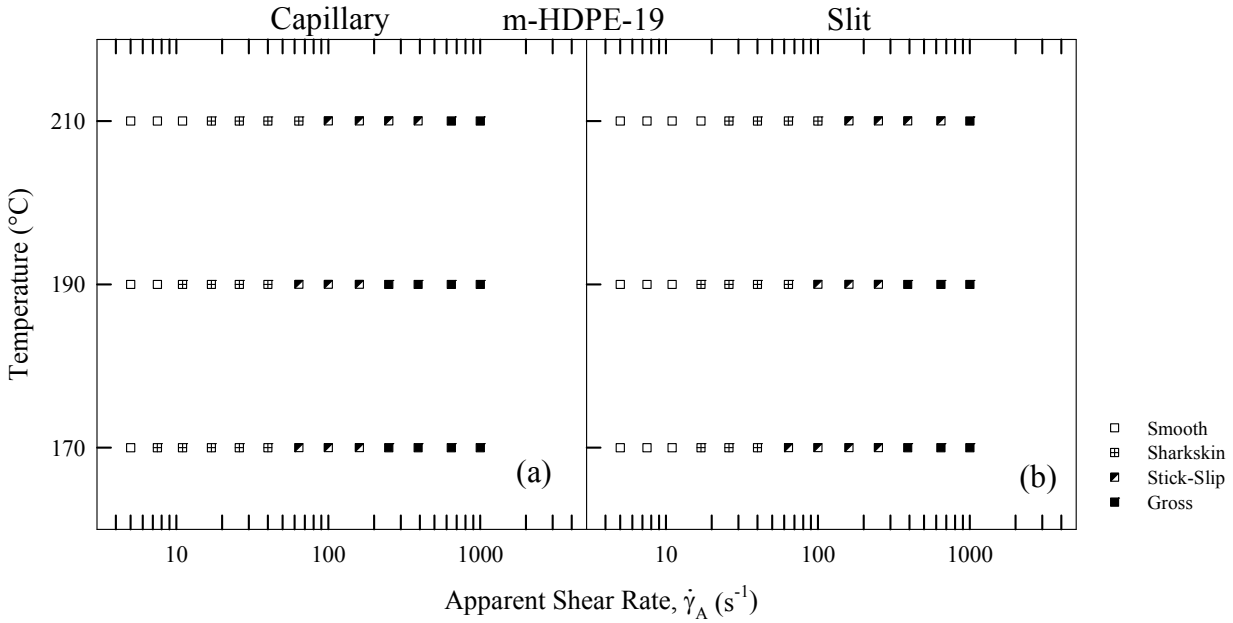

Figure D.9. *Processability map of resin m-HDPE-19 in extrusion through capillary and slit dies as a function of apparent shear rate and temperature.*

Table D.9. *Critical apparent shear rates and shear stresses for the onset of melt fracture in capillary and slit dies for resin m-HDPE-19 at different temperatures.*

Temperature (°C)	*Capillary*		*Slit*	
	$\dot{\gamma}_{A,cr}$ (s^{-1})	$\sigma_{A,cr}$(MPa)	$\dot{\gamma}_{A,cr}$ (s^{-1})	$\sigma_{A,cr}$(MPa)
170	6.12	0.17	13.67	0.20
190	9.08	0.16	13.67	0.18
210	13.67	0.16	21.02	0.20

APPENDIX E – MOONEY ANALYSIS

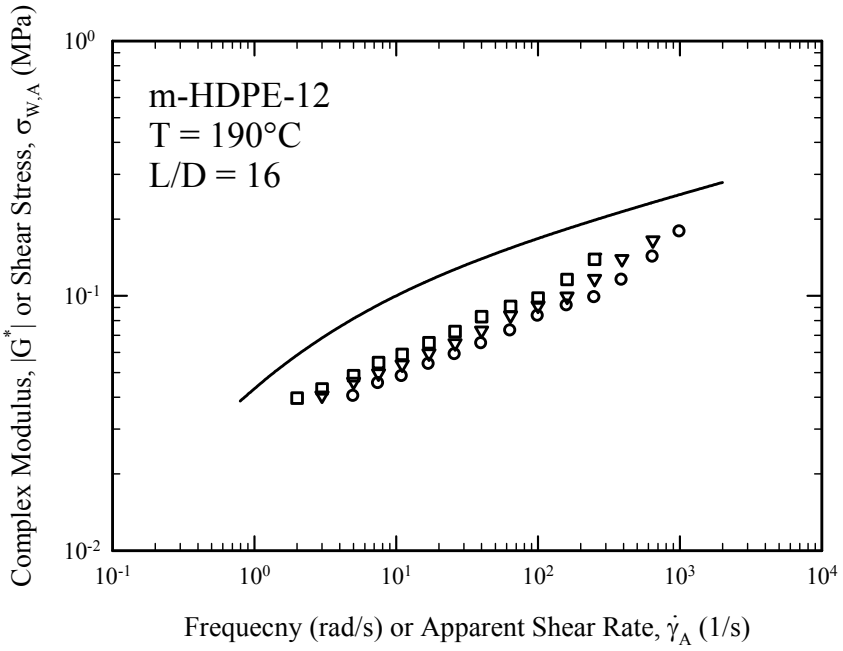

Figure E.1. *Bagley corrected flow curves of resin m-HDPE-12 for different diameters at T=190°C. The diameter dependence and the significant deviation from the LVE data (failure of the Cox-Merz rule) is consistent with the assumption of slip.*

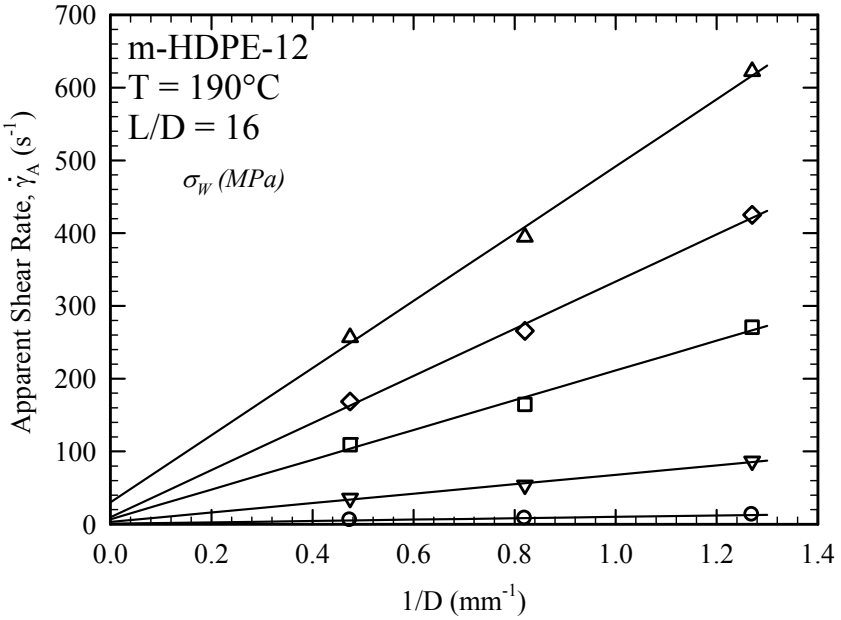

Figure E.2. *Mooney plot using the data plotted in Fig. E.1. The slopes of the lines are equal to $8u_s$ (Eq. 7.1) for the corresponding value of stress. The slopes increase with increase of shear stress.*

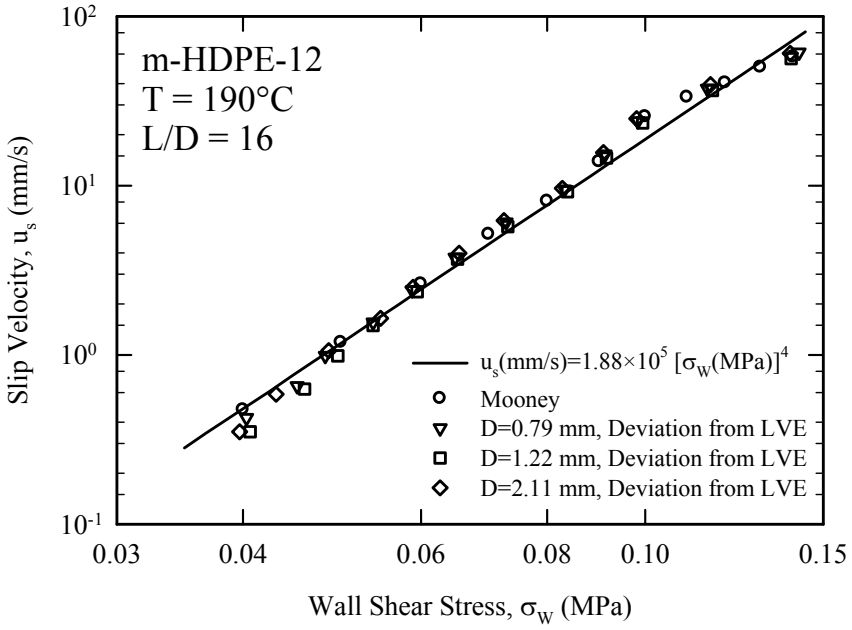

Figure E.3. *The slip velocity as a function of shear stress for resin m-HDPE-12 at T=190°C. The solid line represents the slip law given by Eq. 7.3.*

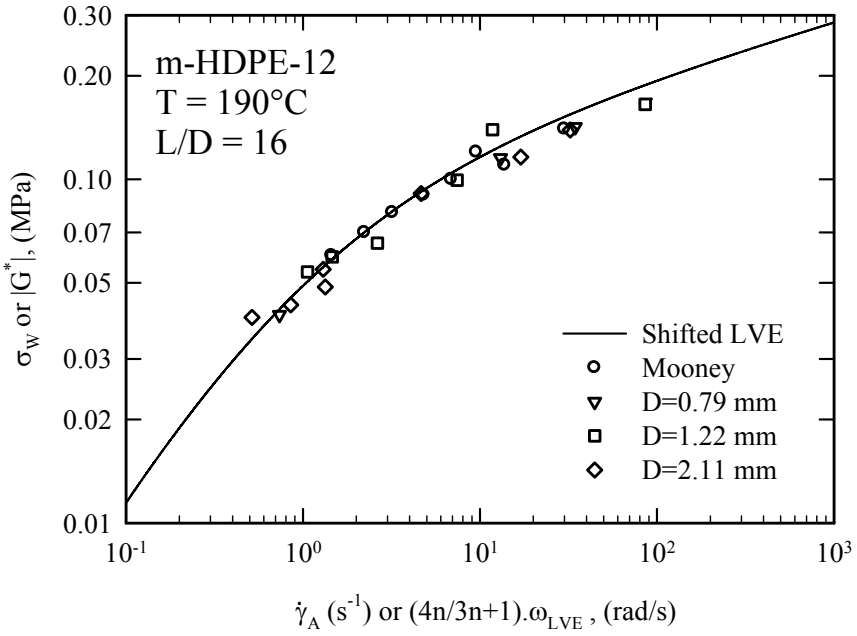

Figure E.4. *The slip corrected flow curve of resin m-HDPE-12 at T=190°C compared with the LVE data. Excellent agreement is shown, demonstrating the validity of the Cox-Merz rule.*

APPENDIX F – FLOW CURVE CONSTRUCTION

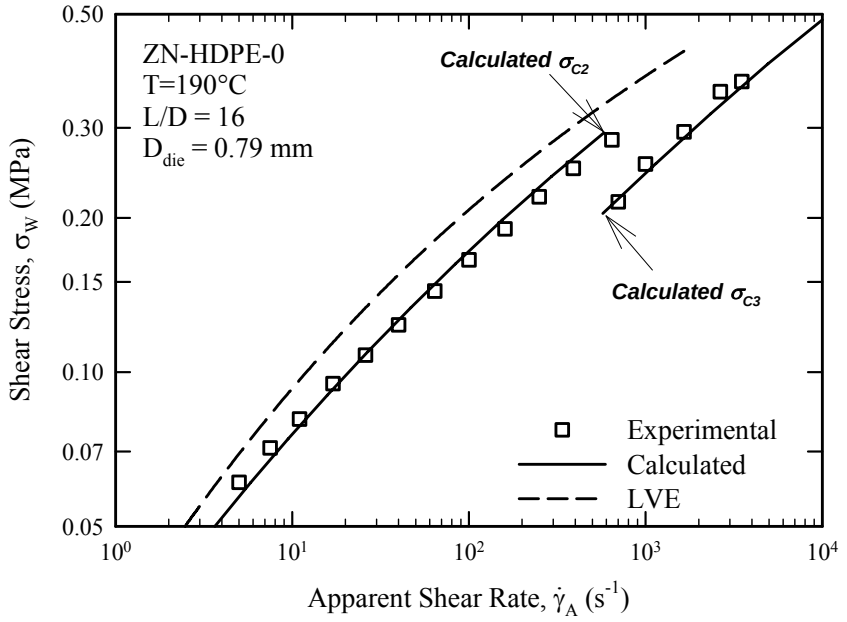

Figure F.1. *Constructing the flow curve of ZN-HDPE-0 starting from LVE data.*